nagra
National Cooperative for the
Disposal of Radioactive Waste

TECHNICAL REPORT 03-01

Grimsel Test Site
Investigation Phase V

The CRR final project report series I: Description of the Field Phase - Methodologies and Raw Data

December 2004

A. Möri (editor)

Hardstrasse 73, CH-5430 Wettingen/Switzerland, Telephone +41-56-437 11 11

nagra
National Cooperative for the
Disposal of Radioactive Waste

TECHNICAL REPORT 03-01

Grimsel Test Site
Investigation Phase V

The CRR final project report series I: Description of the Field Phase - Methodologies and Raw Data

December 2004

A. Möri (editor)

Contributors:

W.R. Alexander[1)], C. Degueldre[2)], J. Eikenberg[2)], Th. Fierz[3)], H. Geckeis[4)], F. Geier[4)], W. Hauser[4)], A. Möri[5)], Th. Schaefer[4)], P.A. Smith[6)]

[1)] Nagra, Wettingen, Switzerland

[2)] Paul Scherrer Institut, Villigen PSI, Switzerland

[3)] Solexperts, Schwerzenbach, Switzerland

[4)] FZK-INE, Karlsruhe, Germany

[5)] Geotechnical Institute, Bern, Switzerland

[6)] SAM, North Berwick, United Kingdom

Hardstrasse 73, CH-5430 Wettingen/Switzerland, Telephone +41-56-437 11 11

This report was prepared on behalf of Nagra. The viewpoints presented and conclusions reached are those of the author(s) and do not necessarily represent those of Nagra.

ISSN 1015-2636

Foreword

Concepts for the disposal of radioactive waste in geological formations depend crucially on a thorough knowledge of relevant processes in the host rock and on an understanding of the whole repository system, comprising both engineered and geological barriers. The Grimsel Test Site (GTS) is a first-generation underground rock laboratory which is used to investigate many of these processes in hard, fractured rocks. It has been operated since 1984 by the Swiss National Cooperative for the Disposal of Radioactive Waste (NAGRA).

The laboratory is located in the crystalline rock of the Central Aar Massif, 450 m below the eastern flank of the Juchlistock at an altitude of 1730 m. It is reached via a 1200 m horizontal access tunnel, operated by the hydropower plant KWO. The layout of the tunnels that comprise the GTS allowed the establishment of a radiation controlled zone (IAEA type B/C) in 1990 in which experiments with radioactive tracers are carried out. With increasing experience in the implementation of in-situ experiments, improved process understanding and more advanced repository concepts, the experimental programmes at the GTS have gradually become more complex and more directly related to open questions defined by performance assessors or by regulatory bodies. Demonstration of disposal concepts by performing large- or full-scale, long-term experiments has also become a key aspect of investigations in the rock laboratory.

The current investigation phase (Phase V; 1997 - 2002) was initiated in 1997 in close cooperation with international partner organisations. Seven experimental programmes and projects are included in Phase V, covering a broad spectrum of investigations.

This report documents the field results of the Colloid and Radionuclide Retardation (CRR) project, the aims of which were: examination of the migration of bentonite colloids in fractured rocks, investigation of the interactions between safety relevant radionuclides and bentonite colloids and, in addition, testing of the applicability of numerical codes for representing colloid-mediated radionuclide transport.

In addition to the in situ dipole tracer experiments carried out at the Grimsel Test Site (GTS), the project partners, namely ANDRA (F), ENRESA (E), FZK-INE (D), JNC (J), Nagra (CH) and the USDoE/Sandia (USA), funded an extensive programme of laboratory and modelling investigations, the results of which are reported elsewhere in the CRR final report series (NTB 03-02, 03-03 and 03-04).

Vorwort

Bei der Entsorgung radioaktiver Abfälle wird aus Sicherheitsüberlegungen die Endlagerung in geologischen Formationen vorgesehen. Dafür sind Kenntnis über das Wirtgestein sowie ein vertieftes Verständnis der technischen Sicherheitsbarrieren von entscheidender Bedeutung.

Seit 1984 betreibt die Nagra (Nationale Genossenschaft für die Lagerung radioaktiver Abfälle) ein standortunabhängiges Felslabor im Grimselgebiet (FLG), in den granitischen Gesteinen des Zentralen Aar Massivs.

Das FLG liegt 450 m unter der Ostflanke des Juchlistocks auf einer Höhe von 1730 m ü.M. und kann durch einen 1200 m langen horizontalen Zugangsstollen der Kraftwerke Oberhasli AG (KWO) erreicht werden. Im Jahr 1990 wurde in einem der Stollenabschnitte des FLG's eine kontrollierte Zone (IAEA Typ B/C) für Versuche mit radioaktiven Tracern eingerichtet.

Mit zunehmender Erfahrung in der Durchführung von Feldversuchen, verbessertem Systemverständnis der geologischen und technischen Barrieren sowie der weiterentwickelten Lagerkonzepte, verlagerten sich die Programm-Schwerpunkte zu komplexen, direkt auf die Anforderungen der Sicherheitsanalyse ausgerichteten Versuche. Langzeitdemonstrationsversuche gewannen in den letzten Jahren immer mehr an Bedeutung.

Die Untersuchungsphase V (1997 - 2002) wurde in enger Zusammenarbeit mit den Partnerorganisationen geplant. Sie beteiligen sich wesentlich bei der Durchführung der insgesamt 7 Versuchsprogramme, die ein breites Spektrum wissenschaftlicher und technischer Fragestellungen abdecken.

Der vorliegende Bericht präsentiert die Resultate der Felduntersuchungen, welche im Rahmen des Projekts Kolloid und Radionuklid Retardation (CRR) durchgeführt wurden. Die Hauptzielsetzungen des CRR Experimentes waren die Untersuchung des Transportverhaltens von Bentonit Kolloiden in einer Scherzone, die Interaktionen von sicherheitsrelevanten Radionukliden mit Bentonit Kolloiden sowie die Überprüfung und Weiterentwicklung von Transportmodellen zur Vorhersage von Kolloidunterstütztem Radionuklidtransport.

Zusätzlich zu einer Vielzahl von in-situ Dipol-Tracer-Experimenten, welche im Felslabor Grimsel (FLG) durchgeführt wurden, ermöglichten die beteiligten Projektpartner ANDRA (F), ENRESA (E), FZK-INE (D), JNC (J), USDoE/Sandia (USA) and Nagra (CH) die Durchführung von umfangreichen Laborexperimenten und Transportmodellierungen, welche ebenfalls in der Serie der Schlussberichte zum CRR Projekt dokumentiert sind (NTB 03-02, 03-03 und 03-04).

Préface

Le stockage définitif des déchets radioactifs est prévu, pour des questions de sécurité, dans des formations géologiques. La connaissance détaillée des roches d'accueil et une compréhension approfondie des processus se déroulant dans la roche et dans les barrières techniques de sécurité sont d'une importance décisive.

Le laboratoire souterrain du Grimsel (LSG) est un laboratoire de première génération en fonction depuis 1984, exploité par la Société coopérative nationale pour l'entreposage de déchets radioactifs (CEDRA).

Le laboratoire est situé à une altitude de 1730 m dans les roches granitiques du Massif Central de l'Aar, à 450 m de profondeur sous le flanc est du Juchlistock. On l'atteint par un tunnel d'accès horizontal exploité par la centrale électrique Oberhasli AG de la société KWO. En 1990, on a aménagé dans le LSG une zone de radiation contrôlée (type B/C de l'AIEA) pour des essais avec traceurs radioactifs.

Avec l'expérience croissante dans la conduite d'essais in-situ, une meilleure compréhension des barrières géologiques et techniques, le programme de recherche s'est orienté vers des essais toujours plus complexes liés aux exigences des analyses de sécurité. La démonstration de faisabilité de concepts de dépôt à grande échelle et sur de longues durées est devenue l'un des points forts des recherches dans le laboratoire souterrain.

La phase de recherche actuelle (phase V 1997 - 2002) a été planifiée en concertation étroite avec des partenaires internationaux. Elle comprend sept projets et programmes d'essais couvrant un large spectre de questions scientifiques et techniques.

Ce rapport documente les résultats obtenus au cours du projet Colloids and Radionuclide Retardation (CRR) dont les objectifs étaient: le contrôle de la migration in situ des colloïdes de bentonite dans les roches fracturées, l'investigation en laboratoire et in situ des interactions entre les radionucléides et les colloïdes de la bentonite, et en complément, le test d'applicabilité de codes numériques représentant le transport des radionucléides par les colloïdes.

Outre une série d'expériences de traceur de dipôle in situ qui ont été menées dans le laboratoire souterrain de Grimsel (GTS Grimsel Test Site), les partenaires du projet, à savoir ANDRA (F), ENRESA (E), FZK-INE (D), JNC (J), USDoE/Sandia (USA) et Nagra (CH), ont établi un vaste programme d'essais en laboratoire et d'investigations sur la modélisation, dont les résultats sont documentés dans la série de rapports finals du projet CRR (NTB 03-02, 03-03 and 03-04).

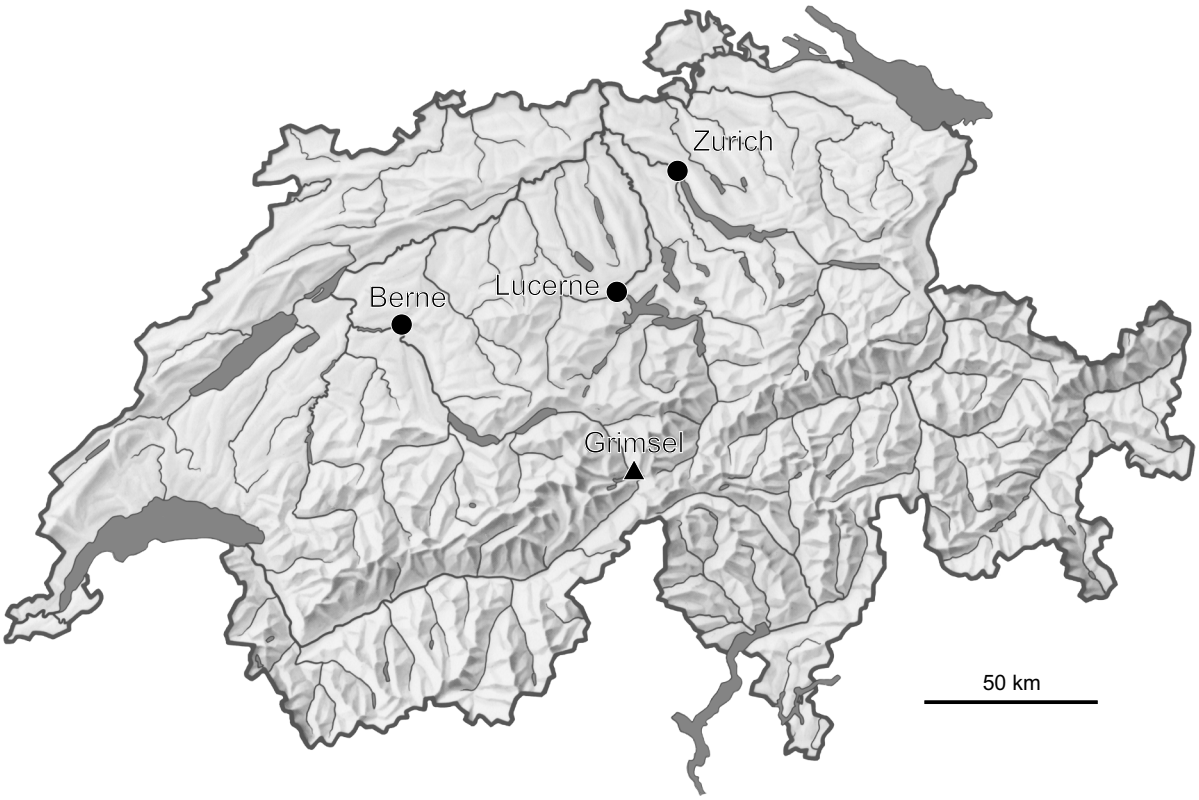

Location of Nagra's underground test facility at the Grimsel Pass in the Central Alps (Bernese Alps) of Switzerland

Grimsel area (view to the west)

1 Grimsel Test Site 2 Lake Raeterichsboden 3 Lake Grimsel 4 Juchlistock

Grimsel Test Site (GTS)

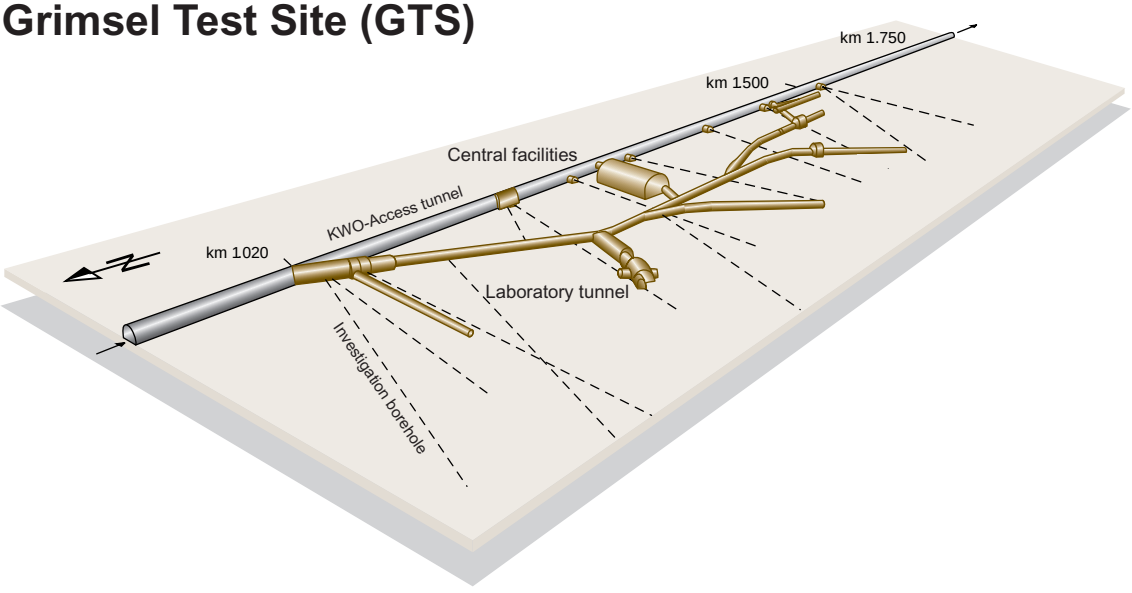

Grimsel Test Site
GTS

KWO-Access tunnel

Laboratory tunnel

Central Aaregranite (CAGR)
High biotite content CAGR

Grimsel-Granodiorite

Shear zone

Lamprophyre

SB — Investigation borehole

ZB — Central facilities

GTS Phase V 1997-2002

HPF — Hyperalkaline Plume

CRR — Colloid and Radionuclide Retardation

GAM — Gastransport in the Geosphere

FEBEX — 1:1 EBS – Demonstration (HLW)

GMT — Gas Migration Test in the EBS

GMB — Geophysical Methods in Boreholes

EFP — Effective Parameters

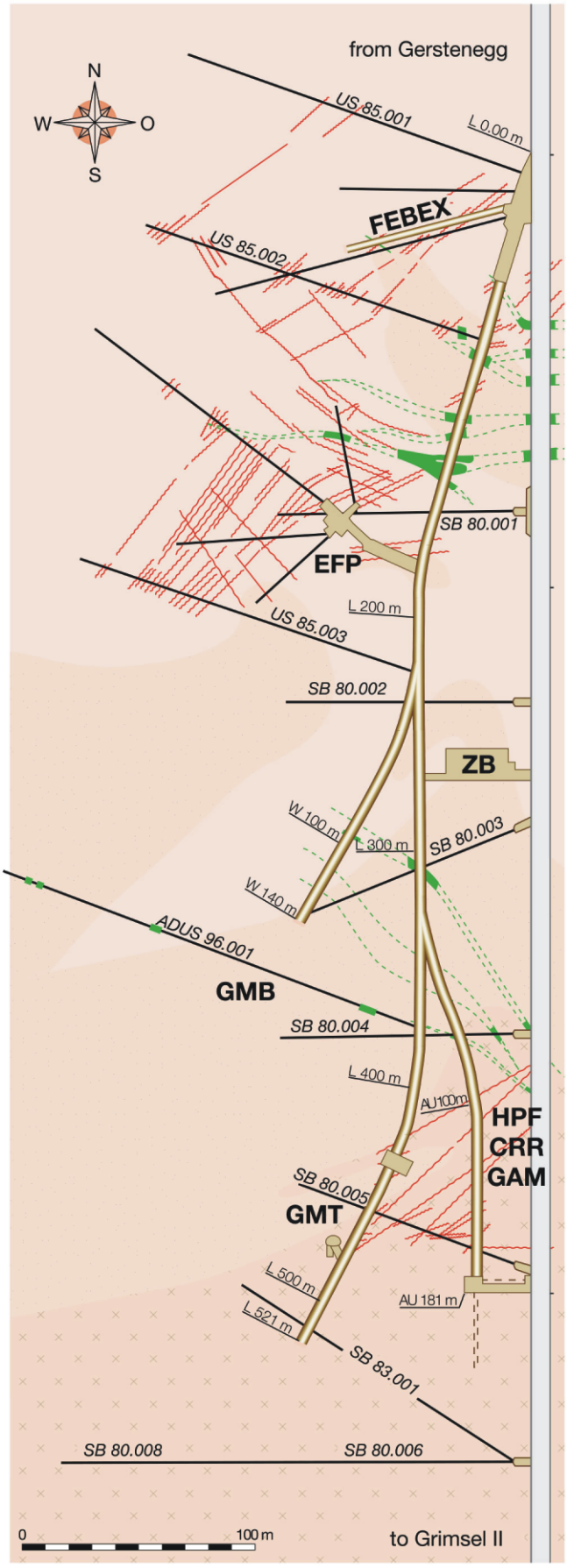

Abstract

The Colloid and Radionuclide Retardation Experiment (CRR) is dedicated to improve the understanding of the *in situ* retardation of colloid-associated, safety-relevant actinides and fission products in the vicinity of the Engineered Barrier System (EBS)/host rock interface. In addition to a series of *in situ* dipole experiments that were carried out at the Grimsel Test Site (GTS), the project partners, namely ANDRA (F), ENRESA (E), FZK-INE (D), JNC (J), USDOE/Sandia (USA) and Nagra (CH), funded an extensive programme of laboratory and modelling investigations. The aims of CRR were: examination of the *in situ* migration of bentonite colloids in fractured rocks, investigation of the interactions between safety relevant radionuclides and bentonite colloids in the laboratory and *in situ* and, in addition, testing of the applicability of numerical codes for representing colloid-mediated radionuclide transport.

The present report is the first of a quadruplet of final project reports that summarise the findings of the CRR project. In addition to this field report, the series includes laboratory and modelling reports along with a final, synthesis report. This report summarises and discusses the results of the field investigations that were carried out in 2001 and 2002 as part of the overall CRR project.

The overall concept behind CRR is based on the fact that, in most high-level radioactive waste repository designs, the waste is packed in massive metal canisters which are surrounded by a large volume of bentonite clay (collectively known as the Engineered Barrier System, or EBS). The canisters will slowly degrade and eventually fail, releasing some radionuclides, most of which are expected to be retained and to decay within the bentonite. However, it is conceivable that erosion of the bentonite at the EBS/host rock interface will produce bentonite colloids and that a limited amount of radionuclides escaping the EBS may become associated with these colloids and migrate through water conducting features in the geosphere towards the biosphere.

The central part of the CRR project was a series of dipole tracer tests that were carried out in a well-defined shear zone, in which dipole flow fields of 2.2 and 5 m length were generated. Preliminary tracer tests were performed with uranine, followed by tests with bentonite colloids and homologue elements for the tri- and tetravalent actinides (Tb for Am, Hf and Th for Pu, respectively). The tests culminated in the injection of the final tracer cocktails containing different isotopes of Am, Np, Pu, U, Tc, Th, Cs, Sr and I in the absence and presence of bentonite colloids.

The field installations consisted of several on-line measurement devices such as a downhole uranine detection device for the determination of the tracer input functions, a High Purity Germanium (HPGe) detector for γ-spectrometric measurements as well as a Laser Induced Breakdown Detector (LIBD) and a Photon Correlation Spectroscopy (PCS) apparatus for on-site colloid detection. The analytical techniques that were used off-site consisted of α-/γ-spectrometry and ICP-MS (Inductively Coupled Plasma-Mass Spectrometry) measurements for radionuclide detection as well as of Single Particle Counting (SPC) for the determination of the different colloid size classes. The interaction of the strongly sorbing tri- and tetravalent actinides with the equipment was avoided by producing as many as possible of those parts of the *in situ* equipment that were in direct contact with the tracers in PEEK (an inert plastic).

The natural colloid background of the groundwater in the experimental shear zone showed an average colloid diameter around 200 nm and a stable colloid concentration around 5 μgL^{-1}. Increased colloid concentrations observed temporarily at the beginning of the experiments were most likely due to mechanical stress induced by pressure pulses generated during installation of

the test setup. The four different colloid detection techniques, namely LIBD, ICP-MS[1] , PCS and SPC, produced internally consistent breakthrough data of the injected bentonite colloids. The bentonite colloids arrived slightly earlier than did the conservative dye uranine and the recovery was about 90%. Filtration effects varied depending on the colloid size and measurement technique employed and, as such, require further investigation .

Homologue pre-tests proved to be very useful for the prediction of the *in situ* behaviour of tri- and tetravalent actinides. In the absence of bentonite colloids, a clearly lower recovery was found for the homologues than when injected together with bentonite colloids and the peak maxima of the homologue breakthrough were slightly shifted to earlier arrival times compared to that of the uranine.

The tracer cocktail composition for the final tracer injections covered the entire range of oxidation states from -I to VI and was decided based on the results of laboratory experiments, the kinetics of redox reactions and practical constraints on the *in situ* use of these elements. The preparation of an injection cocktail which contains tri- and tetravalent actinides proved to be problematic, as shown by the presence of a variable colloidal fraction for Am, Pu and Th, even in the absence of bentonite colloids. However, the injection cocktail, which included bentonite colloids, showed high colloid association and long term stability for the tri- and tetravalent actinides with the bentonite colloids, indicating that a significant proportion of the radionuclides were associated with the added bentonite colloids.

In the first run (without bentonite colloids), the tri- and tetravalent actinides Am, Th and Pu displayed lower recovery, less tailing and a peak time which was about 10 minutes earlier than U, Np and I (which is assumed to behave in a conservative fashion), indicating that a fraction of these actinides was transported in a colloidal state. With regard to the varying colloid content in the injection cocktail, the source of these colloids cannot yet be uniquely defined (homogeneous- or heterogeneous radiocolloids) and artifacts, for example, during cocktail preparation, cannot yet be ruled out completely.

With the addition of bentonite colloids, an increased recovery of Am, Pu and Th compared to the first run was observed. The shape of the breakthrough curves did not change significantly as the peak in the first experiment was also affected by a colloidal fraction. Only about 1% of the Cs was colloidally transported which implies that 90% of the initially colloid bound Cs in the injection cocktail (10% Cs in the injection cocktail was in colloidal form) desorbed during migration.

Finally it should be noted that the field experiments constitute only a part of the overall CRR project and interpretation and transfer of these data needs to be carried out taking into account the results of the laboratory experiments along with the effects of site groundwater chemistry, very short test duration and other technical constraints.

---

[1] ICP-MS was used to determine the total Al concentration in the groundwater as tests indicated that this accurately mirrored the Al-rich clay fraction of the bentonite (in this particular groundwater).

Zusammenfassung

Das Kolloid- und Radionuklid-Retardationsexperiment (CRR) erweitert das Verständnis für die *in-situ*-Retardation von sicherheitsrelevanten Aktiniden und Spaltprodukten in Anwesenheit von Kolloiden in geklüfteten Medien im Stollennahfeld. Zusätzlich zu einer Vielzahl von *in-situ*-Dipol-Tracer-Experimenten, welche im Felslabor Grimsel (FLG) durchgeführt wurden, ermöglichten die beteiligten Projektpartner ANDRA (F), ENRESA (E), FZK-INE (D), JNC (J), USDoE/Sandia (USA) und Nagra (CH) die Durchführung von umfangreichen Laborexperimenten und Transportmodellierungen. Die Hauptzielsetzungen des CRR-Experimentes waren die Untersuchung des Transportverhaltens von Bentonit-Kolloiden in einer Scherzone, die Interaktionen von sicherheitsrelevanten Radionukliden mit Bentonit-Kolloiden sowie die Überprüfung und Weiterentwicklung von Transportmodellen zur Vorhersage von Kolloid-unterstütztem Radionuklidtransport.

Der vorliegende Bericht ist der erste von vier Schlussberichten, welche die Erkenntnisse aus dem Projekt CRR zusammenfassen. Die Serie enthält neben dem Feldbericht einen Schlussbericht zu den Laborexperimenten sowie zu den Modellierungen. Der vierte Bericht liefert eine Synthese sämtlicher Resultate. Dieser Bericht präsentiert und diskutiert die Resultate aus den Feldexperimenten, welche zwischen 2001 und 2002 im Rahmen des CRR Projektes durchgeführt wurden.

Das Konzept des CRR-Experimentes basiert auf der Grundlage, dass der radioaktive Abfall in den meisten Endlagerkonzepten in massiven Stahlbehältern, umgeben von grösseren Mengen von Bentonit-Ton (Technisches Barrierensystem) gelagert werden soll. Im weiteren wird angenommen, dass die Behälter mit der Zeit langsam korrodieren und dabei Radionuklide freigesetzt werden können. Auch wenn der Grossteil dieser Radionuklide im Bentonit bis zu deren Zerfall zurückgehalten wird, wird angenommen, dass sich an der Kontaktstelle Bentonit/ Wirtgestein Kolloide bilden und freigesetzte Radionuklide zusammen mit den Kolloiden über die Geosphäre Richtung Biosphäre transportiert werden können.

Das Kernstück des CRR-Projektes bildet eine Serie von *in-situ*-Dipol-Tracer-Experimenten, welche in einer gut charakterisierten Scherzone in Fliessfeldern von 2.23 bis 5 m Länge durchgeführt wurden. Erste Vorversuche fanden mit Uranin statt, gefolgt von Tracer-Versuchen mit Bentonit-Kolloiden und Homolog-Elementen für die drei- und vierwertigen Aktiniden (Tb für Am, Hf und Th für Pu). Die beiden Tracer-Cocktails für das Hauptexperiment enthielten verschiedene Isotope von Am, Np, Pu, U, Tc, Th, Cs, Sr und I und wurden einmal mit und einmal ohne Bentonit-Kolloide in die Scherzone injiziert.

Die Uranin-Inputfunktionen wurden online mittels eines Bohrlochdetektors erfasst und die Durchbrüche der gammaemittierenden Radionuklide wurden mit einem Germanium-Detektor ebenfalls online registriert. Kolloiddurchbrüche konnten sowohl mittels Laser als auch mittels Spektroskopie vor Ort gemessen werden (Laser Induced Breakdown Detector, LIBD und Photon Correlation Spectroscopy, PCS). Die Laboranalysen beinhalteten α-/γ-Spektrometrie sowie ICP-MS-Messungen für die Radionuklide und Single Particle Counting (SPC) zur Bestimmung einzelner Kolloidgrössenklassen. Um die Interaktion zwischen den stark sorbierenden drei- und vierwertigen Aktiniden mit den Geräten zu minimieren, wurden Oberflächen, welche in direktem Kontakt mit dem Tracer waren, wenn immer möglich aus PEEK (einem inerten Kunststoff) hergestellt.

Der natürliche Kolloidhintergrund im Grundwasser der Scherzone besitzt einen durchschnittlichen Kolloiddurchmesser von 200 nm und eine stabile Kolloidkonzentration von ca. 5 μgL^{-1}.

Erhöhte Hintergrundkolloidkonzentrationen wurden kurzzeitig am Anfang der Experimente beobachtet und haben ihren Ursprung höchstwahrscheinlich in installationsbedingten Druckschwankungen im Fliessfeld. Die vier verschiedenen Kolloidnachweistechniken LIBD, ICP-MS[2], PCS und SPC produzierten konsistente Durchbruchsdaten. Die Bentonit-Kolloide erreichten die Extraktionsseite etwas früher als der konservative Farbstoff Uranin. Ihre Rückgewinnung betrug ca. 90%. Filtrationseffekte waren unterschiedlich und zeigten eine Abhängigkeit von der Kolloidgrösse und den verwendeten Messtechniken. In diesem Zusammenhang sind weitere Untersuchungen nötig.

Vorbereitende Experimente mit Homologen erwiesen sich als sehr nützlich für die Vorhersage des *in-situ*-Verhaltens der drei- und vierwertigen Aktiniden. Ohne Bentonit-Kolloide war die Rückgewinnung deutlich geringer als mit den Bentonit-Kolloiden und die Durchbruchskurven verschoben sich, verglichen mit Uranin, hin zu leicht früheren Ankunftszeiten.

Die Oxidationsstufen der Aktiniden und Spaltprodukte in den Tracercocktails reichen von -I bis VI und wurden mit Hilfe von Laborexperimenten zur Kinetik der Redox-Reaktionen und im Hinblick auf Einschränkungen, welche sich aus der Machbarkeit der Experimente ergaben, festgelegt. Die Herstellung eines Tracercocktails aus drei- und vierwertigen Aktiniden stellte sich als sehr anspruchsvoll heraus. Probleme zeigten sich vor allem in der Bildung von Kolloiden bei einem Teil des Am, Pu und Th, auch wenn keine Bentonit-Kolloide beigegeben wurden. Demgegenüber zeigte der Cocktail mit den Bentonit-Kolloiden eine deutliche und über lange Zeit stabile Gebundenheit eines Grossteils dieser Aktiniden an die Bentonit-Kolloide.

Im ersten Versuch ohne Bentonit-Kolloide zeigten die drei- und vierwertigen Aktiniden Am, Th und Pu eine niedrigere Rückgewinnung, weniger „Tailing“ und eine um ca. 10 Minuten verfrühte Peak-Zeit als U, Np und I (I repräsentiert einen typischen, konservativen Tracer). Dies lässt darauf schliessen, dass ein Teil dieser Aktiniden kolloidal transportiert wurde. Berücksichtigt man den stark schwankenden Kolloidanteil im Injektionscocktail ist es schwierig festzustellen, ob es sich um homogene- oder heterogene Radiokolloide handelt und ob es sich dabei um Artefakte, zum Beispiel von der Herstellung des Tracercocktails, handelt.

Mit der Zugabe von Bentonit-Kolloiden zum Tracercocktail stieg die Rückgewinnung von Am, Pu und Th gegenüber dem ersten Versuch deutlich an. Die Form der Durchbruchskurven änderte sich nur unbedeutend, da der Peak im ersten Versuch ebenfalls schon von Kolloiden beeinflusst war. Ungefähr 1% des injizierten Cs wurde ebenfalls in kolloidaler Form transportiert. Dies bedeutet, dass 90% des ursprünglich kolloidal gebundenen Cs im Injektionscocktail (10% des ursprünglich eingegebenen Cs war in einer kolloidalen Form) während seinem Transport durch die Scherzone von den Kolloiden desorbierte.

Abschliessend muss erwähnt werden, dass die Feldexperimente nur einen Teil des CRR-Experimentes darstellen und für die Interpretation bzw. den Transfer der Resultate immer auch die Ergebnisse der Laborexperimente sowie mögliche Einflüsse der örtlichen Grundwasserchemie, der kurzen Dauer des Experiments sowie anderer technischer Einschränkungen mitberücksichtigt werden müssen.

---

[2] ICP-MS wurde zur Bestimmung der Al-Konzentration im Grundwasser verwendet, da mittels Experimenten gezeigt werden konnte, dass diese im vorherrschenden Grundwasser die Al-reiche Tonfraktion des Bentonits widerspiegelt.

Résumé

En vue des analyses de sûreté l'expérience de Retardement des Colloïdes et des Radionucléides (CRR Colloid and Radionuclide Retardation Experiment) est consacrée à l'amélioration de la compréhension du retardement *in situ* des colloïdes associés aux actinides et les produits de fission à proximité de l'interface du système de barrières ouvragées (EBS Engineered Barrier System) et de la roche avoisinante. Outre une série d'expériences de dipôle *in situ* qui ont été menées dans le laboratoire souterrain de Grimsel (GTS Grimsel Test Site), les partenaires du projet, à savoir ANDRA (F), ENRESA (E), FZK-INE (D), JNC (J), USDOE/ Sandia (USA) et Nagra (CH), ont établi un vaste programme d'essais en laboratoire et de recherche de modélisations. Les objectifs du CRR étaient: le contrôle de la migration *in situ* des colloïdes de bentonite dans les roches fracturées, l'investigation en laboratoire et *in situ* des interactions entre les radionucléides et les colloïdes de la bentonite, et en complément, le test d'applicabilité de codes numériques représentant le transport des radionucléides par les colloïdes.

Le présent rapport est le premier d'une série de quatre rapports finals qui résument les résultats de recherche du projet CRR. En complément de ce rapport d'activités, la série inclut des rapports de laboratoire et de modélisation, le tout avec un rapport final de synthèse. Ce rapport résume et discute les résultats des investigations qui furent menés en 2001 et 2002 dans le cadre du projet CRR.

Le concept général du CRR est basé sur le fait que, dans la plupart des designs de dépôt de déchets de haute radioactivité, les déchets sont empaquetés dans des containers massifs en acier lesquels sont entourés d'un grand volume de bentonite (formant le système de barrières ouvragées EBS). Les containers vont lentement se dégrader et éventuellement faillir, relâchant un certain nombre de radionucléides dont la plupart sont supposés être retenus et décroître au travers de la bentonite. Pourtant, il est concevable que l'érosion de la bentonite à l'interface du système de barrières ouvragées et de la roche avoisinante produise des colloïdes de bentonite et qu'un nombre limité de radionucléides s'échappant du système de barrières s'associent à ces colloïdes pour migrer de la géosphère vers la biosphère au travers des fissures contenant de l'eau.

La partie centrale du projet CRR s'est appuyée sur une série de tests de traceur de dipôle. Ceux-ci ont été réalisés dans une zone de cisaillement bien définie dans laquelle des champs de flux de dipôle de 2.2 et 5 m de long ont été générés. Des tests préliminaires sur les traceurs ont été pratiqués avec l'uranine, suivis de tests avec des colloïdes de bentonite et des éléments homologues des actinides tri- et tétravalents (Tb pour Am, Hf et Th pour Pu, respectivement). Finalement des cocktails de traceurs, contenant les différents isotopes de Am, Np, Pu, U, Tc, Th, Cs, Sr et I en l'absence ou en présence de colloïdes de bentonite, ont été injectés.

Les installations de terrain sont composées de plusieurs instruments de mesure en ligne tels qu' un appareil de détection de l'uranine au fond du forage pour la détermination des fonctions d'alimentation de traceurs, un détecteur de haute pureté au germanium pour les mesures de spectrométrie-γ ainsi qu'un Laser Induced Breakdown Detector (LIBD) et un appareil de spectroscopie à corrélation de photon (PCS Photon Correlation Spectroscopy) pour la détection des colloïdes sur site. Les techniques analytiques qui ont été utilisées hors-site ont consisté en des mesures de spectrométrie α-/γ- et ICP-MS (Inductively Coupled Plasma-Mass Spectrometry) pour la détection des radionucléides ainsi qu'en l'utilisation de Single Particle Counting (SPC) pour la détermination des différentes classes de taille des colloïdes. L'interaction des actinides tri- et tétravalents fortement sorbants avec l'équipement a été évité en limitant autant que possible le contact direct *in situ* des parties de l'équipement en utilisant du PEEK (une matière synthétique inerte) avec les traceurs.

Les données sur les colloïdes naturels dans l'eau souterraine de la zone de cisaillement expérimentale ont révélé un diamètre moyen de colloïdes de l'ordre de 200 nm et une concentration en colloïdes stable aux alentours de 5 μgL^{-1}. L'augmentation des concentrations en colloïdes observée temporairement au début des expériences a été vraisemblablement due aux contraintes mécaniques induites par des pulsations de pression générées lors de l'installation de l'appareillage de test. Les quatre différentes techniques de détection, à savoir LIBD, ICP-MS[3], PCS et SPC, ont produit des données internes consistantes sur les colloïdes de bentonite injectés. Les colloïdes de bentonite sont arrivés légèrement plus tôt que le colorant conservatif d'uranine, et le recouvrement a été de 90%. Les effets de la filtration ont montré une dépendence des techniques appliquées et des diamètres des colloïdes.

Les tests d'homologues préliminaires se sont avérés très utiles pour la prédiction du comportement *in situ* des actinides tri- et tétravalents. En l'absence de colloïdes de bentonite, le recouvrement des homologues est légèrement plus faible que lorsque ceux-ci sont injectés avec les colloïdes de bentonite. Le pic maximum est légèrement décalé vers les temps d'arrivée plus courts comparé à celui de l'uranine.

La composition du cocktail de traceurs pour les injections finales de traceurs d'actinide ont couvert la gamme entière des états d'oxydation de -I à VI et ceci fut le résultat d'expériences de laboratoire, des cinétiques des réactions redox et des contraintes d'ordre pratique de l'utilisation de ces éléments *in situ*. La préparation d'un cocktail d'injection contenant des actinides tri- et tétravalents s'est avérée problématique comme démontré par la présence d'une fraction colloïdale variable de Am, Pu et Th, et ceci même en l'absence de colloïdes de bentonite. Pourtant, le cocktail d'injection qui incluait les colloïdes de bentonite a montré une haute association de colloïdes et une stabilité à long terme pour les actinides tri- et tétravalents avec les colloïdes de bentonite. Ceci indique qu'une proportion de radionucléides a été associée aux colloïdes de bentonite rajoutés.

Dans la première injection (sans les colloïdes de bentonite), les actinides tri- et tétravalents Am, Th et Pu ont montré un recouvrement moindre, moins filant et un pic de temps qui apparaissait 10 minutes plus tôt que celui de U, Np et I (qui est supposé réagir de manière conservative), indiquant qu'une fraction de ces actinides a été transportée dans un état colloïdal. Du fait de la concentration variable en colloïdes dans le cocktail d'injection, la source de ces colloïdes ne peut pas être encore définie de façon unique (radio-colloïdes homogènes ou hétérogènes) et des artéfacts, par exemple pendant la préparation du cocktail, ne peuvent pas être complètement écartés.

Avec l'addition de colloïdes de bentonite, un recouvrement plus important de Am, Pu et Th par rapport à la première injection a été observé. La forme des courbes n'a pas changé de façon significative puisque le pic dans la première expérience a aussi été affecté par une fraction des colloïdes. Autour de 1% de Cs a été transporté par des colloïdes, ce qui implique que 90 % du Cs contenu dans le cocktail (10 % du Cs dans le cocktail d'injection était sous forme colloïdale) a désorbé pendant la migration.

Finalement, on peut noter que les expériences de terrain constituent seulement une partie de l'ensemble du projet CRR et que l'interprétation et le transfert des ces données ont besoin d'être menés en tenant compte des résultats des expériences en laboratoire, des effets de la composition chimique de l'eau souterraine du site, des tests de courte durée et des autres contraintes techniques.

---

[3] ICP-MS a été utilisé pour déterminer la concentration totale en Al de l'eau souterraine, puisque les tests ont indiqué que cela reflétait la fraction de bentonite dans l'argile riche en Al (dans cette eau souterraine particulière).

Table of Contents

List of Tables

List of Figures

1 Introduction

W. R. Alexander, A. Möri and P.A.Smith

1.1 Background of the CRR project

The Colloid and Radionuclide Retardation Project (CRR) began in 1998 with the aim of studying the *in situ* migration behaviour of selected actinides and fission products in the absence and presence of bentonite colloids. An extensive programme of *in situ* work was conducted in a water-conducting feature (shear zone) at Nagra's Grimsel Test Site (GTS) in southern Switzerland and this was backed up by an intensive programme of laboratory studies and modelling at various institutions around the world.

Colloids are natural and ubiquitous in groundwater and may also be generated by physical and chemical processes resulting from the presence of a geological repository for radioactive waste. In most repository designs for vitrified high-level waste (HLW) and spent fuel (SF), the waste is packed in massive metal canisters which are surrounded by a large volume of bentonite clay, all of which constitute the engineered barrier system (EBS)[4]. The canisters will slowly degrade and eventually fail, releasing some radionuclides, most of which are expected to be retained and to decay within the bentonite.

Although bentonite is expected to act as a colloid filter, the outer surface of the bentonite may itself act as a source of colloids due, for example, to erosion by flowing water in host rock fractures. For these colloids to have any affect on radionuclide transport in the host rock, the radionuclides in question must be able (i), to migrate to the bentonite/host rock interface before they decay, and (ii) subsequently sorb on the bentonite colloids that are generated there (the colloids themselves must also fulfil a number of criteria, as discussed in Section 1.2). If the bentonite barrier operates as expected, transport of any sorbing radionuclides will be slow and the above conditions are unlikely to be met for most safety-relevant radionuclides. There are, however, conceivable scenarios that would allow more rapid transport of some sorbing radionuclides through the bentonite barrier, including, for example, the creation of temporary flow paths (see Fig. 1.1) through the bentonite by repository produced gas (from canister corrosion *etc*; see Nagra, 2002). The impact of natural groundwater colloids on transport is also a concern in the case of fractured hard rocks.

Due to a lack of relevant *in situ* data on colloid and colloid-mediated radionuclide transport, most performance assessment (PA) studies treat such scenarios conservatively (or over-conservatively). Therefore HSK (the Swiss Federal Nuclear Safety Inspectorate) noted that "...the generation of colloids at the bentonite surface cannot be excluded" and that "...possible colloid associated transport of radionuclides remains an important open question." (HSK, 1998).

CRR is therefore dedicated to improve the understanding of the *in situ* retardation of colloid associated, safety relevant radionuclides in the vicinity of the EBS/host rock interface and to examine the implications of these findings on the far-field transport of safety relevant radionuclides. To this end, laboratory results and predictions from reactive transport modelling have been tested against *in situ* dipole tracer injections of radionuclides and bentonite colloids in the experimental shear zone at the GTS.

---

[4] Designs for other waste types also include bentonite barriers and so the relevance of the work presented here is not restricted to HLW/SF.

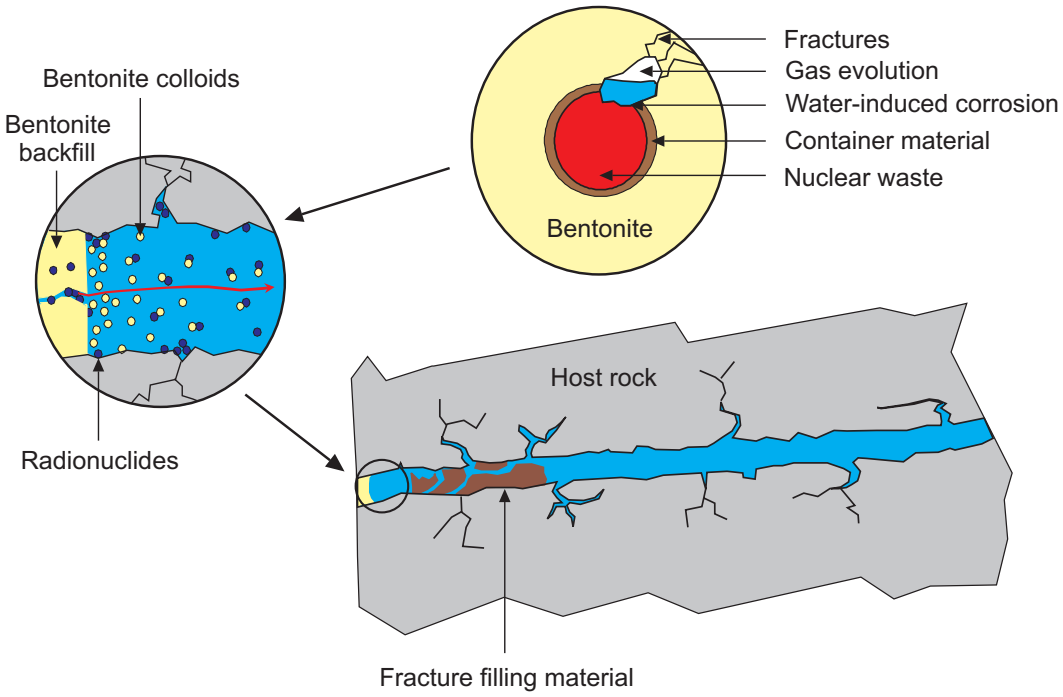

Fig. 1.1: CRR scenario for radionuclide release and bentonite colloid formation

1.2 Key safety-relevant issues related to colloids

CRR addresses the transport of radionuclide-bearing colloids in a fractured hard rock. In general, there exist good arguments for assuming efficient filtration of any colloids in unfractured rocks with fine pore structures (e.g. Baeyens *et al*. 1985). It should be noted, however, that even in such a potential repository host rock, the Boom Clay, field experiments have demonstrated the diffusion-dominated transport of ^{14}C-labelled natural organic matter (NOM) colloids over distances in the order of 0.5 m (Dierckx *et al*. 2000).

Several recent PAs have considered the possibility that radionuclides released from a repository become sorbed on colloids, or incorporated within them, and subsequently transported by advection/dispersion in flowing groundwater. Colloids may not be subject to some of the processes that retard the transport of radionuclides in solution. Indeed, they may move faster than the average groundwater flow velocity, because both their physical size and electrostatic effects can keep them away from solid surfaces where friction slows the flow of groundwater. There are, however, retardation and immobilisation processes that could affect radionuclides associated with colloids.

In fractured media, they could conceivably diffuse into stagnant water in the rock matrix. Their diffusion coefficient would be lower than un-complexed ions and the extent to which they penetrated into the matrix (if at all) would depend on the sizes of matrix pores with respect to the size of the colloids, as well as charge effects. The investigations of James and Chrysikopoulos (1999), for example, which considered the influence of matrix diffusion on the breakthrough of polydispersed colloids in rough fractures, showed that larger particles are the least retarded and smaller particles are more slowly transported. Colloids may in some circumstances become unstable through aggregation or dissolution. They may also come into contact with fixed solid surfaces, such as fracture walls and the pore surfaces of fracture infill material, to which they can become attached (although the negative charge often found on the

surfaces of both colloids and solid phase surfaces acts against this process), or become trapped at constrictions in fractures or in the pore space of the rock matrix because they are too large to pass through. These processes are termed filtration: mechanical filtration, where large colloids become trapped in small pores or narrow channels, and chemical filtration, where colloids become chemically attached to fracture or pore surfaces.

Colloids may have either beneficial or detrimental effects on repository performance. In particular, effects would be beneficial if radionuclides become irreversibly bound to colloids that are later immobilised, e.g. by filtration. The effects would be detrimental if radionuclide-bearing colloids are mobile, and are excluded from matrix pores. In general, it can be stated that colloid facilitated transport may be important and detrimental to performance if the following conditions are met (Chapman *et al*. ,1993).

1. There is a large population of colloids occurring naturally in groundwater or arising from the presence of the repository.
2. Fracture apertures and other pore spaces conducting flowing groundwater are sufficiently large to allow colloids to pass without significant physical or chemical filtration.
3. The groundwater chemistry is conducive to colloid stability.
4. Radionuclide sorption on colloids is favoured by electrostatic attraction and groundwater chemistry
5. Desorption processes are irreversible, or at least slow relative to transport times through the geosphere.This combination of conditions is illustrated schematically in Fig. 1.2. As pointed out in Gardiner *et al*. (2001), no chemical process, such as the sorption of radionuclides by colloids, is strictly speaking irreversible. The key issue here is whether the process is reversible over the timescales of interest in safety assessment.

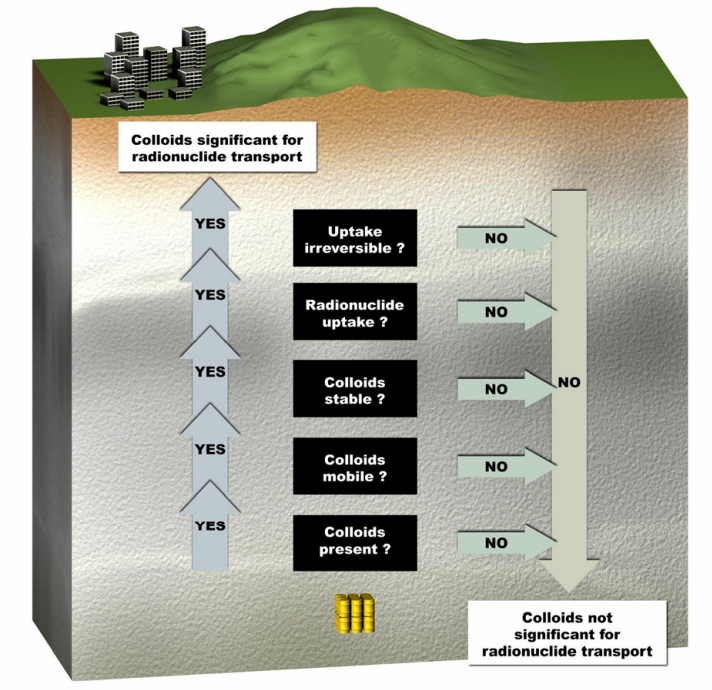

Fig. 1.2: The "colloid ladder", which indicates when colloid facilitated radionuclide transport is likely to become relevant to the long-term safety of a deep geological repository (after Chapman et al. 1993).

1.3 Concept of the CRR project

The general conceptual model behind the *in situ* experiment assumes that radionuclides released from the bentonite become associated with bentonite colloids, produced by erosion at the near-field/far field interface. These colloid-associated radionuclides then pass through the bentonite porewater/groundwater mixing zone and are released into a water-conducting feature where they are expected to be transported in the natural groundwater. The specific concept of the experiment in the GTS is shown in Figure 1.3 where the FEBEX[5]/Grimsel granodiorite interface is assumed with the CRR experiment beginning in the Grimsel groundwater, immediately after the mixing zone.

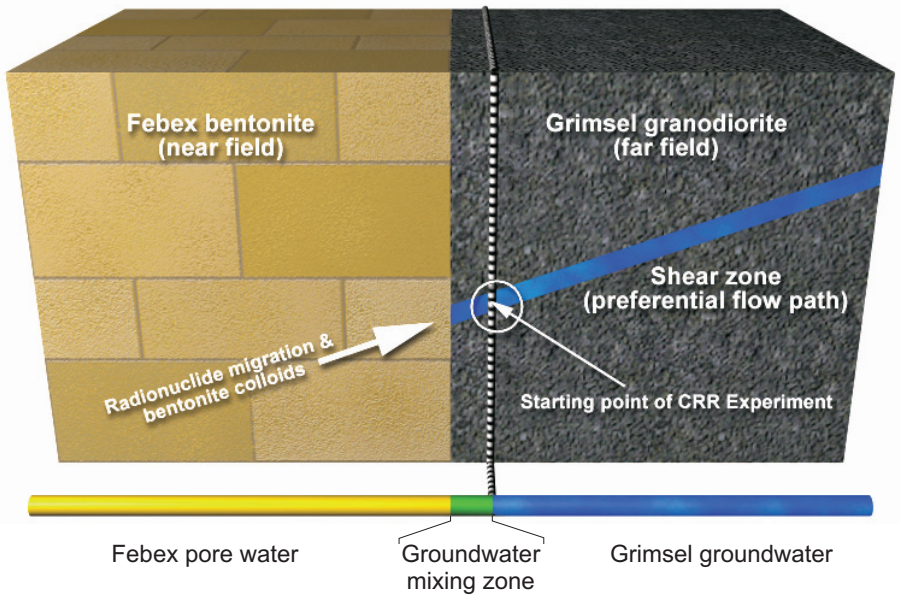

Fig. 1.3: Conceptual model of the CRR experiment

One of the key issues of the project was to ensure that the results of this highly complex field experiment will be of widespread use, in particular for PA. Therefore it is very important to carefully design the *in situ* experiment in such a way as to minimise experimental artifacts as much as possible. Moreover, in such an *in situ* experiment, where actinides and bentonite colloids are used in combination with the natural GTS groundwater, the chemical and hydraulical experimental conditions have to be optimised as far as possible. However, the final layout of this experiment naturally consisted of several compromises which have to be taken into account in the final discussion and interpretation of the experiment (discussed further below).

[5] FEBEX = Full-scale Engineered Barrier Experiment – see Huertas et al. (2000) for details.

1.4 Project overview

1.4.1 Tasks and time schedule

The CRR experiment was divided into two main Phases, each containing several tasks:

- Phase I, in which the feasibility of conducting *in situ* tracer tests was examined, site characterisation, scoping calculations on radionuclide solubility limits and radioprotection requirements, a preparatory laboratory programme and predictive transport modelling, and
- Phase 2, which consisted of the tests themselves, various supporting field and laboratory studies, further transport modelling and final reporting.

The time schedules for these various tasks are summarised in Tab. 1.1.

Tab. 1.1: Major tasks and time schedule of the CRR project

Phase	Task	1998		1999		2000		2001		2002		2003	
Phase 1 Feasibility	Site characterisation												
	Preliminary calculations												
	Preparatory laboratory programme												
	Predictive transport modelling												
Phase 2 In situ experiment	Preparatory colloid and homologue tests												
	Field experiment												
	Natural colloid background study												
	Supporting laboratory programme												
	Transport modelling												
	Final reporting												

1.4.2 The *in situ* tracer tests

The *in situ* tracer tests are reported in detail in this report. The tests were conducted in four different artificial asymmetric dipole flow fields in the shear zone, established by pumping water into one borehole (the injection borehole) and withdrawing water at a higher rate at a second borehole (the extraction borehole).

In preparation for CRR, three new 86mm diameter boreholes (BOCR 99.001, 99.002 and 00.003) were drilled almost perpendicular to the experimental shear zone and equipped with triple packer systems. Other boreholes (BOMI 86.004, 86.005, 87.007, 87.008, 87.010 and 87.011) were already available from the earlier GTS Migration Experiment (MI) conducted in the same shear zone (see Frick et al., 1992, for details). Fig. 1.4 gives an overview of the boreholes and the different flow fields that were established between the packed off intervals (black arrows). In each dipole, the direction of water flow was towards the gallery, thus coinciding with the unperturbed groundwater flow direction.

In the tracer tests test, once the flow field had been established, individual tracers or tracer cocktails were injected at the injection borehole, and the resulting breakthrough curves measured at the withdrawal borehole. An overview of the tracer tests is given in Table 1.2.

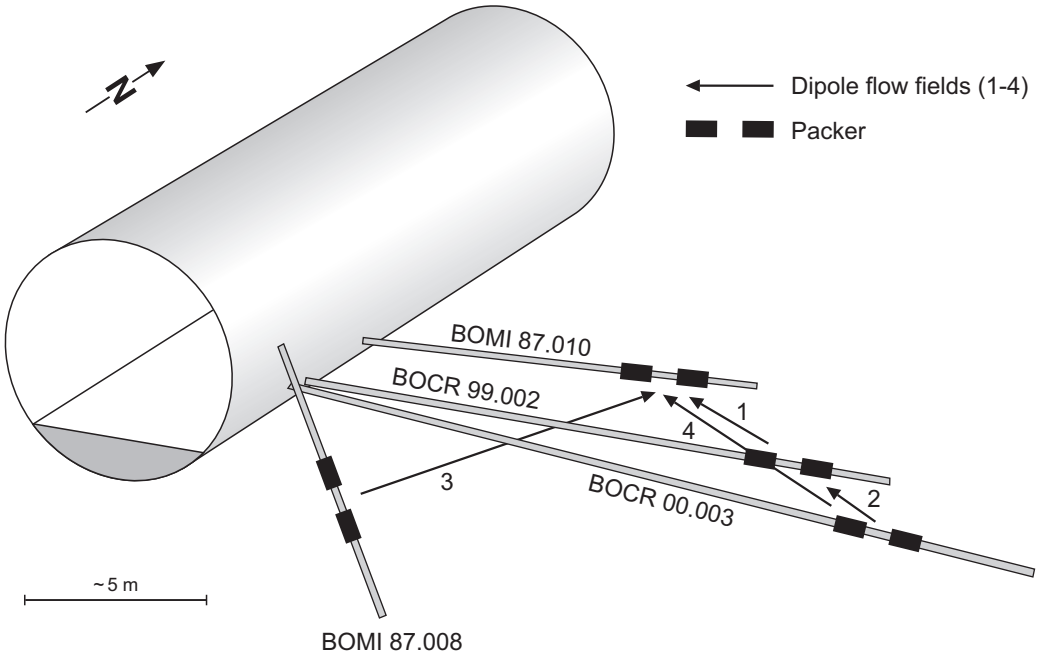

Fig. 1.4: 3D view of the CRR test site, viewed perpendicular to the experimental shear zone

Tab. 1.2: List of dipoles with corresponding boreholes, experimental runs and tracers used

Dipole	**Length** [m]	**Injection/ extraction borehole**	**Flow rates (in/out)** [mL min^{-1}]	**Number of run where this dipole was tested and type of tracer composition**
D-1	2.23	CRR 99.002 /BOMI 87.010	08/120 06/160 08/213 10/150 10/150 10/150 10/150 10/150 10/150 10/150	run #1, uranine run #2, uranine run #3, uranine run #13, uranine run #14, homologues run #21, uranine, ^{85}Sr & ^{82}Br run #28 to 30, uranine, ^{131}I run #31, RN cocktail run #32, RN cocktail & colloids run #33 to 35 uranine, ^{131}I
D-2	1.71	CRR 00.003 /CRR 99.002	10/150 05/075 10/150 10/150 10/150	run #4, uranine run #5, uranine run #9, uranine run #10, homologues run #11, uranine
D-3	5.25	BOMI 87.008 /BOMI 87.010	10/150 10/150 10/150 10/150 10/150 10/150	run #6 & 7, uranine run #6a, bentonite colloid injection run #7a, bentonite colloid injection with homologues run #8, uranine run #15, homologues run #16, uranine
D-4	3.94	CRR 00.003 /BOMI 87.010	10/150	run #12, uranine

Tests using the conservative (non-sorbing) tracer uranine were performed in order to calibrate hydraulic models of flow within the dipoles and to optimise the flow conditions so that a recovery close to 100 % was achieved. ^{129}I was added to the uranine tracer cocktails in order to test whether it was suitable to use as a conservative tracer in later, more complex tests. Two main tracer tests were carried out in dipole 1 with a suite of different radionuclides. These were:

- run #31, in which ^{243}Am, ^{237}Np, ^{242}Pu, ^{238}Pu, ^{238}U, ^{85}Sr, ^{131}I and ^{232}Th were injected in the absence of bentonite colloids and
- run #32, in which ^{241}Am, ^{237}Np, ^{244}Pu, ^{238}Pu, ^{233}U, ^{99}Tc, ^{137}Cs, ^{85}Sr, ^{131}I and ^{232}Th were injected in the presence of 20 mgL^{-1} of bentonite colloids.

1.4.3 Supporting field and laboratory studies

In addition to the *in situ* experiment, a series of supporting field and laboratory experiments and theoretical studies was carried out, addressing, most notably:

- the hydraulic characteristics of the experimental shear zone were further defined and the new data were combined with existing information on the site to develop an updated hydraulic model
- a study of the natural colloid background in the experimental shear zone (and several other sites in the GTS) showed that levels were generally low and stable over time but the populations varied from one site to another.
- bentonite colloid migration tests in the experimental shear zone provided information on filtration/retardation of various sizes of colloids
- calculated tracer solubilities in Grimsel groundwater provided reasonable boundary conditions with which to plan the *in situ* studies
- laboratory studies of radionuclide solubilities in Grimsel groundwater and bentonite porewater indicated some differences from the above calculations which allowed fine-tuning of the *in situ* experiment
- laboratory studies on bentonite erosion processes clearly showed the potential for colloid production at the bentonite/far-field interface
- laboratory studies of colloid stability in Grimsel groundwater and bentonite porewater indicated very high stability in the groundwater and complete instability in the bentonite porewaters
- sorption on shear zone materials (Grimsel granodiorite and fracture filling material) and on bentonite colloids provided data for predicting the outcome of the *in situ* tests and gave some indication of (at least short-term) irreversibility of sorption

All of this work is reported in detail here and in Missana and Geckeis (2004).

1.4.4 Modelling

The aim of the modelling work carried out in support of CRR was to develop understanding of the structures and processes affecting tracer breakthrough by constructing numerical models, and comparing their output with the results of the *in situ* tests. This work is the focus of the report by Guimera et al. (2004).

The models and parameter values used were, to some extent, constrained by field observations and supporting laboratory work conducted as part of CRR, as well as wider experience from the earlier MI and Excavation Experiment (EP) at the GTS and other relevant work conducted internationally. Uncertainties were, however, such that various alternative conceptualisations were possible, some of which were explored in the CRR modelling work.

Models were developed and applied by four modelling teams and two teams carried out predictive modelling in advance of the main experimental runs #31 and #32 in order to test the models and to aid in the planning of the experiments. Most of the modelling was, however, carried out after the main runs and involved a degree of inverse modelling, whereby parameter values are adjusted until the closest possible fit is obtained to the measured breakthrough curves.

1.5 Reporting

The raw data are reported in a series of unpublished Nagra internal reports and are referenced in the corresponding sections below. Publications which have been produced as part of the CRR project to date are:

C. BIGGIN, A. MOERI, W.R. ALEXANDER, K. OTA, B. FRIEG, W. KICKMAIER and I.G. McKINLEY (2002): *In situ* radionuclide retardation in groundwater conducting systems: overview of the research carried out at Nagra's Grimsel Test site, central Switzerland. Pp207-228 *in* Environmental radiochemical Analysis II (*ed* P.Warwick), RSC, London.

J. GUIMERÀ, L. DURO & J. BRUNO (2000): Radionuclide field tests in a single fracture. Proc. Int. Conf. on tracers and modelling in hydrogeology; Liège, Belgium (Dassargues, Ed); IAHS Pub. 262, 309-314.

W. HAUSER, H. GECKEIS, J.I. KIM and T. FIERZ (2002): A mobile laser-induced break-down detection system and its application for the *in situ*-monitoring of colloid migration. Coll. Surf. A, 203, 37-45.

T. MISSANA & A. ADEL (2000): On the applicability of DLVO theory to the prediction of clay colloids stability. J. Coll. Interface Sci., 230, 150-156.

T. MISSANA, U. ALONSO & M.J. TURRERO (2003a): Generation and stability of bentonite colloids at the bentonite/granite interface of a deep geological radioactive waste repository. J. Contam. Hydrol. (*in press*).

T. MISSANA, M. GARCIA-GUTIERREZ & U. ALONSO (2003b): Kinetics and irreversibility of Caesium and Uranium sorption onto bentonite colloids. Appl. Clay Sci. (*in press*).

A. MOERI, W.R. ALEXANDER, H. GECKEIS, W: HAUSER, TH. SCHÄFER, J. EIKEN-BERG, T. FIERZ, C. DEGUELDRE and T. MISSANA (2002): The Colloid and Radio-nuclide Retardation experiment (CRR) at the Grimsel Test Site: influence of bentonite colloids on radionuclide migration in a fractured rock. Coll. Surf. A, 217, 33-47.

A. PUDEWILLS, W. HAUSER, H. GECKEIS (2002): Numerical modelling of flow and transport phenomena in fractured crystalline rock. Proceedings of 2nd Biot Conf.on Poromechanics, Grenoble, F, August 26-28, 2002, *eds* J.-L. Auriault et al., A.A. Balkema; 527-532.

G. KOSAKOWSKI & P. A. SMITH (2004): Modelling the transport of solutes and colloids in a water conducting shear zone in the Grimsel Test Site. Nagra Technical Report NTB 04-01. Nagra, Wettingen, Switzerland.

This report is the first of a quadruplet of final project reports that summarise the findings of the CRR project:

A. MOERI (*ed*) (2004): The CRR final project report series: I - description of the field phase - methodologies and raw data. Nagra Technical Report NTB 03-01, Nagra, Wettingen, Switzerland.

T. MISSANA & H. GECKEIS (*eds*) (2004): The CRR final project report series: II - results of the supporting laboratory programme. Nagra Technical Report NTB 03-02, Nagra, Wettingen, Switzerland.

J. GUIMERA, G. KOSAKOWSKI, K. IIJIMA, A. PUDEWILLS & P. A. SMITH (2004): The CRR final project report series: III - results of the supporting modelling programme. Nagra Technical Report NTB 03-03, Nagra, Wettingen, Switzerland.

W.R. ALEXANDER, A. MOERI & P.A. SMITH (2004): The CRR final project report series: IV – project overview and synthesis of results. Nagra Technical Report NTB 03-04, Nagra, Wettingen, Switzerland.

1.6 Structure and objectives of this report

This report presents the results and conclusions of the different field activities which were carried out at the Grimsel Test Site between 1998 and 2003.

Chapter 1 provides an overview to the background and concept of the project.

Chapter 2 contains a description of the test site and the experimental shear zone, the bore-holes and dipoles as well as the layout for the hydro- and tracer testing.

Chapter 3 summarises the results of the dipole selection procedure, the natural colloid back-ground study and of the preparatory tracer tests which were carried out with homologues and bentonite colloids in order to ascertain the feasibility of the final tracer tests.

Chapter 4 contains the results of the final actinide tracer tests and the supporting uranine and iodine tracer tests. The influence of bentonite colloids on the migration behaviour of selected actinides will be discussed under the given test prerequisites.

Chapter 5 gives a summary of the field results and draws conclusions on the *in situ* experiments.

2 Experiment overview

A. Möri, Th. Fierz, H. Geckeis, J. Eikenberg, Th. Schaefer, W. Hauser and F. Geyer

2.1 Site description and geological overview

The CRR *in situ* experiments were carried out at Nagra's underground rock laboratory, the GTS, which is located at about 1730 m above sea level under a ~450 m thick overburden of crystalline rock (Grimsel granodiorite and granite). The experimental shear zone which was selected for the CRR dipole experiment is located at the former MI (Migration Experiment) site at tunnel position AU 96. This shear zone is well characterised due to preceding experiments such as MI and the EP (Excavation Project) and details are provided in Frick et al. (1992), Möri et al. (2004) and Smith et al. (2001).

The host rock of the experimental shear zone is the Grimsel granodiorite, which is a medium to coarse grained crystalline rock transected by a series of shear zones and scattered lamprophyric and aplitic dykes. The granodiorite consists mainly of 28 vol% quartz, 29 vol% plagioclase, 24 vol% potassium feldspar and 18 vol% sheet silicates (biotite, muscovite and chlorite).

Early ductile structures (mylonites) have been overprinted by brittle deformation, which is characterised by destruction of the mylonitic fabric followed by brecciation of the material. The thickness of fault breccia horizons range from a few mm to 1 cm. Brittle deformation led to the formation of fault gouge within the shear zones and preferential flow paths were created within these horizons. Fault gouge porosity is in the range of 10 to 40% and the mineralogy does not significantly differ from the mylonitic composition (albite ca. 28 vol%) although the biotite content (41 vol%) is increased compared to the mylonite and the clay content in the fault gouge ranges from 0 to 1 vol%.

The experimental shear zone itself is largely described in Bossart & Mazurek (1991), Möri & Adler (2001) and in Möri et al. (2004) and is characterised as a WSW-ENE striking, steeply dipping (to the SSE) cleavage-parallel plane. The original shear direction was sub-vertical, parallel to the mineral stretching lineation with a minimum value for shear displacement of 3 m. The thickness of the experimental shear zone varies between 0.15 and 0.90 m.

2.2 Boreholes and dipoles

Three new 86 mm outer diameter boreholes labelled BOCR 99.001[6], 99.002 and 00.003 were drilled in the frame of the CRR project from the AU gallery into the experimental shear zone. Together with the existing boreholes BOMI 86.004, 86.005, 87.007, 87.008, 87.010 and 87.011 from the former MI experiment, they provided various possibilities for new dipole configurations. Figure 1.4 gives an overview of the boreholes tested in CRR and the different dipole flow fields which were established between the packed off intervals (black arrows). Table 2.1 provides the relevant technical data for the boreholes.

The orientation of the boreholes was almost perpendicular to the experimental shear zone. In order to minimise any effects of the gallery (such as the excavation disturbed zone, high hydraulic gradients, oxidation or desaturation phenomena) on the flow fields, it was a primary requirement that the intersection points of the boreholes with the experimental shear zone had,

[6] Abandoned after about 3.5 m due to a broken drill crown.

within operational requirements, to be as far as possible from the tunnel surface. The perpendicular distance between the shear zone intersection points of boreholes BOCR 99.002, BOCR 00.003, BOMI 87.008 and BOMI 87.010 and the tunnel surface was 5.08 m, 6.78 m, 2.85 m and 2.91 m respectively.

Tab. 2.1: Borehole technical data

Borehole	**Start** Y X Z a.s.l.	**End** Y X Z a.s.l.	**Depth** [m]	**Diameter** (o.d.) [mm]	**Distance to shear zone** [m]	**Shear zone interval** [m]	**Azimuth of dip** [°]	**Dip** [(2)] **angle** [°]
BOCR 99.001[(1)]	667473.782 158964.093 1732.038	667474.623 158967.316 1731.031	3.48	86	---	---	14.62	-16.82
BOCR 99.002	667473.623 158965.350 1731.985	667477.029 158975.665 1728.002	11.57	86	9.55	9.32 - 9.85	18.27	-20.14
BOCR 00.003	667473.831 158964.576 1732.196	667478.775 158976.943 1726.463	14.50	86	11.43	11.00 - 11.70	21.79	-23.29
BOMI 86.004	667466.958 158984.015 1732.179	667464.040 158960.696 1726.840	24.10	86	20.65	20.59 - 20.85	187.13	-12.80
BOMI 86.005	667470.826 158981.991 1732.107	667480.932 158970.325 1727.817	16.02	86	10.35	10.22 - 10.58	139.10	-15.53
BOMI 87.007	667471.126 158957.668 1732.456	667465.419 158969.525 1727.886	13.93	86	10.64	10.58 - 10.80	334.30	-19.15
BOMI 87.008	667471.068 158968.246 1731.244	667471.133 158970.862 1726.090	5.78	86	3.34	2.21 - 3.34	1.42	-63.08
BOMI 87.010	667473.529 158966.990 1732.116	667475.140 158974.907 1729.347	8.54	86	6.59	5.06 - 6.63	11.50	-18.92
BOMI 87.011	667471.247 158953.767 1733.260	667452.897 158964.778 1738.142	21.95	86	18.27	18.20 - 19.47	300.97	12.85

[(1)] BOCR 99.001 was abandoned due to a broken drilling crown
[(2)] negative values indicate descending boreholes

The geometry of the resulting dipole flow fields was also designed so as to allow the potential excavation of the dipole flow fields by overcoring of the experimental shear zone from the tunnel surface (*cf* Möri et al., 2004). The reason for this requirement is two fold: first, it is of great interest to know the retardation sites of the injected radionuclides and, if possible, also of colloids along their flow paths and, second, it was a radioprotection licensing requirement that recovery of any contaminated rock material would be technically possible if necessary – in this case, by simple overcoring. Thus the potential test dipoles (see dipoles 1, 2 and 4 in Figure 1.4) were oriented perpendicular to the tunnels to simplify potential overcoring (see comments in Alexander et al., 2003).

The boreholes were equipped with triple packer systems, which contain pressure and flow lines in each interval. Table 2.2 gives an overview of the dipoles, the applied flow rates during tracer testing and the tracers employed in the different tracer tests. Dipoles 1 and 2 have lengths of 2.23 and 1.71 respectively, whereas dipole 4 is a combination of both dipoles and has a total length of 3.94 m. Dipole 3 shows an orientation almost parallel to the gallery and was previously used in former MI experiments. This longer dipole (5.25 m) was only used during the preparatory tracer tests with homologues and colloids as it was not intended to use this dipole for the final actinide runs where cross-contamination of the dipole with bentonite colloids from other tests had to be avoided.

Tab. 2.2: List of dipoles with corresponding boreholes, experimental runs and tracers used

Dipole	**Length** [m]	**Injection/extraction borehole**	**Flow rates (in/out)** [mL min^{-1}]	**Number of run where this dipole was tested and type of tracer composition**
D-1	2.23	CRR 99.002/ BOMI 87.010	08/120	run #1, uranine
			06/160	run #2, uranine
			08/213	run #3, uranine
			10/150	run #13, uranine
			10/150	run #14, homologues
			10/150	run #21, uranine, ^{85}Sr & ^{82}Br
			10/150	run #28 to 30, uranine, ^{131}I
			10/150	run #31, radionuclide cocktail
			10/150	run #32, radionuclide cocktail & colloids
			10/150	run #33 to 35 uranine, ^{131}I
D-2	1.71	CRR 00.003/ CRR 99.002	10/150	run #4, uranine
			05/075	run #5, uranine
			10/150	run #9, uranine
			10/150	run #10, homologues
			10/150	run #11, uranine
D-3	5.25	BOMI 87.008/ BOMI 87.010	10/150	run #6 & 7, uranine
			10/150	run #6a, bentonite colloid injection
			10/150	run #7a, bentonite colloid injection with homologues
			10/150	run #8, uranine
			10/150	run #15, homologues
			10/150	run #16, uranine
D-4	3.94	CRR 00.003/ BOMI 87.010	10/150	run #12, uranine

2.3 Tracers and tracer cocktails

27 tracer tests were performed in the frame of CRR project within the four dipoles (see Table 2.3; for more details see Fierz et al., 2001 and Geckeis et al., 2003a,b).

Tracer tests with the conservatively transported dye, uranine, were performed in all four CRR test dipoles in order to calibrate the hydraulic models and to optimise the dipole flow conditions to achieve 100% recovery of a conservative tracer at maximum residence times of the tracer in the experimental shear zone (requested by the regulator in the licence for the active tracer tests). At a later date, the two active conservative tracers ^{131}I and ^{82}Br were added to the uranine tracer cocktails as it was intended to substitute uranine in the final tracer injections by bromine or

iodine because of the possibility of interference (it was suspected that the large uranine organic molecules would build complexes with the strongly sorbing actinides). The disadvantage of this substitution was that the downhole measured input function can only be determined from the uranine (via a downhole fluorescence measuring system, for details see Frick et al., 1992). Therefore several tracer tests with uranine and ^{131}I were made before, between and after the actinide injections in order to check the stability of the input functions during the main tests.

Preparatory tracer tests with ^{159}Tb, ^{178}Hf and ^{232}Th as homologues for the tri- and tetravalent actinides were performed to test the *in situ* applicability of these homologues. Further on, these data provided an additional dataset of tracer breakthrough curves for predictive modelling of the behaviour of the actinides in the dipole experiments, both in presence and absence of bentonite colloids. Homologues were injected in dipoles 1, 2 and 3 whereas all preparatory tests with bentonite colloids took place in dipole 3, which was never intended to be used for the final tracer tests.

Tab. 2.3: Overview of tracer cocktails

Run	Date	Dipole	Tracer	M_0 [mg or Bq]	C_0 [Bq mL^{-1} or mg mL^{-1}]
#1	14.09.1999	1	uranine	2.31E+02 mg	1.00E+01 mg mL^{-1}
#2	22.09.1999	1	uranine	3.37E-01 mg	1.00E-02 mg mL^{-1}
#3	27.10.1999	1	uranine	3.25E-01 mg	1.00E-02 mg mL^{-1}
#4	04.07.2000	2	uranine	3.01E+00 mg	1.00E-01 mg mL^{-1}
#5	12.07.2000	2	uranine	1.51E+00 mg	1.00E-01 mg mL^{-1}
#6	22.08.2000	3	uranine	3.96E-01 mg	1.00E-02 mg mL^{-1}
#6a	23.08.2000	3	colloids	2.04E+00 mg	2.00E-02 mg mL^{-1}
#7	23.08.2000	3	uranine	1.96E+00 mg	1.00E-01 mg mL^{-1}
#7a	25.08.2000	3	colloids	1.65E+00 mg	2.00E-02 mg mL^{-1}
			^{232}Th	2.52E-03 mg	3.00E-05 mg mL^{-1}
			^{178}Hf	2.14E-03 mg	2.60E-05 mg mL^{-1}
			^{159}Tb	2.32E-03 mg	2.80E-05 mg mL^{-1}
#8	25.08.2000	3	uranine	2.00E+00 mg	1.00E-01 mg mL^{-1}
#9	07.11.2000	2	uranine	9.19E-01 mg	1.00E-02 mg mL^{-1}
#10	07.11.2000	2	^{232}Th	6.78E-05 mg	9.20E-07 mg mL^{-1}
			^{178}Hf	6.63E-05 mg	9.00E-07 mg mL^{-1}
			^{159}Tb	8.02E-05 mg	1.10E-06 mg mL^{-1}
#11	07.11.2000	2	uranine	7.00E-01 mg	1.00E-02 mg mL^{-1}
#12	16.01.2001	4	uranine	1.00E+00 mg	1.00E-02 mg mL^{-1}
#13	23.01.2001	1	uranine	1.00E+00 mg	1.00E-02 mg mL^{-1}
#14	25.01.2001	1	^{232}Th	1.84E-04 mg	2.10E-06 mg mL^{-1}
			^{178}Hf	2.01E-04 mg	2.30E-06 mg mL^{-1}
			^{159}Tb	1.77E-04 mg	2.00E-06 mg mL^{-1}
#15	26.01.2001	3	^{232}Th	1.94E-04 mg	2.10E-06 mg mL^{-1}
			^{178}Hf	1.85E-04 mg	2.00E-06 mg mL^{-1}
			^{159}Tb	1.57E-04 mg	1.70E-06 mg mL^{-1}

The main tracer tests with the actinides were carried out in dipole 1 with a suite of radionuclides. It was agreed that the injection should be performed in two different runs: a first run

containing a cocktail of radionuclides and a second run containing a cocktail very similar to the first injection, but also containing bentonite colloids. The reason to perform the injection with the bentonite colloids after the injection of the pure radionuclide cocktail, was to avoid any disturbances of the original flow field. For example, due to possible colloid retention within the flow field that could affect the behaviour of the radionuclides injected afterwards. Different isotopes of the same element (see Table 2.3) were used in the different runs so that, following any excavation of the site, differing retardation behaviour in the run with and the run without bentonite could be easily ascertained.

Tab. 2.3: Overview of tracer cocktails (*cont.)*

Run	**Date**	**Dipole**	**Tracer**	**M_0** [mg or Bq]	**C_0** [Bq mL^{-1} or mg mL^{-1}]
#16	26.01.2001	3	uranine	8.00E+00 mg	1.00E-01 mg mL^{-1}
#21	03.07.2001	1	uranine	1.00E+00 mg	1.00E-02 mg mL^{-1}
			^{82}Br	1.12E+05 Bq	1.12E+03 Bq mL^{-1}
			^{85}Sr	1.05E+05 Bq	1.05E+03 Bq mL^{-1}
#28	16.01.2002	1	uranine	4.93E-02 mg	4.92E-04 mg mL^{-1}
			^{131}I	6.55E+04 Bq	6.53E+02 Bq mL^{-1}
#29	17.01.2002	1	uranine	4.93E-02 mg	4.92E-04 mg mL^{-1}
			^{131}I	6.68E+04 Bq	6.67E+02 Bq mL^{-1}
#30	17.01.2002	1	uranine	4.93E-02 mg	4.92E-04 mg mL^{-1}
			^{131}I	7.20E+04 Bq	7.19E+02 Bq mL^{-1}
#31	23.01.2002	1	^{243}Am	1.08E+03 Bq	1.06E+01 Bq mL^{-1}
			^{237}Np	5.91E+02 Bq	5.82E+00 Bq mL^{-1}
			^{242}Pu	3.55E+01 Bq	3.50E-01 Bq mL^{-1}
			^{238}Pu	6.80E+02 Bq	6.70E+00 Bq mL^{-1}
			^{238}U	2.86E-01 Bq	2.82E-03 Bq mL^{-1}
			^{85}Sr	9.65E+04 Bq	9.52E+02 Bq mL^{-1}
			^{131}I	7.57E+04 Bq	7.46E+02 Bq mL^{-1}
			^{232}Th	1.07E-03 Bq	1.06E-05 Bq mL^{-1}
#32	19.02.2002	1	^{241}Am	2.05E+03 Bq	2.04E+01 Bq mL^{-1}
			^{237}Np	6.74E+02 Bq	6.72E+00 Bq mL^{-1}
			^{244}Pu	1.12E-01 Bq	1.11E-03 Bq mL^{-1}
			^{238}Pu	7.22E+02 Bq	7.20E+00 Bq mL^{-1}
			^{233}U	7.24E+03 Bq	7.22E+01 Bq mL^{-1}
			^{99}Tc	6.57E+01 Bq	6.55E-01 Bq mL^{-1}
			^{137}Cs	6.09E+05 Bq	6.07E+03 Bq mL^{-1}
			^{85}Sr	8.26E+04 Bq	8.24E+02 Bq mL^{-1}
			^{131}I	5.58E+04 Bq	5.56E+02 Bq mL^{-1}
			^{232}Th	1.03E-03 Bq	1.03E-05 Bq mL^{-1}
			colloids	2.01E+00 mg	2.00E-02 mg mL^{-1}
#33	06.02.2002	1	uranine	4.63E-01 mg	4.63E-03 mg mL^{-1}
			^{131}I	6.61E+04 Bq	6.61E+02 Bq mL^{-1}
#34	20.02.2002	1	uranine	4.97E-01 mg	4.95E-03 mg mL^{-1}
			^{131}I	6.67E+04 Bq	6.65E+02 Bq mL^{-1}
#35	27.02.2002	1	uranine	4.98E-01 mg	4.98E-03 mg mL^{-1}
			^{131}I	6.75E+04 Bq	6.75E+02 Bq mL^{-1}

2.3.1 Composition of main tracer cocktails

Initial project discussions focussed on the definition of the suite of safety relevant radionuclides to be utilised in the experiment. Further discussions included aspects such as the radionuclide concentration in the cocktail, type and concentration of colloids, the moment the bentonite colloids should be injected (before, after or simultaneously with the radionuclides) and the chemical and physical conditions under which the cocktail should be prepared and injected.

The radionuclides of relevance to HLW/SF repositories vary slightly from national programme to national programme depending on the waste mix, repository design and host rock type (for an overview, see Neall & Smith, 2004).The list includes activation/fission products (*eg* Ni, Se, Zr, Tc, Pd, Sn and Cs) as well as members of different actinide chains (*eg* Np, U, Pu and Th). In addition, due to a wide range of experimental constraints, PA relevant radionuclides might be replaced by shorter-lived isotopes of the same element or by elements which behave in a very similar fashion but which are more amenable to the available spectrometric methods *etc*.

The selection of the radionuclides for CRR was therefore a compromise between the PA wishes of the project partners and experimental requirements and some of the points considered are listed here:

- Release of oxidised species: this scenario is based on the assumption that open fractures are produced within the bentonite barrier due to the formation of gas pressure from waste corrosion. This scenario could lead to enhanced and fast nuclide transport through the bentonite where the nuclide species from the waste could arrive at the EBS/geosphere interface in an oxidised status (due to near-field radiolysis reactions).
- Reduced species: numerous PA studies assume that any gas channels in the bentonite would immediately close due to bentonite self-healing properties. The nuclides would then be reduced by the *in situ* conditions in the EBS, be transported by diffusion through the bentonite and would finally enter the geosphere in a reduced state.

The laboratory results and the reasoning for the selection of the above mentioned radionuclides and their appropriate *in situ* oxidation states are outlined in detail in the CRR laboratory report (Missana et al. 2004). However, the final tracer cocktail reflects compromises between safety relevance of the selected radionuclides, PA wishes of the project partners, the different release scenarios (oxidation states), technical feasibility and radioprotection. Therefore, results obtained by such studies have to be carefully reviewed and possible artefacts due to the layout of the experiment have to be addressed and taken into account before any conclusions are drawn..

The radionuclides that were selected at the end of the tracer evaluation were:

- ^{243}Am, ^{237}Np, ^{242}Pu, ^{238}Pu, ^{238}U, ^{85}Sr, ^{131}I and ^{232}Th for the first run in the absence of bentonite colloids and
- ^{241}Am, ^{237}Np, ^{244}Pu, ^{238}Pu, ^{233}U, ^{99}Tc, ^{137}Cs, ^{85}Sr, ^{131}I and ^{232}Th for the second run in the presence of 20 mgL^{-1} of bentonite colloids.

2.3.2 Radionuclide solubility

The likely solubilities of selected radionuclides in GTS groundwater were calculated during the feasibility phase of the experiment (see also comments in the preceding chapters). The solubility and speciation with the correspondent predominance diagrams for each nuclide shown below are reported in Duro (2000).

Table 2.4 summarises the calculated solubilities and the selected input concentrations (M_0) for the radioactive tracer cocktails which were injected. The applied concentrations for a particular element may differ between the two runs because of the presence of bentonite colloids in run #32 which takes into account that the "apparent" solubility of most of the radionuclides increases due to the formation of heterogeneous radiocolloids (radionuclides attached to bentonite colloids) as confirmed by various laboratory experiments (Missana & Geckeis, 2004). The concentrations of ^{232}Th, ^{99}Tc, and $^{238/242/244}$Pu in the tracer cocktail are limited by their solubility in the GTS groundwater. In the case of ^{85}Sr, $^{241/243}$Am and ^{137}Cs, the concentration utilised is not a reflection of solubility control, rather it is defined by the maximum permitted activity of these radionuclides at the site[7].

Tab. 2.4: Solubility values, solid phases and oxidation states of the relevant radionuclides.

Nuclide	Calculations			*In situ* experiment		
	Solid phase	**Oxidation state**	**Calculated solubility M** [molL^{-1}]	**Assumed oxidation state**	**Run #31: input concentration M_0** [molL^{-1}]	**Run #32: input concentration M_0** [molL^{-1}]
Tc	(TcO_2)	IV	10^{-8}	IV	---	^{99}Tc: 1.0E-08
Am	($AmOHCO_3$(am))	III	10^{-7}	III	^{243}Am: 5.9E-09	^{241}Am: 6.6E-10
Th	($Th(OH)_4$(am))	IV	10^{-8}	IV	^{232}Th: 1.1E-08	^{232}Th: 1.1E-08
U	U(IV)solids U(VI)solids	IV VI	10^{-8} 10^{-4}	VI	^{238}U: 9.5E-07	^{233}U: 8.7E-07
Np	($Np(OH)_4$(am)) $Np(V)O_2(OH)$	IV V	10^{-8} 10^{-4}	V	^{237}Np: 9.4E-07	^{237}Np: 1.1E-06
Pu	($Pu(OH)_4$(am))	IV	10^{-10}	IV	^{238}Pu: 4.4E-11 ^{242}Pu: 9.9E-09	^{238}Pu: 4.8E-11 ^{244}Pu: 6.7E-09

2.3.3 Bentonite colloids

The FEBEX bentonite colloids that were used in the CRR experiments are characterised in detail in the CRR laboratory project report (Missana et al., 2004). Based on investigations on colloids in different natural granitic groundwater and on the results from the laboratory experiments, a proposition for the bentonite colloid concentration to be used in the *in situ* experiment was made by the experimental team. The colloid concentration should be sufficiently high to influence significantly the speciation of those radionuclides that are assumed to undergo colloid formation (especially the actinides) and to allow detection by the analytical tools. In addition, the bentonite colloid cocktail in the GTS groundwater should be stable over the entire test duration (*eg* no aggregation of smaller colloid to large particles *etc*). Finally, the concentration utilised should reflect experimental data on bentonite erosion.

During the laboratory experiments, it was observed that bentonite colloid concentrations up to 1000 mgL^{-1} remained stable in suspensions in the GTS groundwater over several weeks, clearly showing that quite high concentrations of bentonite colloids can be stabilised in GTS groundwater. However, Degueldre et al. (1996) mention that, in natural granitic groundwater

[7] Higher activities (and therefore concentrations) are permissable, but only by re-licensing the site as a IAEA Level B laboratory (as was the case during the EP experiment: see Alexander et al., 1996 for details).

systems, the colloid concentrations were found to be much smaller (*eg* 0.35 ± 1.06 mgL^{-1} in the granitic bedrock in Sweden and 0.34 ± 0.34 mgL^{-1} in the Whiteshell research area in Canada). The natural colloid background in the GTS groundwater was found to be 0.005 mgL^{-1} (see section 3.2 of this report).

Further, two studies on the sorption capacity of natural and bentonite colloids in the GTS groundwater were performed by PSI and FZK (both reported in Geckeis et al., 2003a) in order to estimate whether there would be enough naturally occurring colloids or bentonite colloids in the GTS groundwater to bind all the radionuclides which will be injected. According to both studies, the calculations with bentonite colloids revealed that there could be enough sorption sites on 20 mgL^{-1} bentonite colloids to bind all the injected radionuclides. Laboratory studies performed in the frame of CRR also showed that this colloid concentration should be sufficient with regard to the available surface sites (see Missana & Geckeis., 2004).

2.4 Hydraulic testing

Constant rate injection tests with different test durations (approximately 12 seconds, 120 seconds and 2 hours) were performed prior to proceeding with the tracer tests (for details see Fisch, 2002). The aim of the hydraulic testing was to supply the hydraulic parameters necessary for designing the tracer tests and for providing input data for the hydraulic models.

The tests were carried out in the new boreholes BOCR 99.002 and BOCR 00.003. During testing, interference pressure reactions were observed in the other boreholes of the experimental shear zone which are BOMI 86.004, 86.005, 87.007, 87.008 and 87.010.

Flow was controlled using a Shimadzu HPLC-pump (range from 0 to 150 mL min^{-1}) and measured with a magnetic inductive flow meter (Fisher + Porter Instruments 0-450 mL min^{-1}). The specifications of the tested and monitored borehole intervals, along the static heads, are given in Tables 2.5 and 2.6.

Tab. 2.5: Specification of tested and monitored borehole intervals

Borehole and interval	**Interval position** [m]	**Interval length** [m]	**Nominal interval volume** [l]	**Pressure transducer offset** [1)] [kPa]	**Vertical position of transducer above tunnel floor** [m]	**Pressure transducer range** [bar]
BOCR 99.002-i2	9.30-9.70	0.40	2.3	88.7	1.62	20
BOCR 00.003-i2	11.25-11.56	0.31	1.8	82.9	1.41	20
BOMI 86.004-i2	1.50-24.07	22.57	131.1	90.3	1.26	20
BOMI 86.005-i2	9.57-11.38	1.81	10.5	85.5	1.36	20
BOMI 87.007-i1	10.05-13.93	3.88	22.5	81.3	0.96	20
BOMI 87.008-i2	1.74-3.45	1.71	9.9	84.2	0.93	20
BOMI 87.010-i2	6.40-6.80	0.4	2.3	85.8	1.62	20

[1)] Transducer signal at atmospheric pressure, measured on June 23, 2000; 13:25

Tab. 2.6: Static heads

Borehole and interval	Interval position [m]	Interval length [m]	Pressure June 29, 2000 09:20 [kPa]	Pressure Transducer Offset [kPa]	Vertical position of transducer above tunnel floor [m]	Head above tunnel floor [m]
BOCR 99.002-i2	9.30-9.70	0.40	197.7	88.7	1.62	12.73
BOCR 00.003-i2	11.25-11.56	0.31	207.1	82.9	1.41	14.07
BOMI 86.004-i2	1.50-24.07	22.57	209.8	90.3	1.26	13.44
BOMI 86.005-i2	9.57-11.38	1.81	205.3	85.5	1.36	13.57
BOMI 87.007-i1	10.05-13.93	3.88	161.7	81.3	0.96	9.16
BOMI 87.008-i2	1.74-3.45	1.71	153.9	84.2	0.93	8.03
BOMI 87.010-i2	6.40-6.80	0.4	141.9	85.8	1.62	7.34

A summary of the analysis methods applied in the CRR Project is presented in Table 2.7. Descriptions of the various test types and standard analysis techniques are given for example in Adams & Wyss (1994).

Tab. 2.7: Summary of analysis methods

Test Type	Analysis Method	Reference
Constant-rate test	Log-log diagnostics (Burden-derivative)	Bourdet et al. (1989)
Homogeneous radial flow model	Straight-line analysis (transient flow period)	Cooper & Jacob (1946)
	Type curve analysis	Gringarten, Bourdet (cited in SABET, 1991)
Constant-Rate Test Homogeneous flow model	Straight-line analysis, plotting $\Delta P/q$ versus superposition time	Birsoy & Summers (cited in Kruseman & De Ridder, 1990)
Pressure recovery after constant-head/rate tests	Diagnostics: using "equivalent time" (AGARWAL) for ΔP/derivative plots	Agarwal (1980) & Bourdet et al. (1989)
	Straight-line analysis (transient flow period)	Agarwal (1980)

2.5 Tracer testing

2.5.1 Experimental set-up

Specially designed packer systems were installed in the boreholes in such a way that the shear zone interval of the borehole was tightly sealed. The boreholes were subdivided into three intervals using a triple packer system. Intervals I-1 and I-3 were equipped with pressure measurement devices and the shear zone interval (I-2) was equipped with a pressure measurement line, a flow line and a quartz fibre pair for downhole detection of the fluorescent uranine dye. The volume of the shear zone intervals was kept as small as possible (115 mL in the injection interval and 83 mL in the extraction interval) and all parts within the interval exposed to GTS groundwater and later to the tracers were PEEK (polyether etherketone) coated in order to minimise tracer sorption on the test equipment. Experiments on actinide sorption on different types of material (stainless steel, LDPE, HPP and PFA) showed that sorption on container walls also plays an important role for tri- and tetravalent actinides and finally high-density polyethylene (HDPE) bottles were found to be appropriate for tracer storage (see below and Fierz et al., 2001 for details). However, the sorption of strongly sorbing radionuclides on the equipment can never be completely ruled out (*cf* Alexander et al., 2003) and therefore it was decided to quantify the amount of sorbed radionuclides on the equipment and the tubing after the main injections. This was achieved by washing the parts with a 2% HNO_3 solution followed by determination of the nuclide concentration in the solution.

The control units of the packer system consist of three major parts:

- The packer control unit is connected to the packer inflation lines and consists of an individual inflation port for each packer and a precise manometer for inflation pressure control.
- The flow control unit is connected to the flow lines and equipped with two-way valves for injection or withdrawal of fluid.
- The pressure control unit is connected to the pressure measurement lines. Precise manometers and pressure sensors, which are linked to the data acquisition system, enable pressure observation within the interval. Keller PAA 23 pressure sensors were used for pressure measurements.

Data acquisition was ensured by an on-site Geomonitor system which recorded flow, Eh, pH and dissolved oxygen at the injection and extraction side, pressures in all CRR and MI boreholes, the input function of the uranine and the output function of uranine and of the γ-emitting radionuclides. Pressures, flow rates and uranine input concentrations and chemical parameters (Eh, pH, and dissolved oxygen) were monitored with a sampling rate of 30 seconds during the first two hours after tracer dosage. Afterwards, the sampling rate was set to 2 minutes. The extraction uranine data were sampled every 10 seconds.

2.5.1.1 Injection side

The surface equipment consisted of several, independently functioning, devices and the precise layouts varied with respect to the precise tracer composition and to the analytical requirements (see Figure 2.1). Starting point on the injection side was always a stainless steel water storage tank in which GTS groundwater previously collected from the experimental shear zone was stored under N_2 atmosphere in order to prevent the solution becoming contaminated with O_2 and CO_2. Before being released into the injection interval, the stored GTS groundwater first passed through a filter (0.4 μm mesh size) and was then pumped with a HPLC pump (Shimadzu LC8) through pH, O_2 and Eh flow-through cells and a flow meter. All these devices were directly linked to the data acquisition system.

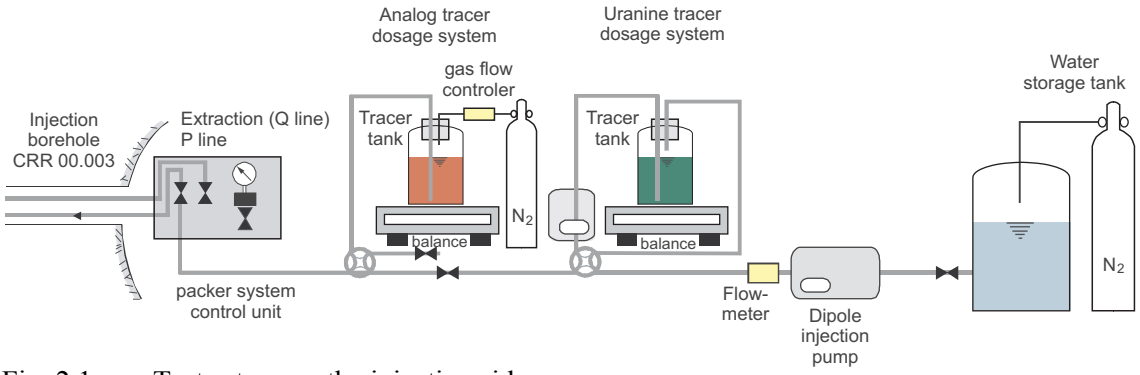

Fig. 2.1: Test set-up on the injection side

Uranine and the $^{82}Br/^{85}Sr$ tracer cocktail were injected by a tracer injection pump. The homologues and the final tracer cocktails were injected with the newly developed tracer injection system using pressurised N_2 (see also analogue tracer dosage system in Figure 2.1). The injection solutions, which were stored and transported in high-density polyethylene (HDPE) bottles and kept under an Ar-atmosphere, were directly connected to the injection flow line and the N_2 on site. By applying an appropriate injection pressure, the tracer solution was injected into the PEEK tubing of the injection line. The injection flow rate evaluated during the preparatory uranine tracer test was set to 10 mL min^{-1} and was controlled by balancing the mass loss within the HDPE bottle.

2.5.1.2 Extraction side

The extraction side consists of another HPLC pump (Labomatic), pH, O_2 and Eh flow through cells and a flow meter. When required, the following additional units could be linked to the extraction line (see also Figure 2.2 below):

- a fluorimeter flow-through cell for down-hole and in-tunnel uranine detection
- an on-line HPGe detector for the detection of γ-emitting radionuclides
- a Laser Induced Breakdown Detector (LIBD)
- a Photon Correlation Spectrometer (PCS)

The extracted water finally passed through the sampling port and any excess water was collected in the wastewater tanks for appropriate radioprotection checks and storage prior to disposal or to treatment and disposal.

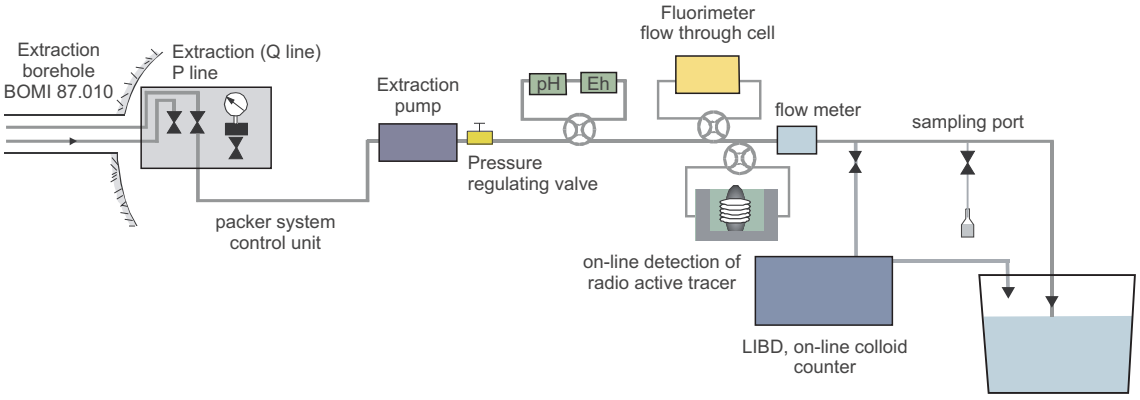

Fig. 2.2: General test set-up on the extraction side for active tracer tests

2.5.2 Sampling

During the tracer breakthrough in the two main runs, it was intended to sample almost the entire extracted groundwater. The flow at the outlet borehole was set to be 150 mL min^{-1}. From this flow 20 mL were used by the LIBD/PCS unit for on-site colloid analysis. The remaining 130 mL min^{-1} were continuously sampled by the on-site crew (see Table 2.8). Samples for α/γ-spectrometry and ICP-MS were stored in plastic bottles (HDPE) and acified with NHO_3 whereas the samples for the single particle counter were stored in glass bottles. Sampling started 15 minutes after the injection started. The first 3 hours were continuously sampled (ca. every 4 minutes at first, but at longer intervals later). Additional samples in the tail of the break-through curves were taken for RIMS (resonance ionisation mass spectrometry) analysis, performed at the Institut für Kernchemie, Universität Mainz, Germany.

Tab. 2.8: Requested samples for analysis

	α-spectrometry PSI	γ-spectrometry PSI	ICP-MS FZK	Single particle counting PSI	LIBD FZK
Requested sample volume	50 mL	50 mL	15 mL	50 mL	20 mL

2.5.3 On-site instrumentation

2.5.3.1 Uranine detection device

Uranine was analysed on-line at both the injection and the extraction side. On the injection side, the uranine input function was detected by a downhole measurement device using two optrodes which were installed in the injection interval. At the end of the extraction flow line (just after the extraction pump), the uranine breakthrough curves were recorded by a fibre optic fluori-meter.

During the CRR field campaign in 2002, the fluorimeter was tested for linearity and accuracy at different uranine concentration levels. The linearity of the measurement device was found to be better than 2% and the standard errors are listed in Table 2.9 below.

Tab. 2.9: Accuracy of uranine detection at the extraction side

Uranine concentration range [ppb]	**Standard errors** [%]
50	0.2
5	0.7
1	1.7
0.5	2.6
0.1	14
0.05	24
0.02	147

Based on the data listed in Table 2.9, an exponential error function describing the relation between measured uranine concentration and the standard error of the uranine measurement was derived. The calculated errors are composed of 3σ standard errors plus a systematic error of 2%.

2.5.3.2 On-site HPGe detector

A portable P-type co-axial, solid-state, intrinsic high purity Germanium detector was used for *in situ* γ-spectrometric measurements for the radiotracers analysed at the extraction site (water extraction line wrapped in a spiral around the detector; *cf* Frick et al., 1992). The detector employed (type X-cooler, Ortec Company) was equipped with a cryogenic cooling system, which replaced the standard liquid N_2 cooling process. The high-resolution γ-spectrometric system was connected with standard electronics (amplifier, ADC, MCA) and *in situ* γ-spectra were continuously acquired via scanning software and monitored via a PC notebook. A high counting sensitivity was achieved by a high detector efficiency of 30% (with respect to 3"x 3" NaI scintillation detectors at 1173 keV), high peak to Compton ratios (60 : 1 for ^{40}K at 1461 keV) and high peak energy resolution (full width half maximum from 1.5-2.2 keV in the range 50-2000 keV). The activities of the radionuclides were calculated using the software package "Inter-Winner 4.1" (Canberra-Eurisis). This Windows-based program uses least square algorithms for fitting of photo peaks and to resolve the peaks from background and Compton scatter. The software additionally accounted for interferences of γ-lines with similar energies. By setting the energy range from 0-2 MeV and by using an 8 kilobyte multichannel analyser, a photo peak separation of 0.25 keV per channel was obtained, in this case the best option for the peak fitting algorithm. Calibration of the raw data obtained from *in situ* acquisition was carried out subsequently by high precision γ-activity determinations of bulk water samples in a well-defined counting geometry at the PSI accredited radioisotope laboratory.

The accuracy of the on-line ^{131}I data depends on the integration time set for the HPGe equipment. The shorter the integration time, the lower the resolution of the measuring device is. The fast concentration change within the extraction flow during the tracer breakthrough required a fast sampling rate. Therefore the resulting accuracy of the ^{131}I data decreased.

2.5.3.3 Laser Induced Breakdown Detector (LIBD)

The principle of LIBD is based on the generation of a dielectric breakdown in the focus region of a pulsed laser beam. As the threshold energy (irradiance) to induce a breakdown is lower for solids than for liquids or gas, the breakdown can be generated selectively in particles dispersed in solution at suitable pulse energies.

A schematic diagram of the mobile LIBD set-up used in the present work is shown Figure 2.3. A pulsed laser beam with a frequency of 15 Hz at 532 nm wavelength from a small Nd-YAG-laser (Continuum Minilite I) is focused (15 mm focal length) into the centre of a flow-through detection cell or cuvette, after passing through a variable attenuator and a beam splitter. The plasma generated at a breakdown event is monitored by a microscope equipped with a CCD monochrome camera triggered by the incident laser pulse and recorded by a PC-controlled image processing system. A breakdown shock wave propagated in the sample solution is detected simultaneously by an acoustic sensor (piezoelectric transducer) that is connected to the surface of the cell. Both the energy and the acoustic signal are recorded by an analogue-digital converter interface in a PC. Colloid concentrations are derived from the respective breakdown probability, represented by the number of breakdown events per number of laser shots, and the range of breakdown events within the laser beam axis determined by optical inspection of the laser focus area. Colloid populations (Pt L^{-1}) are given relative to a calibration with polystyrene

reference colloids. Mass concentrations are calculated by assuming an average colloid density of 2.7 g mL^{-1} and spherical particle shape. A more detailed description of data evaluation is given in Hauser et al. (2002).

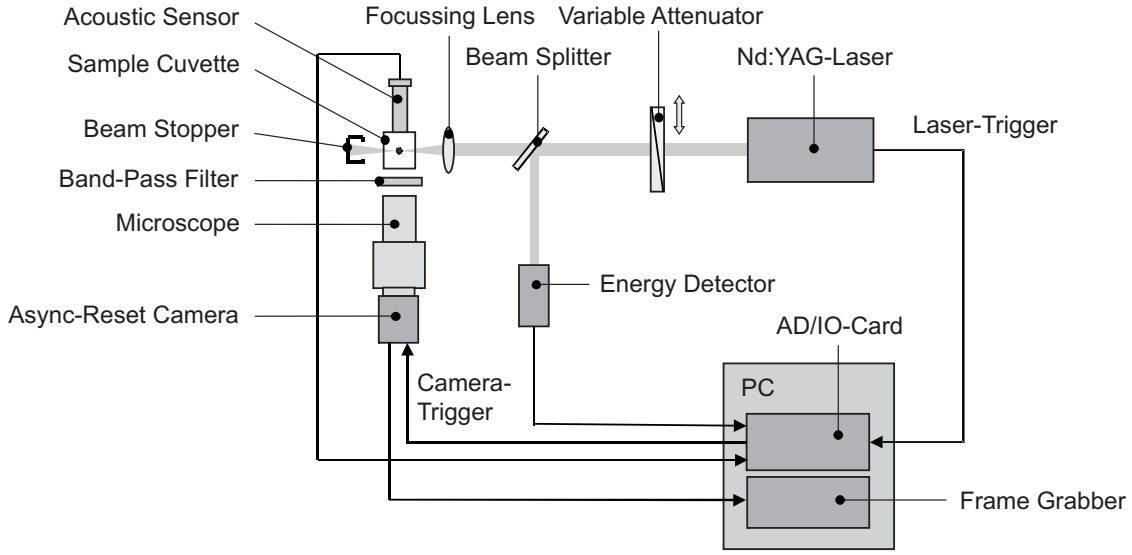

Fig. 2.3: Schematic diagram of the mobile LIBD

The mobile instrumentation of the LIBD is combined with a Millipore ultra-pure water processing unit for on-line flushing of the flow-through detection cell and to allow for regular determination of instrument drift. The whole system is set up on a compact mobile unit for the field experiment. The LIBD has been operated in the CRR migration experiments under low pressure conditions with commercially available quartz detection cells (fluorescence cells) for batch (laboratory experiments) or flow-through sampling. These cells have a sample volume of 3 mL at 10 mm absorption length. For higher water pressures (as for example in the access tunnel to the Kraftwerke Oberhasli (KWO) neighbouring the GTS), a new flow-through PEEK detection cell has been developed. The new cell has an external stainless steel housing with four optical windows, one on each side for the laser light transmission (absorption length 12 mm), one for the microscope and one for inspection. They consist of 2 mm thick sapphire. The groundwater flow enters the inner cell volume of 0.8 mL from the base via PEEK tubing. The outlet is on the top of the cell. The high-pressure detection cell has been successfully tested for water pressure up to 60 bars.

The quantitative evaluation of colloids in the field migration experiment requires the stable alignment of all optical components of the LIBD system. The exact adjustment of the beam alignment is performed by optical inspection with a laser beam profiler. The laser pulse energy is adjusted to a constant value at which the highest signal-to-background ratio is attained for the colloid detection. Such operational energy is selected by comparing the breakdown probability of “ultra-pure water” with that of a colloid dispersion as a function of the laser pulse energy (Figure 2.4). The breakdown probability is appraised by the ratio of the observed breakdown events to the total number of laser trigger pulses. The LIBD sensitivity, as determined with the pure water dispersion of polystyrene reference particles for the smallest size available (19 nm diameter), is attained down to a few ppt at the threshold energy of 1.4 mJ.

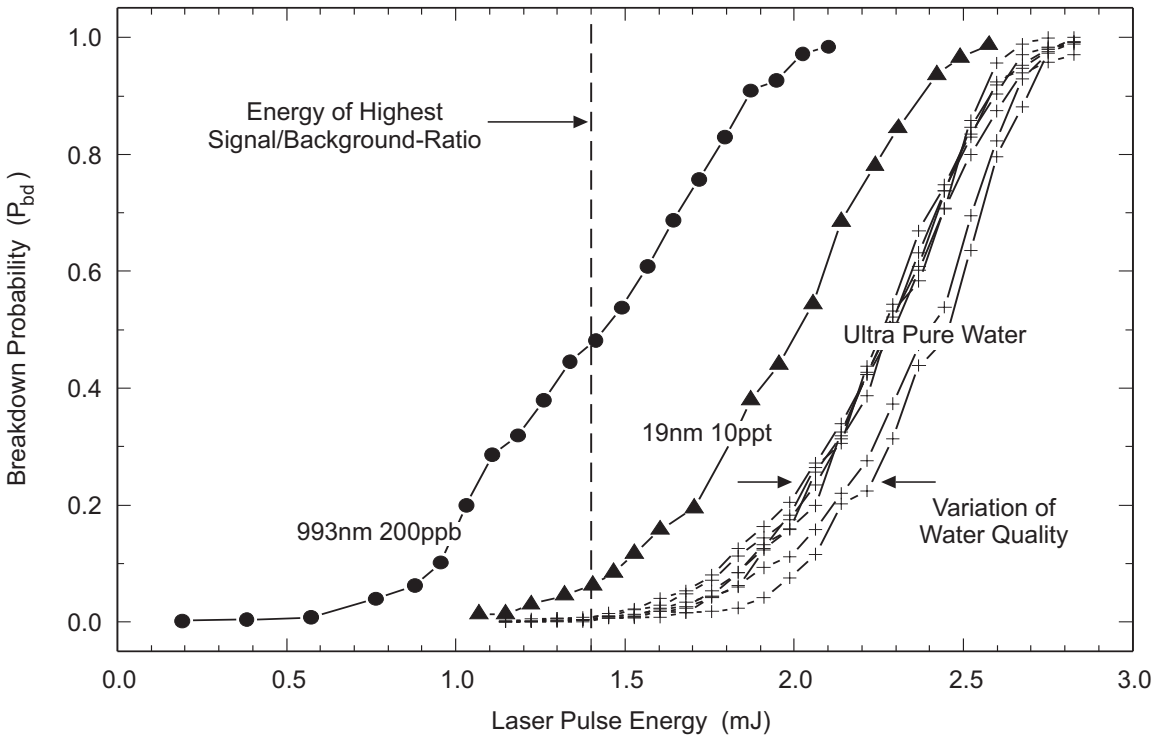

Fig. 2.4: Breakdown probability as a function of the laser pulse energy

A calibration of the colloid mass concentration, or number density, was made by measuring the breakdown probability for different particle sizes as a function of the laser pulse energy. Polystyrene reference particles/colloids are taken for this purpose, because they are available over a wide range of mono-dispersed sizes and robust in terms of the dispersion stability.

Along the photo-acoustic detection path, the plasma generated on the breakdown events is monitored with a CCD-camera adapted to a microscope. The optical recording system stores a series of pictures of breakdown events in the computer memory. The evaluation is subsequently made off-line. The emission intensity is represented by contours and light shades, showing the maximal intensity at the x_c-y_c co-ordinate. Using image processing software, the location of the individual events is evaluated within the laser pulse focus region by surveying the 2-dimensional co-ordinates x, y of breakdown emission. The spatial extension of the breakdown event distribution in the laser pulse focus area is found to be a direct function of the particle size. Such a distribution is determined in the direction of the laser beam axis (x-co-ordinate) by monitoring the number of breakdown events in the 2-D spatial area along the x-axis. For details on the concentration and particle size calibration see Hauser et al. (2002).

2.5.3.4 Photon Correlation Spectroscopy (PCS)

Colloid size determination by photon correlation spectroscopy (PCS) is conducted using a homodyne (single-beam) laser light scattering (LLS) device (ZetaPlus, Brookhaven Inc.) equipped with a 50 mW solid-state laser (λ = 532 nm). All measurements were performed in quartz glass SUPRASIL® cuvettes (Hellma 117.100F or 176.751) and the scattered light is analysed at a constant angle perpendicular to the incident laser beam. On-line measurements in the GTS during run #32 were performed by purging the flow through the cuvette for one minute and measuring three autocorrelation functions (ACF) at an accumulation time of 60 s. The scans

were analysed individually and averaged to a mean intensity distribution G(Γ) as well as combined to one mean ACF, giving the combined intensity distribution G(Γ). The average LLS intensity was determined by the combination of the three separate measurements and the limit of variation (error bars in Figure 2.5) represents the maximum and minimum value of the three single measurements. The ACFs were evaluated by applying the BI-ISDA software (Brookhaven Instruments Corporation, 1990) which allows the quadratic weighted cumulant analysis (QC) as well as a series of multimodal size distribution (MSD) analyses including the techniques of multiple pass, non-negatively constrained least squares (NNLS), CONTIN, exponential sampling and double-exponential sampling. In this study only the mean diameter of the above mentioned MSD algorithm calculations and the QC analysis were compared to show the variety of analytical results calculated from one measured ACF. The performed analysis procedure was especially chosen to evaluate critically the dependency of the calculated mean diameter on the chosen algorithm of the MSD software.

The quantification of colloid concentrations was performed by a laser light scattering (LLS) intensity calibration using different dilutions of the bentonite colloid stock solution CRR-TS2 (Figure 2.5). A good linear correlation of the log/log data ($r^2 = 0.99921$) was found down to a concentration range of ~75 μgL^{-1} whereas, at lower concentration, the LLS intensity asymptotically reached the background level. Possibly due to the change in humidity in the INE-laboratory (25-30%) as compared to that in the GTS (65-70%), a 25% decrease of the intensity for a diluted stock solution (CRR-TS2 diluted to 20 mgL^{-1}) was observed at the GTS. This difference in intensities was taken into account for the colloid quantification. At colloid concentrations < 75 μgL^{-1}, the QC derived mean colloid size of the standard was found to increase slightly from originally 222 nm (measured at higher colloid concentration) to 258 nm and the half width of the measured size distribution (FWHM) increased drastically from 93.5 nm to 210 nm. Therefore, the PCS detection limit for the CRR-TS2/GTS groundwater suspension system was set to 75 μgL^{-1} or 2.6 kcps (Figure 2.5).

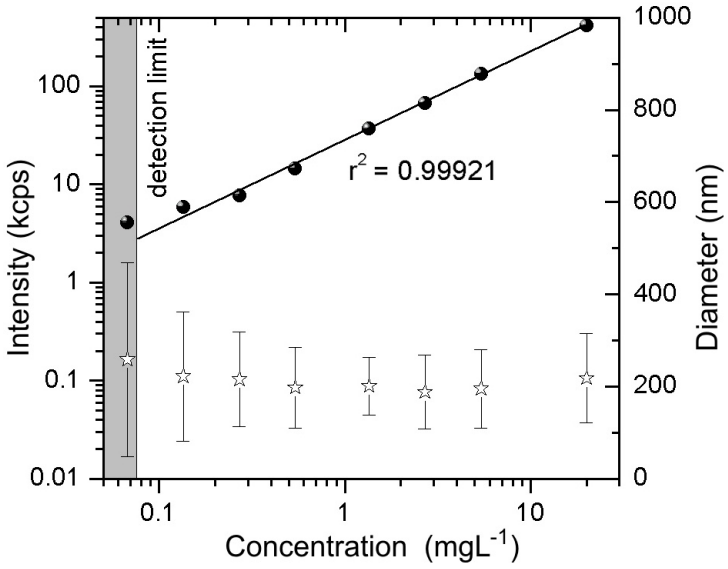

Fig. 2.5: Correlation of the FEBEX bentonite colloid mass concentration in GTS groundwater with the average light scattering intensity ⚬ determined by PCS; the mean colloid diameter (☆ FWHM as error bars) is determined according to the QC method (see text)

2.5.4 Off-site analytical techniques

2.5.4.1 Off-site γ-spectrometry

The activity of the radionuclides decaying by γ-emission was calculated automatically according to the following relationship:

$$A = \frac{I - I_0}{t_m \cdot P_W(Z,A) \cdot \varepsilon_\gamma(E)} \quad (1)$$

where I refers to the registered photo-pulses during counting time t_m, and I_0 to the background count rate induced from cosmic rays, terrestrial γ-radiation (short-lived uranium and ^{232}Th series nuclides such as ^{214}Bi/^{214}Pb) and Compton scatter of the radionuclide cocktail itself. $P_W(Z,A)$ is the photon emission probability (which depends on atomic mass and number) and $\varepsilon_\gamma(E)$ the detector efficiency (which is dependent on the energy of the incident photons).

For the calculation of the α-activities determined with the surface barrier detectors, the parameters I_0, $\varepsilon_\alpha(E)$ and $P_W(Z,A)$ can be omitted, since (i) the background count rate is extremely small for α-spectrometry, (ii) within the range of typical α-emission energies (*ie* between 4 and 8 MeV) the particle detection efficiency of the counter, E_α, is almost constant and (iii) the particle emission probability of all α-nuclides investigated here is close to 100%.

Measurement uncertainty and detection limits for all nuclides analysed were calculated according to ISO-norm 11929-1:2000(E). The detection limit for most of the injected γ-radionuclides was about 0.1 Bq mL^{-1} (*in situ* analysis), while in the 1L and 50 mL water samples, activities even below 0.005 Bq mL^{-1} could be determined when counting the samples for about 10^4 seconds (2.8 hours). Since the laboratory samples were measured in a high-precision geometry, the overall measurement uncertainty was mainly dominated by the counting statistics. Typical 2σ-errors for γ-emitting ^{85}Sr, ^{82}Br and ^{131}I in the region of the peak-breakthrough were 2 – 4%, while the overall uncertainty (2σ) for the α-emitting isotopes was significantly higher (about 15 – 20%). Two reasons are responsible for these higher values; (i) poorer counting statistics (due to smaller sample quantity, *ie* 10 mL instead of 50 mL used for γ-spectrometry) and (ii) the counting efficiency of the evaporated planar sources could be determined only with a precision of $\pm$ 10%. Significantly higher precision for all samples would have required highly time intensive radiochemical separation procedures, something which would be impractical during a relatively short-term field experiment.

2.5.4.2 Off-site α-spectrometry

To monitor the breakthrough of α-emitting isotopes, 10 mL aliquots of the water samples were evaporated onto a stainless steel planchet and measured with solid-state α-spectrometry. To obtain a reasonable counting efficiency (which is dependent on the sample self-attenuation), two approaches were chosen: (i) comparison of the α-count rate with results obtained from γ-spectrometric measurement of aliquot samples (*eg* applicable for α/γ-emitting ^{243}Am in run #3) and (ii) via radiochemical separation on selected samples that were collected during run #32. In both cases, it turned out that the average counting efficiency was 8.0 $\pm$ 0.8%.

The radionuclide couples ^{233}U/^{237}Np and ^{238}Pu/^{241}Am respectively were not separated in these laboratory analysis. However, a chemical separation of these radionuclides was performed on one sample (collected after 1.19 hours of test duration). The 2σ measurement uncertainty was found to be smaller than 5%. The subsequent analysis of each element revealed the following

activities (in Bq mL^{-1}): ^{233}U = 164, ^{237}Np = 11, ^{238}Pu = 35 and ^{241}Am = 80. Back-calculating these values to the previously analysed radionuclide pairs reveals good consistency with the former values (see Table 2.10 below).

Tab. 2.10: Colloid bound radionuclide concentrations as calculated and measured (colloid concentration: 20 mgL^{-1})

Separation of radionuclides for analysis	**Total activity of $^{233}U/^{237}Np$** [Bq mL^{-1}]	**Total activity of $^{238}Pu/^{241}Am$** [Bq mL^{-1}]
Without separation	164	114
Radionuclides separated	175	115

2.5.4.3 ICP-MS measurements

Analysis of the individual radionuclide samples was carried out by an ICP-MS (Elan 6000, Perkin & Elmer) equipped with an ultrasonic nebuliser and a desolvation device (USN 6000 AT+, CETAC Inc.). Samples are acidified prior to analysis and ^{103}Rh added as an internal standard. Calibration for the actinides is made by using standard solutions of ^{238}U and ^{232}Th. Due to the high sensitivity of the nebuliser-ICP-MS combination, the low background in the heavy element mass region and the low salt content of the GTS groundwater, it is possible to analyse the actinides at relatively low concentrations (see Table 2.11). Variations in the sensitivity are due to changes in the instrumental parameters.

Tab. 2.11: Estimated detection limits for the actinide analysis by ICP-MS

Isotope	**Detection limit** (3σ)
^{232}Th	1-2.3 ngL^{-1}
^{238}U	1.7 ngL^{-1}
^{99}Tc	0.4 ngL^{-1}
^{237}Np, ^{242}Pu, ^{244}Pu, ^{233}U, ^{241}Am, ^{243}Am	0.07-0.2 ngL^{-1}

2.5.4.4 Single Particle Counting (SPC)

Determination of colloid size classes was performed by single particle counting carried out at PSI (for details see Degueldre et al., 1996). Groundwater samples were diluted in a stream of ultrapure water (Milli-Q from Millipore). The collected 200 mL groundwater samples were injected in the 500 $mL \cdot min^{-1}$ stream of ultrapure water. This injection is performed with a Dosamat pump and the time between injection and detection is less than one second for the detectors. Analyses were performed with injection flow rates of 0.17-16.67 $mL \cdot min^{-1}$ according to the colloid concentration in the studied water. The loop included two optical PMS units (Particle Measuring Systems, Boulder, USA), namely a HSLIS-M50 single particle monitor (PDS) and a single particle spectrometer (LPS) HVLIS-C200-Cor. Both the single particle monitor and the spectrometer are coupled down-stream from the Milli-Q unit allowing specific counting of 13 size classes from 50 to 5000 nm. The colloid concentrations were determined for size class 50-100, 100-150, 150-200 nm with the monitor and 200-300, 300-500, 500-700, 700-1000, 1000-1500, 1500-2000, 2000-5000 and over 5000 nm with the spectrometer.

The MilliQ water (blank) was previously cross filtered using a flat membrane of 200 nm pore size. This blank was used to define the detection limit (3 x σ_{blanc}). In the blank, the concentration for the smallest class of colloids (50 – 100 nm) was found to be around 3300 mL^{-1} and the σ_{blank} is around 2500 mL^{-1} for 10 times 1 min measurements. For this blank the detection limit would be 7500 mL^{-1} for an average size of 75 nm, corresponding to a concentration of about 10 ppt (1.0E-08 gL^{-1}) for a colloid density of 2 g cm^{-3}.

2.5.5 Radioprotection

An *in situ* experiment which uses radioactive tracers (including actinides) requires special radioprotection measures and licensing from the relevant authorities. The radioprotection concept for *in situ* experiments at the GTS was developed between the Swiss Federal Nuclear Safety Inspectorate (HSK) and the radioprotection officer from Nagra over 15 years of safe application of radionuclide tracers *in situ* at the GTS during the former MI and EP experiments, carried out at the same experimental shear zone as the CRR experiment.

Full details of the planned experiment were submitted to HSK and discussed further. A site visit to the GTS was carried out to approve the facilities before licensing was approved. During the course of the experiment, the laboratory would operate as an 'IAEA Type C' radiochemistry laboratory. This laboratory is in a separate tunnel to the rest of the GTS and isolated with a locked door and a changing area. Access to the laboratory is restricted and requires the permission of the radiation protection officer. To be permitted to work in this laboratory, the test crew were registered with the authorities as occupationally radiation-exposed workers and subject to medical checks. The entrance to this laboratory displays the safety information for persons wishing to enter this zone, including the radiological significance. In the vicinity of the CRR test area, the floor and tunnel wall were covered by plastic sheeting to prevent any contamination of the surface. During work with radionuclides, a radiation protection officer was always present to measure external dose rates and carry out contamination monitoring. To monitor the doses received by personnel during the experiments, TLD (thermo-luminescent dosimeters) were worn by the test crew. Analysis of these badges showed no dose rates above background. Furthermore, no contamination of personnel or the laboratory occurred and external dose rates in all places accessible for workers were below the statutory limits.

The breakthrough solution containing the radionuclide tracers, if not sampled, was collected within six 2000 L PVC tanks. Representative samples were collected from these tanks and analysed for their radionuclide concentration at PSI. Solid radioactive wastes were collected and transported to PSI. Solid wastes, containing only the short-lived radionuclide ^{131}I (half life = 8.04 days), were stored behind lead shielding within the radiochemisty laboratory to wait until radioactive decay rendered them safe. Solid wastes, containing longer lived radionuclides were transported to PSI for treatment and disposal.

The details of the radiation protection measurements have been summarised and reported to HSK. Within this report, a mass balance of the radionuclide tracers is also presented, this examines the concentration of radionuclides injected and extracted to make predictions on the radioactivity still within the flow field. The construction of this mass balance is discussed later in section 4.5.1. No radioactive waste remains at the GTS and long term monitoring of the CRR extraction borehole is carried out 4 times per year. The results of this monitoring are also reported annually to HSK.

2.5.5.1 Transportation

The requested radionuclides were ordered by FZK for the actinide cocktails (runs #31 and #32) and by PSI for the supporting ^{131}I injections. The cocktails were stored at FZK and PSI in HDPE vials for the planned cocktail characterisation and for transportation to the GTS. The actinide tracer cocktails prepared at FZK, the remaining cocktails from the tracer injections and the active samples of the breakthrough solutions were all delivered to FZK by a specialist transportation company whereas samples for the PSI were transported by the radioprotection officer.

2.5.5.2 Radiological mass balance

A radiological mass balance was created to fully account for the radioactive tracers added in the CRR experiment. This was similar to that carried out in the earlier MI and EP projects at the GTS. The aim of the mass balance is to estimate, as accurately as possible, the activity of radionuclides that are still in the test zone and assess the radiological significance of these activities.

In the simplest sense, the mass balance of the CRR experiment was created as follows: the activity of the radionuclides injected minus the activity recovered at the outflow end was equal to the activity that remains in the rock.

The activity recovered was calculated via on-line gamma spectrometry of the extracted water and using the results of laboratory based α-spectrometry and ICP-MS measurements on samples collected from the outflow. The activity that remained in the rock was then corrected for radioactive decay and assumed to be spread throughout the fracture. Knowledge of the dipole area allowed the activity to be calculated as an activity per kilogram. For comparison, the natural radioactivity in the granite can be used to highlight the radiological significance of any remaining activity. The calculations made in the mass balance were conservative and based on worst possible recoveries (from the analytical error) and this allows the maximum radionuclide concentration in the rock and its significance to be calculated.

3 Preparatory field tests

H. Geckeis, Th. Fierz, C. Degueldre, W. Hauser and A. Möri,

3.1 Dipole selection

A preparatory field campaign consisting of hydro- and tracer tests was carried out in the experimental shear zone in order to evaluate the most appropriate dipole geometry and flow conditions. Tracer breakthrough curves of conservative tracers along with data on the hydraulic parameters were used for the elaboration of the hydraulic models for the predictive transport modelling (see Guimera et al., 2004). The flow field for the final *in situ* experiments had to fulfil several boundary conditions:

- 100% recovery of a conservative tracer[8],
- the residence time of a conservative tracer in the experimental shear zone should be in the order of hours and
- it should be possible to overcore the flow field.

With these boundary conditions it is obvious that compromises are necessary as some of the requirements conflict with each other (*eg* tracer recovery versus residence time).

3.1.1 Hydraulic testing

3.1.1.1 Constant rate tests

Constant rate tests were performed at three time intervals of 12 s, 120 s and 7,200 s in the shear zone interval of the boreholes BOCR 99.002 and BOCR 00.003. Before starting a test, the HPLC pump injected water at a constant flow rate within a circuit. The injection test was initiated by switching the flow direction into the interval using a 3-way-valve (note that the injection flow rate varied during the first 5-8s after the start of the test). For reasons unknown, the first recorded pressure reading after opening the interval valve indicated, in most cases, an initial decrease of interval pressure, followed by a steep pressure rise (for details see Fisch, 2002). Gringarten-Bourdet type-curves were used in order to estimate the transmissivity T, the well bore storage constant C and the skin factor. The recorded pressure and time data were converted to dimensionless parameters during the visual matching process (see Figure 3.1 for an example for 120s constant rate tests and the evaluation with type curves). The result of this procedure is of limited precision because of the inherent non-uniqueness of type-curve-fitting.

As the type-curve analysis do not allow independent determination of either of the hydraulic parameters storativity (S) or skin (s), either the skin factor must be known to evaluate storativity, or vice versa. Storativity values within a large but plausible range (S = 1.0E-05, 1.0E-06 and 1.0E-07; see Table 3.1) were assumed for all matches conducted in order to obtain corresponding skin factors. The obtained skin factors indicate the presence of a relatively high positive skin in both borehole intervals which could be interpreted as clogging of the shear zone near the borehole. This could possibly be a result of the drilling process, with fine material transported into the shear zone due to elevated pressures. Alternatively, the observed positive skin effect is due to a decrease in the aperture (compared to the general shear zone aperture) of

[8] This is for two reasons: first, it simplifies the transport modelling and, second, in the case of long-lived radionuclides, HSK require, as far as possible, complete recovery of the tracers.

the shear zone close to the borehole. The resulting transmissivity values were in good agreement with the results obtained from the 2 hour constant rate injection tests (see below).

The constant rate injection tests in the boreholes BOCR 99.002 and 00.003 showed a rising pressure derivative after a short initial stabilization period. The shape of the derivative may reflect the effect of a nearby situated less permeable rock mass or a region with a flow dimension smaller than 2. A flattening of the derivative curve is observed towards of the end of both constant rate injection tests which could be due to a distant zone of increased transmissivity (constant head type boundary).

3.1.1.2 Interference pressure reactions

During the 2 hour constant rate injection tests in the shear zone intervals of boreholes BOCR 99.002 and BOCR 00.003, the pressure interference reactions in other packer intervals of the experimental shear zone were observed. The details of the test analyses are presented in Tables 3.2 and 3.3 and the RI-test in BOCR99.002 (interval 2) and the response in BOCR 00.003 (interval 2) are shown in Figure 3.2.

The interference tests show a good hydraulic connectivity between the actively tested wells BOCR 99.002 and BOCR 00.003 and also between the shear zone intervals of boreholes BOMI 86.004 and BOMI 86.005 and the active wells. Distinct, but slower, pressure reactions were recorded in the shear-zone intervals of boreholes BOMI 87.008 and BOMI 87.010. Pressure in the interval BOMI 87.007 was not affected by the RI-tests in BOCR 99.002 and BOCR 00.003. During the RI-Test in BOCR 00.003, the resin-filled borehole BOMI 87.009 was also connected to the data acquisition system and it showed an interference reaction similar to that of the shear zone interval of BOMI 86.004.

3.1.1.3 Shear zone transmissivities in BOCR 99.002 and BOCR 00.003

Single hole testing in boreholes BOCR 99.002 and BOCR 00.003, as well as crosshole tests between these boreholes and the existing MI boreholes, revealed experimental shear zone transmissivities of between ~3.0E-07 m^2s^{-1} and 2.4E-06 m^2s^{-1}. Transmissivity estimates from early-time type curve matches and early time straight-line fits are very similar for the borehole BOCR 99.002 (~2E-06 $m^2\ s^{-1}$) and are within a narrow range for the borehole BOCR 00.003 (1.4E-06 and 4E-06 $m^2\ s^{-1}$). The transmissivities obtained from middle/late time straight-line fitting are distinctly lower and vary between 3E-07 $m^2\ s^{-1}$ and 7E-07 $m^2\ s^{-1}$. The transmissivity values obtained from the observation wells vary between 8E-07 $m^2\ s^{-1}$ and 2E-06 $m^2\ s^{-1}$.

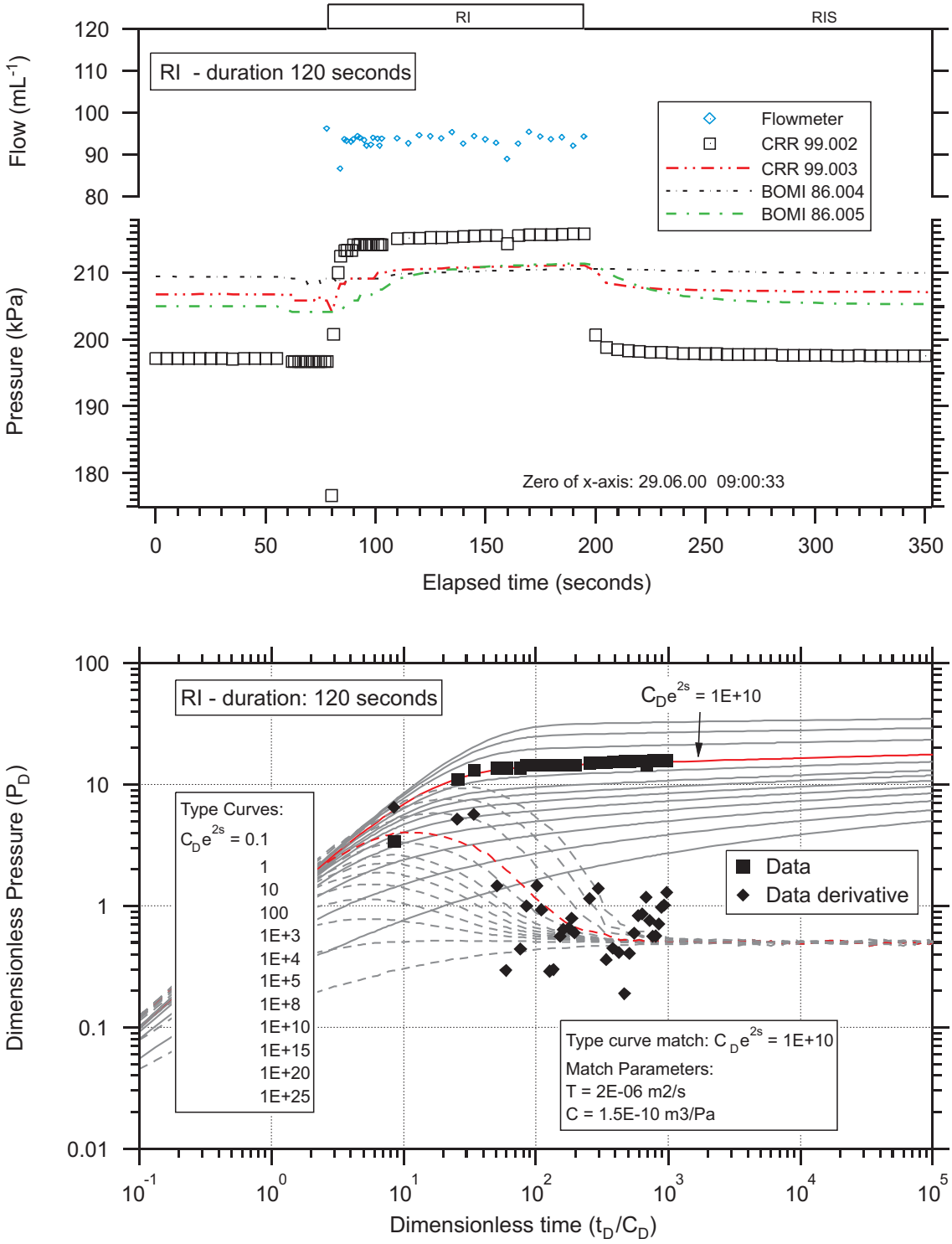

Fig. 3.1: BOCR 99.002-i2/RI-test (120" duration) overview plot and type-curve analysis

Tab. 3.1: Test results obtained from Gringarten-Bourdet type-curve analysis (early time fitting)

Test Interval BOCR 99.002-i2										
Test duration:	->	12 s			120 s			7200 s		
See Appendix			B-1			B-2			C-3	
CD * e2S =	[-]		1.0E+08			1.0E+10			1E+10	
C =	[m3/Pa]		2.0E-10			1.5E-10			1.5E-10	
T [m2/s]	[m2/s]		1.5E-06			2.0E-06			2.2E-06	
K [m/s]	[m/s]		3.8E-06			5.0E-06			5.5E-06	
S [-]	[-]	1.0E-05	1.0E-06	1.0E-07	1.0E-05	1.0E-06	1.0E-07	1.0E-05	1.0E-06	1.0E-07
Ss =	[1/m]	2.5E-05	2.5E-06	2.5E-07	2.5E-05	2.5E-06	2.5E-07	2.5E-05	2.5E-06	2.5E-07
s (Skin)=	[-]	7.8	6.6	5.5	10.2	9.1	7.9	10.2	9.1	7.9
S (if s == 0) =	[-]		1.7E-12			1.3E-14			1.3E-14	
Test Interval BOCR 00.003-i2										
Test duration:	->	11 s/ 16 s			120 s			7200 s		
See Appendix			E-1/ E-2			E-3			F-3	
CD * e2S =	[-]		1E+15			1E+15			1E+15	
C =	[m3/Pa]		3E-10			3E-10			8E-10	
T [m2/s]	[m2/s]		4.0E-6			4.5E-6			4.0E-6	
K [m/s]	[m/s]		1.3E-05			1.5E-05			1.3E-05	
S [-]	[-]	1.0E-05	1.0E-06	1.0E-07	1.0E-05	1.0E-06	1.0E-07	1.0E-05	1.0E-06	1.0E-07
Ss =	[1/m]	3.2E-05	3.2E-06	3.2E-07	3.2E-05	3.2E-06	3.2E-07	3.2E-05	3.2E-06	3.2E-07
s (Skin)=	[-]	15.7	14.5	13.4	15.7	14.5	13.3508	15.2	14.0	12.9
S (if s == 0) =	[-]		2.5E-19			2.5E-19			6.8E-19	

Tab. 3.2: Details of cross-hole analysis (active well: interval BOCR 99.002-i2)

	BOCR 00.003		**BOMI86.004**	**BOMI86.005**	**BOMI87.008**	**BOMI87.010**
Analysis vers. [1)]	a	b	-	-	-	-
Radial dist. [m] [2)]	1.71	1.71	15.53	1.27	6.74	2.5
Fit range (I) [s]	45	4120	605	655	4345	4195
Fit range (II) [s]	340	7215	1205	1205	5550	7215
Fit type	early	late	middle	middle	late	late
u-crit. (I) [s] [3)]	3.0E-03	8.0E-05	4.0E-02	2.0E-04	2.0E-03	2.0E-04
u-crit. (II) [s] [3)]	5.0E-04	4.0E-05	2.0E-02	1.0E-04	1.0E-03	1.0E-04
Intercept [s]	3.098E-02	6.822E+00	3.977E+01	6.044E-02	9.978E+02	1.022E+03
T [m^2/s]	2.4E-06	1.1E-06	1.4E-06	1.5E-06	8.4E-07	8.0E-07
S [-]	5.6E-08	5.9E-06	5.0E-07	1.3E-07	4.2E-05	3.0E-04
R_i (S=5E-7) [m] [4)]	60.2	191.5	85.6	91.1	145.2	161.4
R_i (S = var) [m] [4)]	179.1	55.6	85.5	179.3	15.9	6.6

1) According to early and late time fit ranges
2) Distance to active test interval BOCR 99.002-i2
3) u-criterion: $u = S\ r^2/(4\ T\ t)$
4) The radius of investigation R_i, is roughly estimated using the formula $R_i = 1.5 \sqrt{(T\ t/S)}$

Tab. 3.3: Details of cross-hole analysis (active well: interval BOCR 00.003-i2)

	BOCR-00.003		**BOMI86.004**	**BOMI86.005**	**BOMI87.008**	**BOMI87.010**
Analysis vers. [1)]	a	b	-	-	-	-
Radial dist. [m] [2)]	1.71	1.71	16.79	1.7	8.07	4.19
Fit range (I) [s]	55	2080	975	1570	4925	5145
Fit range (II) [s]	360	7400	2565	2245	7400	7400
Fit type	early	late	middle	middle	late	late
u-crit. (I) [s] [3)]	3.0E-03	2.0E-04	3.0E-02	2.0E-04	2.0E-03	5.0E-04
u-crit. (II) [s] [3)]	5.0E-04	5.0E-05	1.0E-02	1.0E-04	1.0E-03	4.0E-04
Intercept [s]	5.168E-02	1.105E+01	4.916E+01	4.014E+00	1.304E+03	1.324E+03
T [m^2/s]	2.2E-06	9.7E-07	1.1E-06	1.1E-06	7.9E-07	8.2E-07
S [-]	8.5E-08	8.2E-06	4.3E-07	3.5E-06	3.6E-05	1.4E-04
R_i (S=5E-7) [m] [4)]	60.2	191.5	85.6	91.1	145.2	161.4
R_i (S = var) [m] [4)]	179.1	55.6	85.5	179.3	15.9	6.6

1) According to early and late time fit ranges
2) Distance to active test interval BOCR 00.003-i2
3) u-criterion: $u = S\ r^2/(4\ T\ t)$
4) The radius of investigation R_i, is roughly estimated using the formula $R_i = 1.5 \sqrt{(T\ t/S)}$

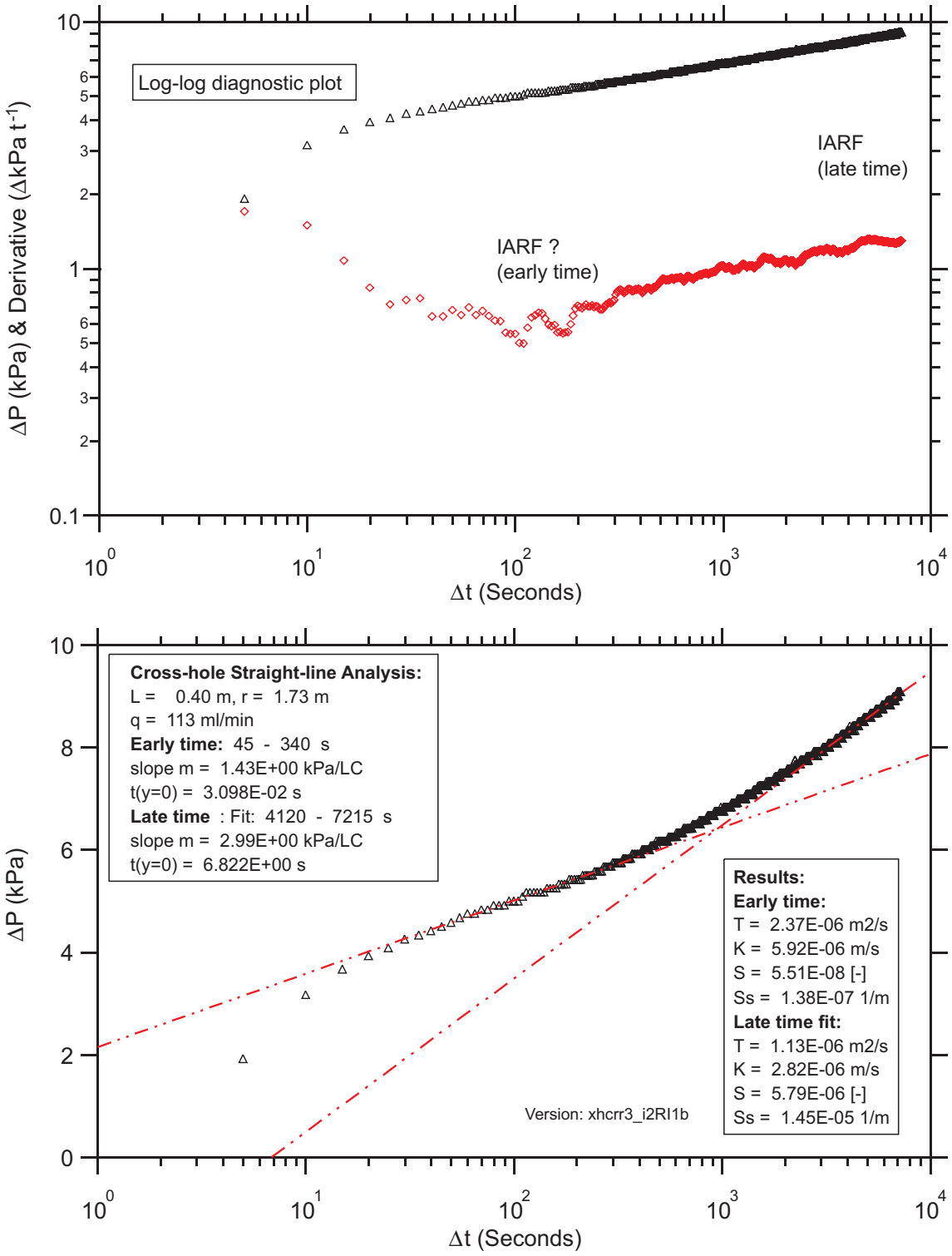

Fig. 3.2: BOCR 99.002-i2/RI; analysis of D-hole reaction in BOCR 00.003-i2

3.1.2 Geostatistical inverse modelling

The model used the data from the hydraulic tests in order to obtain a better understanding of the transmissivity (T) distribution in the experimental shear zone. The existing model was based on the previous geostatistical inverse model utilised in the EP experiment (Meier 1999, 2001) and has been updated and re-calibrated by UPC (Universita Politechnica Catalun) for the CRR experiment.

3.1.2.1 Conceptual model

The model domain is centred on the AU gallery and is 55 m high and 63.25 m wide. The transmissivity is treated as a regionalised variable because of its strong heterogeneity as revealed from the EP experiment results (Meier, 1999, 2001). Therefore, the model domain was divided into 922 T zones (see Figure 3.3). Homogeneous storativity for the model domain was assumed. Additionally, the two back-filled excavation boreholes from the EP experiment were introduced as low flow areas and data from the new cross-hole pumping tests from the CRR boreholes BOCR 99.002 and BOCR 00.003 were included.

Three different hydraulic conditions were considered for defining the boundary conditions: steady-state conditions, without test activities, when all boreholes were closed (SS), steady-state conditions during dipole tracer tests (SSDT) and transient conditions during pumping tests. Constant head boundaries were applied at the outer model domain for SS and SSDT. Flow was prescribed for SS whereas for SSTD conditions, the gallery was treated as a constant head boundary because outflow rates were not measured. The gallery boundary condition can change from a no-flow boundary to an outflow boundary. Inflow through the gallery is not expected. For transient conditions, zero drawdown conditions were imposed on all boundaries, except at the pumping well, where the measured flow rates were imposed. Heads at the outer boundary are the same as calibrated in the EP experiment (Meier 1999, 2001).

Due to the EP overcoring (details in Alexander et al., 2004), the hydraulic properties of the experimental shear zone around the two overlapping, shear zone parallel overcoring boreholes have changed. These boreholes were drilled parallel to the experimental shear zone and follow the direction of the line which links boreholes BOMI 87.009 and BOMI 87.006 (the EP dipole) with the AU gallery. The boreholes were filled with different filling material depending on the borehole depth: in the lower part (between the end of the borehole and the intersection with the former injection borehole BOMI 87.009) the boreholes were filled with sand. Above this, the boreholes were filled with resin up to the intersection with the former extraction borehole BOMI 87.006 (the dipole interval) and the rest until the tunnel surface was filled with a mixture of resin and sand. The hydraulic properties of the drilled boreholes can be split into three different parts (from the bottom up to the intersection between the overcored borehole and the gallery):

- high conductive zone in the lower part of the overcored borehole which was filled with sand,
- low conductive zone in the resin filled part of the overcored borehole and
- medium conductive zone where the boreholes were filled with a mixture of sand and resin. This mixture does not completely seal the overcored borehole because water has been found to flow from the borehole into the access gallery. This part of the borehole makes a hydraulic connection between the experimental shear zone and the AU drift.

Prior information needed to solve the inverse problem using the likelihood method was taken from the EP calibrated transmissivity field. Non-linear estimation of the transmissivity values at

the 922 T zones and storativity was performed with the finite element code TRANSIN II (Medina et al., 1996). Five independent data sets were used simultaneously for model calibration:

- one steady-state data set consisting of the static head values and the inflow rates at the gallery without testing activities and
- four transient drawdown and recovery data sets from pumping tests in boreholes BOMI 87.009 and BOMI 87.006 (performed in the framework of the EP project) and pumping tests in boreholes BOCR 99.002 and BOCR 00.003 (performed in the framework of the CRR project).

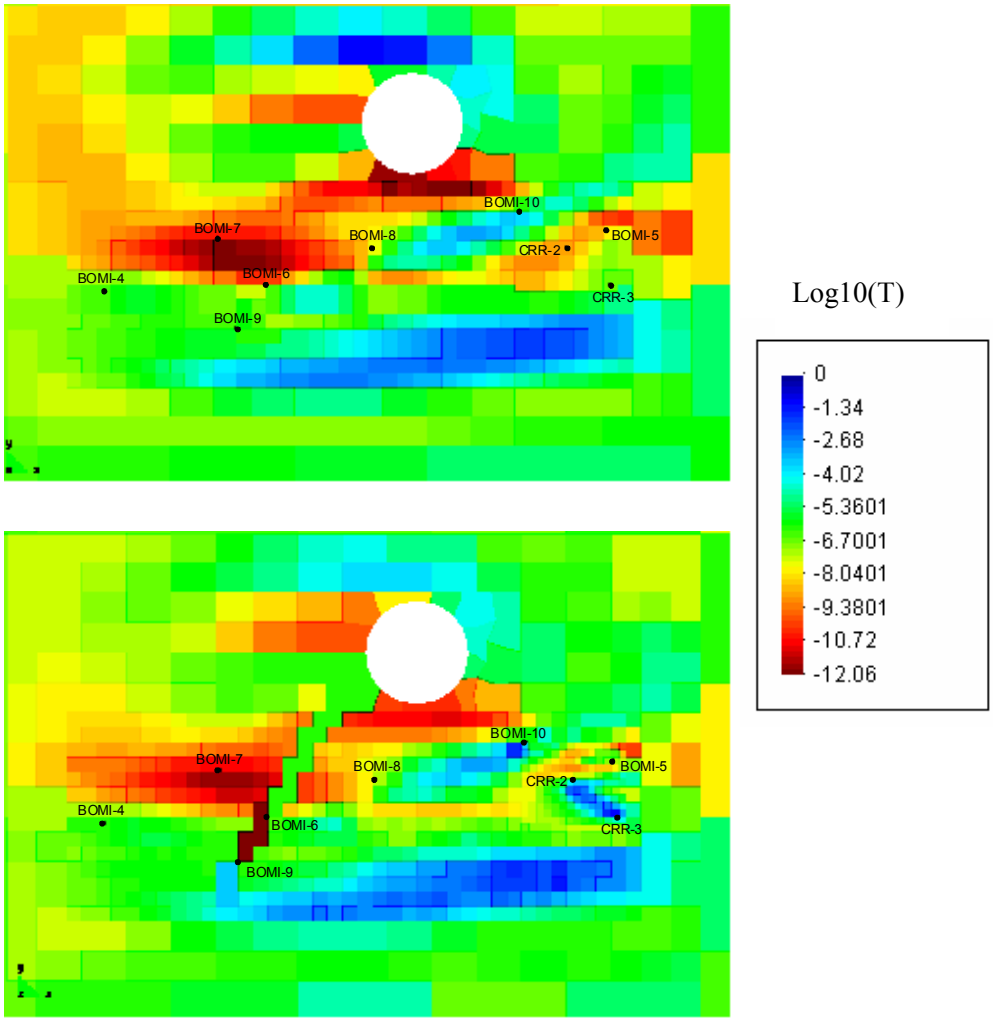

Fig. 3.3: Upper part: log10(T) field obtained from simulation of two constant rate injection tests from the MI experiment; lower part: log10(T) field calibrated for two CRR constant rate injection test, taking into account the EP overcored borehole fracture plane (see Alexander et all, 2004 for details of the borehole). Note that the model domain is 55 m x 63.25 m)

3.1.2.2 Transmissivity fields

The transmissivity field obtained from the inversion (Figure 3.3) shows strong heterogeneity within the experimental shear zone. The model suggests the existence of channels with enhanced transmissivities. These channels have a preferred horizontal orientation. The model also predicts flow barriers with low transmissivity values (Meier 1999, 2001). There is no significant influence of the sealed EP overcoring boreholes on the CRR flow fields.

Transmissivity barriers in the region of the CRR boreholes are mainly located between boreholes BOMI 87.010 and BOCR 99.002 (dipole 1) and "behind" dipole 2. Good hydraulic connections are obvious between the boreholes BOMI 86.005, BOCR 99.002 and 00.003 respectively (dipole 2).

3.1.3 Uranine tracer testing

3.1.3.1 Test programme

The evaluation of the appropriate dipole for the final tracer tests was supported by six uranine tracer tests which were performed in the three CRR dipoles 1, 2 and 4. The uranine was injected at different flow rates as well as at different ratios between injection flow rate and extraction flow rate (termed the β–value) in order to find out the optimum flow conditions for complete recovery at maximum residence time. Table 3.4 gives an overview of the dipoles and the related uranine tests as well as of selected parameters that were derived from the breakthrough curves (see below).

Tab. 3.4: Overview of preparatory uranine tracer tests runs #1, #2, #3, #4, #5, #12 and #13

	Run #1	**Run #2**	**Run #3**	**Run #13**	**Run #4**	**Run #5**	**Run #12**
Dipole [1)]	1	1	1	1	2	2	4
Dipole length [m]	2.23	2.23	2.23	2.23	1.71	1.71	3.94
Injection rate [mL min^{-1}]	8	6	8	10	10	5	10
Extraction rate [mL min^{-1}]	12	160	213	150	250	75	150
β-value	1.5	26.7	26.6	15.0	25.0	15.0	15.0
Peak time input function [h]	0.45	0.58	0.47	0.21	0.51	0.75	0.25
Peak time breakthrough curve [h]	2.10	2.28	2.02	1.41	0.68	1.57	2.90
Residence time of tracer in the shear zone [h]	1.65	1.70	1.55	1.20	0.17	0.82	2.17
Tracer recovery [%]	55	93	95	94	98	65	76

[1)] Dipole 3 was not evaluated with regard to the final *in situ* experiment as this dipole was not intended to be used due to its orientation (overcoring from the tunnel would not be possible)

3.1.3.2 Tracer breakthrough curves

The residence times shown in Table 3.4 were determined by comparing the peak times of the injection and the extraction curves. Tracer recovery was determined by integrating the area below the breakthrough curves (see Figure 3.4).

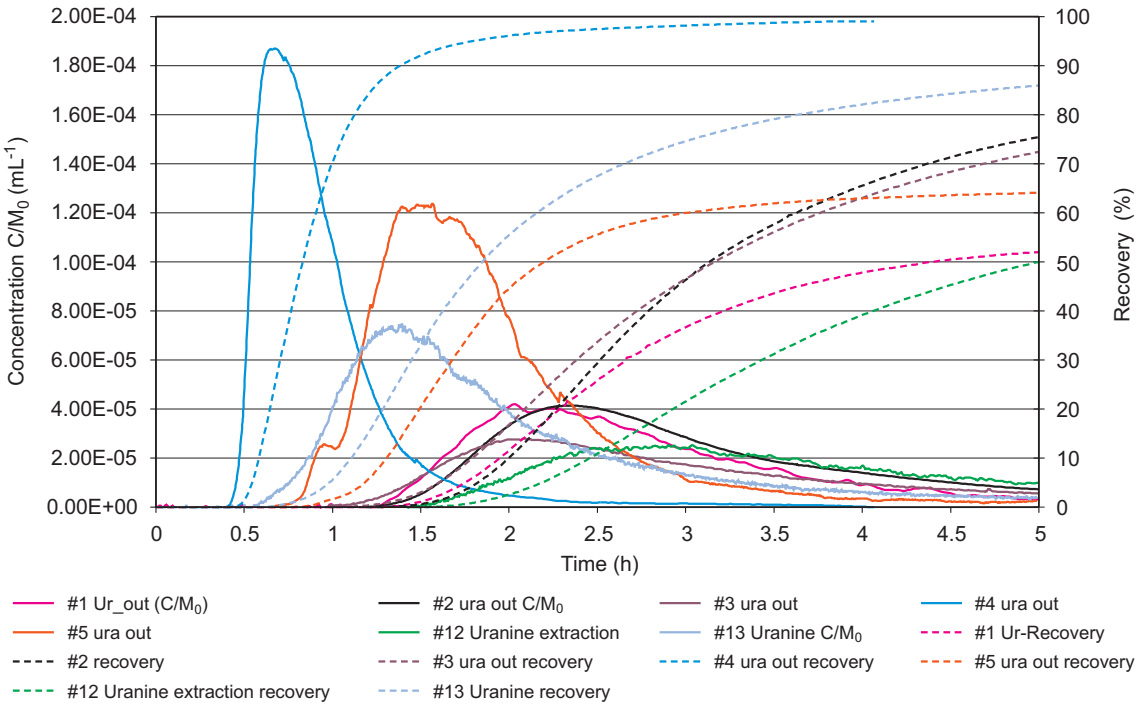

Fig. 3.4: Breakthrough curves of uranine runs #1, #2, #3, #4, #5, #12 and #13

Run #1 in dipole 1 revealed a poor recovery of 55%, indicating that, with the applied β–value of 1.5, almost half of the injected tracer would be lost. Therefore, two other runs were carried out (runs #2 and #3) in this dipole with enhanced β–value of about 27. Both tests showed good tracer recoveries at residence times that lay in the range of about 1.5 hours[9]. A fourth uranine run with a β–value of 15 confirmed the good recovery properties of this dipole at a residence time of about 1.2 hours.

Dipole 2 showed a very short tracer residence time of 0.17 hours while obtaining 98% recovery (with a β–value of 25). Changing β to 15 resulted in an increased residence time of 0.82 hours but revealed a recovery of only 65%. It was concluded that, as predicted from the hydrotesting, this dipole consists of a very direct connection between the injection and extraction borehole. This channel-type flow structure decreases the residence time of the tracers markedly at increased flow rates. The poor recovery that resulted by trying to increase the residence time of the tracer might reflect other channels with high transmissivities which remove a certain amount of the tracer from the dipole.

The almost 4 m long dipole 4 revealed at a β–value of 15 a recovery of only 75% at a not significantly increased residence time of around 2 hours.

---

[9] It is not clear why runs #1 and #3 show the same residence time if the extraction flow rate has almost been doubled at constant injection flow rates and with the very different recoveries. Possibly this reflects residence time dominated by slow flow in the vicinity of the injection hole: increased extraction is just catching more of the injected material (making the dipole narrower)

3.1.4 Summary of dipole selection

The experimental shear zone around borehole BOCR 00.003 showed slightly lower transmissivities than around BOCR 99.002. The observed interference pressure reactions demonstrate a good hydraulic interconnectivity between BOCR 99.002 and BOCR 00.003 and the BOMI 87.004 and BOMI 87.005. However, a transmissivity barrier exists between BOMI 86.008 and BOMI 87.010 and between BOMI 87.010 and BOCR 99.002 (dipole 1). The two MI boreholes BOMI 86.008 and BOMI 87.010 are even better connected to BOMI 86.004 and BOMI 86.005 which intersect the experimental shear zone at greater distances from the tunnel than do the new CRR boreholes. This barrier feature was already predicted by Meier (1999, 2001) and confirmed by the geostatistical inverse modelling exercise.

The main findings of the hydrotesting and geostatistical inverse modelling can be summarised as follows:

- Dipole 1 shows good evidence for a low transmissivity zone between BOCR 99.002 and BOMI 87.010. It can not be predicted whether the tracer travels through this low transmissivity zone at reduced velocities or whether it travels around this zone following distinct channels (*eg* between BOMI 87.008 and BOMI 87.010) which guide the tracers into the extraction borehole BOMI 87.010. A precise prediction of the geometry of the tracer flow field of dipole 1 would be very difficult, suggesting that the entire flow field could not be excavated by only two overcoring boreholes as in the former EP experiment (see Möri et al., 2004 for details). Missing data for interpretation and missing nuclide concentrations for the final mass balance between injected and recovered nuclide activity could be the result and additional site decontamination could then be necessary. On the other hand, this dipole showed good tracer recovery despite the expected low transmissivity zone (mainly due to the very good sink quality of borehole BOMI 87.010) and it showed reasonable tracer residence times.
- Dipole 2 between BOCR 00.003 (injection borehole) and BOCR 99.002 (extraction borehole) showed the same behaviour as dipole 1 with regard to the connection to the BOMI boreholes. Additionally, dipole 2 seems to be more suitable with regard to the prediction of the geometry of the flow field but the residence times of uranine were even lower than in dipole 1.
- Dipole 4 slightly increases the tracer residence time in the experimental shear zone but the disadvantages for the flow field prediction are increased and excavation would be more complicated compared to the other dipoles.

Dipole selection was also supported by the evaluation of the uranine breakthrough curves with TRANSIN II (see Guimera et al., 2004) as well as by predictive modelling of the migration behaviour of sorbing tracers in the frame of the modelling task of CRR. The models were run with matrix diffusion included and excluded. The results of these studies with regard to the dipole selection can be summarised as follows:

- Dispersivity in dipole 2 was found to be much less than in dipole 1 (implying the straight connection within dipole 2 predicted from hydro- and tracer testing may exist).
- The influence of matrix diffusion on the modelled breakthrough curves was found to be smaller in dipole 2 than in dipole 1, due to the short residence times of the tracer in the experimental shear zone and possibly also due to less fracture filling material (fault gouge material) that preferentially serves for “matrix” diffusion in fractures (see discussion in Möri et al., 2004).

Balancing the pros and cons of the three dipoles and taking into account the results of the homologue tracer test that were carried out in dipoles 1, 2 and 3 (see below), led to the selection of dipole 1 as the test dipole for the final actinide tracer experiments. Figure 3.5 shows a schematic drawing of the 2.23 m wide dipole 1. The representation of the borehole walls of the injection borehole BOCR 99.002 and the extraction borehole BOMI 87.010 is based on drillcore mapping and borehole imaging data. The dashed red line displays the interpolation of related fractures between the two boreholes. It is assumed that the major structures (fractures with apertures between 0.1 and 0.5 cm, marked as black horizontal lines in the Figure) are linked together by two flow paths and that flow occurs within these paths. The adjacent matrix and the mylonites bordering the flow paths are not involved in the transport of the tracers at the expected test duration around 1.2 hours (see Möri & Adler 2001 and Möri et al., 2004).

The selected test dipole 1 revealed a residence time for conservative tracers within the experimental shear zone flow field of less than 2 hours. This added a kinetic perspective to the discussion, *ie*, the selection of the injecting solution cannot be simply based on equilibrium or solubility arguments, but must also consider kinetic constraints (see also Smith et al., 2001). This is also important from the point of view of the representativity of the experiment for PA. Accompanying laboratory programmes were run in parallel in order to investigate the stability of the solutions and the sorption behaviour of the different radionuclides (*see* Missana & Geckeis, 2004).

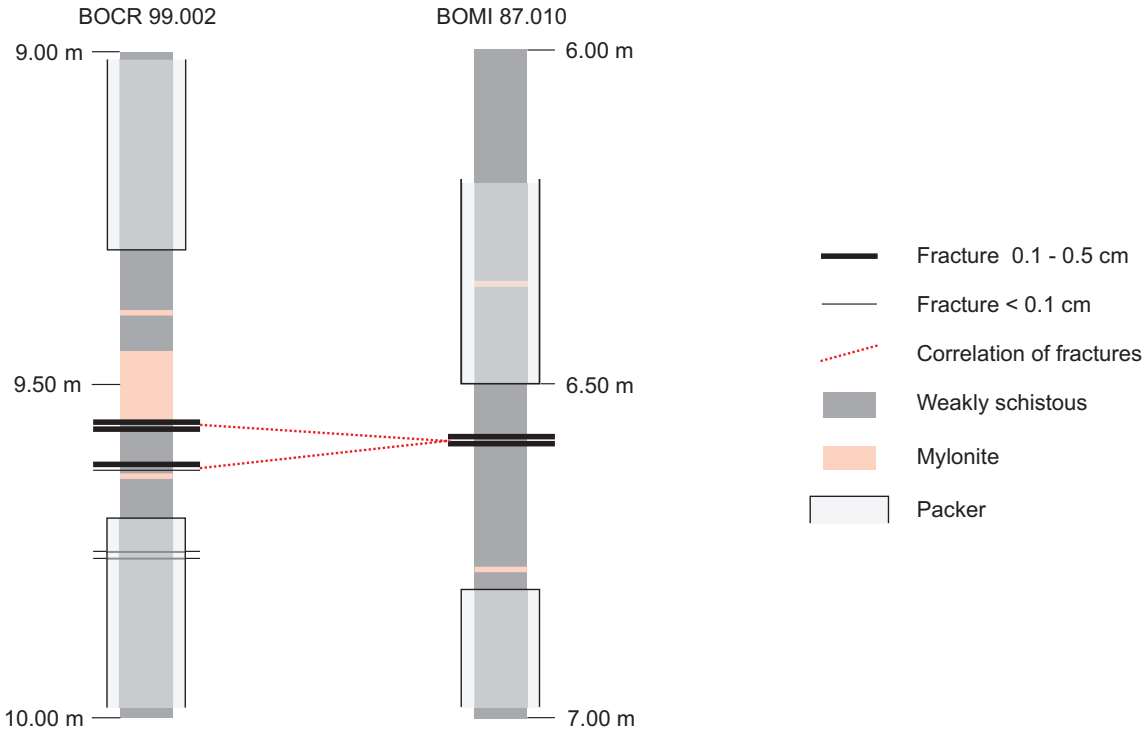

Fig. 3.5: Schematic overview of the packed off shear zone interval of dipole 1 (Figure not to scale)

3.2 Determination of the natural colloid background

The determination of the natural colloid background in the GTS groundwater is a key issue for the evaluation of bentonite colloid breakthrough curves and for the understanding of potential colloid formation in the injection cocktails. Therefore the colloid background was evaluated first in parallel to the preparatory homologue and colloid tests in dipole 3 (runs #6a and #7a) and in a separate colloid background study which took place after the main tracer tests in dipole 1 (see Hauser et al., 2003). In this study, the colloid concentration and the average size distribution of the colloids in the GTS groundwater of the CRR test site at different flow rates from 4 to 150 mL min^{-1} was determined. The LIBD *in situ* detection system was mounted in the gallery at AU96, next to the experimental shear zone. The mobile flow unit was connected to the outflow line of the extraction borehole of the CRR dipoles 1 and 3 and the complete instrumentation was installed in the tunnel close to borehole BOMI 87.010. pH, Eh, O_2 and conductivity of the outflowing groundwater were constantly measured. The LIBD detection cell requires a minimum constant flow rate of 4 mL min^{-1}, whereas the natural outflow at BOMI 87.010 ranges up to 150 mL min^{-1}. Therefore the outflow was divided in two parts: one passed through the detection cells for pH, Eh, O_2 and conductivity measurements and the second passed the LIBD with a constant flow rate of 4 mL min^{-1}. Variation of the flow rate was attained by adjusting the bypass valve. The groundwater outflow rates were set by a flow meter/flow controller device with flow rates from 4 to about 150 mL min^{-1}.

The groundwater outflow from BOMI 87.010 was reduced to the minimal flow of 4 mL min^{-1} 12 days before the test phase started. The higher flow rates were induced by opening the bypass valve step by step. After increasing the flow rate to the next step, it was important to wait with the following measurement until stable flow conditions had been established (constant concentration of background colloids, detected on-line with the LIBD) and the LIBD measurements usually started 5 hours after the desired flow rate had been set. In addition to the on-site measurements, samples were taken for laboratory analysis (LIBD, ICP-MS and SPC).

Additional measurements were made at borehole BOEM 85.012 and, for this, the entire test equipment had to be removed and transported to KWO's main access tunnel. The LIBD instrumentation was installed in a van, which was parked in a niche about 40 m from borehole BOEM 85.012. The geomonitoring unit with the flow controller was directly installed in a niche and the experimental shear zone was flushed for 18 hours at a flow rate of 180 mL min^{-1} prior to starting the measurements (initial hydraulic pressure of 33 bars). The investigated groundwater flow ranged from 4 mL min^{-1} to 954 mL min^{-1}, which is slightly below the upper detection limit of the flow meter.

3.2.1 Size and concentration of the natural colloid background

The background colloid concentration measured with the LIBD prior to the injection of the bentonite colloids in runs #6a and #7a (first study) was found to be about 5 μgL^{-1} and the average colloid sizes were in the range of 202 ± 12 nm. The particle size distribution in the GTS groundwater determined by single particle counting (SPC) analysis revealed also a maximum concentration of natural GTS groundwater colloids for size classes around 200 nm. Increases of the natural colloid concentration at the beginning of the measurements due to changes in the flow rates were eliminated after 1 h of constant flow conditions (see also Figure 3.10).

The values from the first study are in good agreement with the results from the second background study performed in dipole 1 at different flow rates (see Figure 3.6 and 3.7). The flow rates at the extraction borehole of dipole 1 were increased stepwise from 4 to 50, 100 and 150 mL min^{-1}. The scatter in the data at 50 mL min^{-1} represents short interruptions in the power

supply of the flow controller. Colloid concentrations were generally found to be in the range from 2 to 12 µgL^{-1}. The higher colloid concentrations at the beginning of the test seem to be related to mechanical stress in the flow field which was induced by pressure pulses generated during installation of the test setup. However, it appears that the colloid concentration was constant for flow rates of 50, 100 and 150 mL min^{-1}

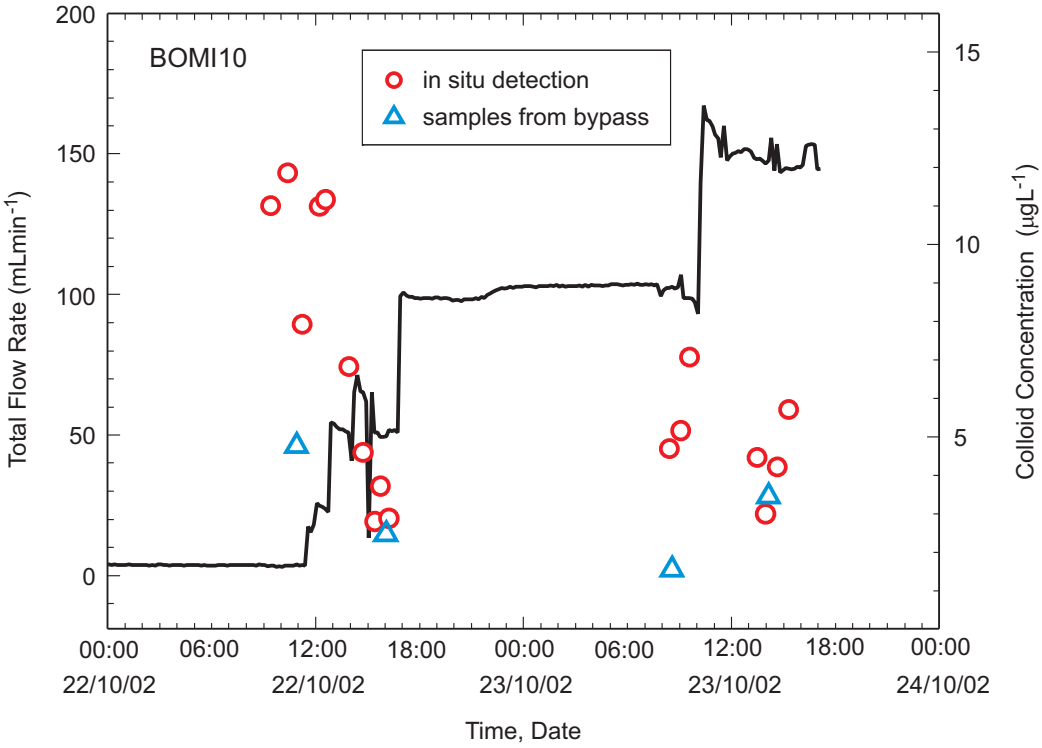

Fig. 3.6: Colloid concentrations in GTS groundwater at BOMI 87.010 at different flow rates (solid line)

Plotting the colloid mass concentration as a function of the flow rate (Figure 3.7 a) shows scattered data with a slight tendency to decrease and approach a steady state at the end of the experiment of around 4-5 µgL^{-1}. Aluminium concentrations[10] may also follow this trend. It is clear that an increase in flow rate up to 150 mL min^{-1} does not greatly influence the colloid population considerably. It is more likely that, despite the preceding flushing of the borehole prior to sampling, colloids were mobilised at the start of the experiments due to experimental manipulations and subsequently washed out to reach a steady state concentration.

Background colloid diameters detected under *in situ* conditions lie between 150 and 250 nm with an average at about 200 nm (Figure 3.7b) and correspond well with the colloid diameters determined during runs #6a and #7a (202 ± 12 nm). Somewhat larger diameter background colloids had been occasionally observed before run #7a due to a mechanical disturbance of the flow field.

It should be noted that the *in situ* detected colloid diameters are larger than those obtained from off-line analysis of samples in the laboratory (Figure 3.7a & b). This fact indicates that either the colloid population in the samples has been influenced during storage and transport or that

[10] Aluminium concentration was foreseen as an indicator for the determination of the bentonite colloid breakthrough as it is one of the major components in the FEBEX bentonite colloids.

sample handling in the laboratory caused this decrease in the average colloid size. A possible explanation could be a contamination of the GTS groundwater samples with smaller sized colloids leaching from the vial walls which, as a consequence, would decrease the average colloid size in the collected samples and thus lead to the somewhat smaller values for the colloid mass concentration measured in the laboratory. The LIBD method applied here is not able to account for colloid size distributions. Colloid populations and mass concentrations are therefore always related to colloidal species of a certain average size derived relative to a calibration with polystyrene reference colloids. Another explanation for the experimental finding might be that a part of the larger natural colloids disappeared due to sorption to the vial surfaces. Nevertheless, a clear reason for the different results of *in situ* and laboratory analyses is presently unavailable as such behaviour has never been observed during previous analyses with samples from the CRR experimental site.

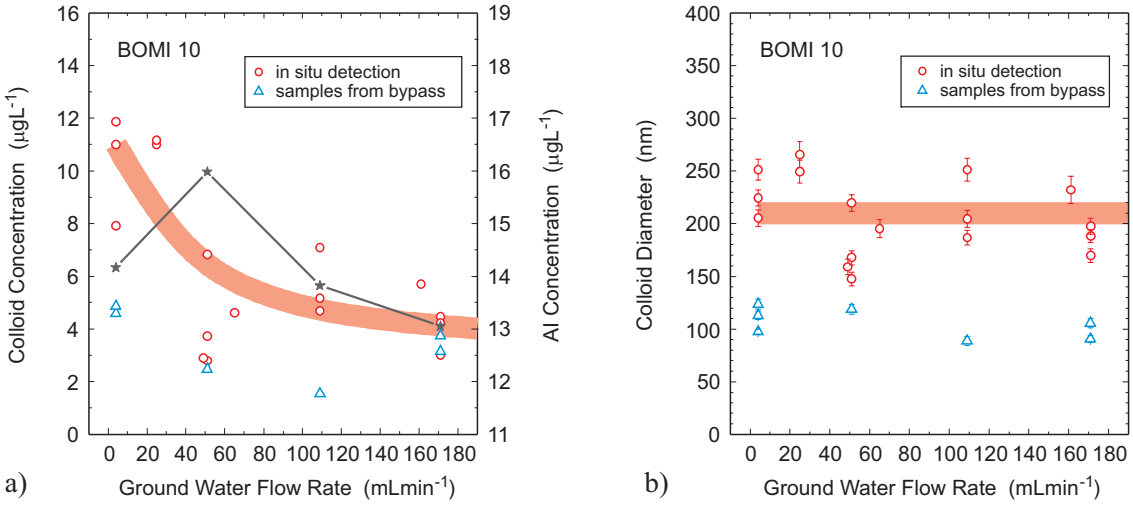

Fig. 3.7: a) Colloid concentration (o; Δ) and aluminium concentrations ✯and b) LIBD detected average colloid diameter

Figure 3.8 shows the time dependent variations of ground water flow rate and the colloid concentrations measured in BOEM 85.012. Initially, there is a clear decrease of the observed colloid concentrations with time, similar to that found at borehole BOMI 87.010. The decrease is, however, much clearer: colloid concentrations decline from 100 – 150 μgL^{-1} to < 50 μgL^{-1}. The change of the flow rate from 100 to 400 mL min^{-1} did not influence colloid concentration significantly. However, increasing the flow to very high rates of 900 mL min^{-1} leads to a clear increase in the colloid concentration to 170 μgL^{-1}.

The reason that the colloid concentrations are up to a factor of 30 higher than in the case of BOMI 87.010 is probably that the BOEM 85.012 borehole still contains a large reservoir of colloidal matter that can be mobilized while BOMI 87.010 has been flushed over a long period of dipole experiments and most mobile colloids have been washed out. Nevertheless, this additional flow rate experiment in BOEM 85.012 demonstrates the effect of erosion at very high ground water flow rates. The very last measurements, however, show again a decrease with time indicating that the mechanical stress induced in the experimental shear zone by the drastic increase of the flow rate has mobilised a quite high colloid amount, which then, in turn, is washed out. The question of whether a steady state colloid concentration is established, as observed in BOMI 87.010, cannot be answered from the present data. Longer observation periods are required.

In addition, the variations in analytical results for GTS groundwater colloids with time and groundwater flow indicate that a steady state is not achieved over the duration of the tests (for details see Hauser et al., 2003). A fully defensible value for the colloid background concentrations at unperturbed natural flow conditions in the borehole BOEM 85.012, therefore, cannot be given. They can only be determined in an experiment where the borehole has been intensively rinsed several days before sampling and detection.

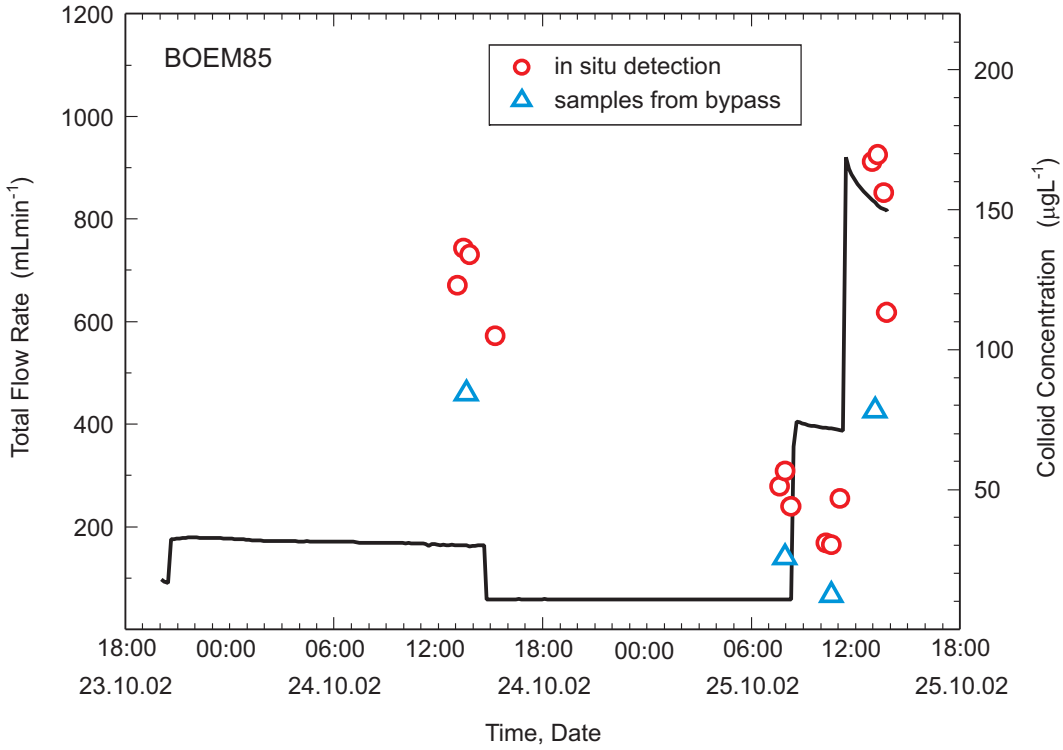

Fig. 3.8: Colloid concentrations in GTS groundwater at BOEM 85.012 at different flow rates (solid line)

3.2.2 Summary of natural colloid background studies

Colloid concentrations determined in the present study in dipoles 1 and 3 reveal that the colloid concentration in the GTS groundwater in the experimental shear zone is rather stable and does not significantly depend on steady state groundwater flow rates up to 150 mL min^{-1} nor does it show significant temporal fluctuations during the sampling period. The average colloid diameter was found to be around 200 nm and the colloid concentration around 5 μgL^{-1}.

Experiments at very high groundwater flow rates (900 mL min^{-1}) determined in an old borehole in the KWO access tunnel reveal a clear increase of colloid concentration indicating the wash-out of colloidal matter. In general, the variations in colloid concentration determined in the present study mainly depend on physical influences and on the borehole history.

Increased colloid concentrations observed temporarily at the beginning of the experiments are, thus, most likely, due to mechanical stress induced by pressure pulses generated during installation of the test setup.

Within the present study, it was found that the characteristics (size and concentration) of background colloids in the GTS groundwater may be influenced by the storage and transportation of the GTS groundwater samples. The reason for that is not clear, as earlier studies within CRR did not show this behaviour.

3.3 Preparatory tracer tests

Homologues are currently used for laboratory and *in situ* experiments in order to replace radionuclides. Besides similarities in their chemical behaviour with the radionuclide they substitute, they should also be as exotic as possible compared to the dominating GTS groundwater composition and analytical tools should be able to trace them also at very low concentrations. Interferences with other elements should be excluded. For the CRR experiment three homologues: ^{159}Tb, ^{178}Hf and ^{232}Th were used. Bentonite colloids were used only in dipole 3, as this dipole was not selected for the final tracer tests. Table 3.5 gives an overview of the different experiments that were carried out in dipoles 1, 2 and 3 with homologues and bentonite colloids. Uranine runs were performed for comparison of the breakthrough curves before and after each homologue injection (*ie* to check for hydraulic stability *etc*).

Tab. 3.5: Homologue and bentonite colloid pre tests

Dipole	**Length** [m]	**Injection / extraction borehole**	**Flow rates (in/out)** [mL min^{-1}]	**Number of run where this dipole was tested and type of tracer composition**	
D-1	2.23	BOCR 99.002/ BOMI 87.010	10/150	run #13	uranine
			10/150	run #14	homologues
D-2	1.71	BOCR 00.003/ BOCR 99.002	10/150	run #9	uranine
			10/150	run #10	homologues
			10/150	run #11	uranine
D-3	5.25	BOMI 87.008/ BOMI 87.010	10/150	run #6 & 7	uranine
			10/150	run #6a	bentonite colloids
			10/150	run #7a	bentonite colloids with homologues
			10/150	run #8	uranine
			10/150	run #15	homologues
			10/150	run #16	uranine

3.3.1 Bentonite colloid migration

Two *in situ* injections with bentonite colloids were performed in the frame of the preparatory tracer tests. Both runs took place in the 5.25 m long dipole 3. Run #6a was performed with a suspension of FEBEX bentonite colloids in GTS groundwater in the absence of any other tracers. In run #7a, the same colloid suspension was injected together with the three homologue elements in order to check the influence of the colloids on the breakthrough of these strongly sorbing elements. Run #6a, the "pure" bentonite colloid run, is discussed below while run #7a is presented in the section on homologues, below.

The breakthrough of the injected bentonite colloids was detected on-line and occasionally also off-line with the LIBD. ICP-MS samples were taken at certain time intervals in order to determine the aluminium content in the water samples. Single particle counting of colloids in collected samples was also carried out in the laboratory.

3.3.1.1 Preparation of bentonite colloid suspension

The FEBEX bentonite used in this study is so called because it has been used in the FEBEX project at the GTS (see Huertas et al., 2000, for details) and it has been proposed as a potential backfill material in the Spanish HLW repository design. FEBEX bentonite is mainly composed of Ca smectite (> 90 wt%) with accessory minerals quartz, cristobalite, feldspar and calcite (ENRESA, 1998). A batch solution of colloids was prepared at FZK by repeatedly washing FEBEX bentonite with GTS groundwater. The bentonite colloid suspension was prepared by five consecutive centrifugation steps (4000 rpm for 40 minutes), decanting of the supernatant and re-suspension in GTS groundwater. The colloid dispersion remained stable for several weeks, as confirmed by photon correlation spectroscopy. 200 mL of the injection solution was prepared by diluting the stock solution to a final colloid concentration of 20 µg mL^{-1} under Ar-atmosphere. The colloid solution remained at pH 9.5, almost identical to the value of the original GTS groundwater (pH 9.6). The colloid injection was made up to a volume of 101 mL, corresponding to a total amount of 2.02 mg of bentonite colloids.

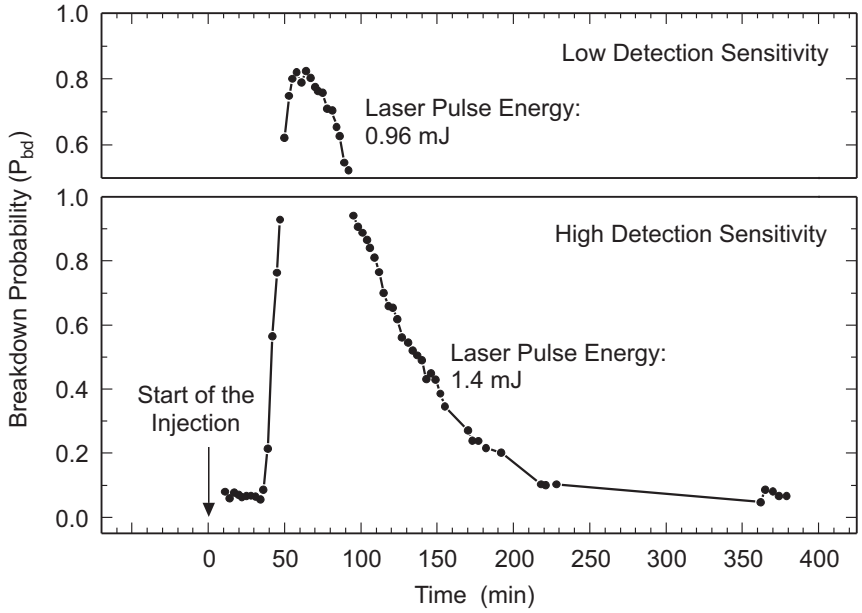

Fig. 3.9: Colloid migration breakthrough monitored on-line by the LIBD breakdown probability

3.3.1.2 LIBD measurements

Figure 3.9 shows the breakthrough of the bentonite colloids. After the colloid injection, the breakdown probability was detected in the range of 5-10% at a high detection sensitivity mode of LIBD (*ie* applying higher laser energy). These signals are attributed to the natural colloid background in the GTS groundwater under the given flow condition and appear significantly above the value of the ultra-pure water. The first arrival of bentonite colloids was observed 40

minutes after the injection. Before reaching the concentration maximum, the breakdown probability approached its saturation state and at this stage the LIBD switched to a lower detection sensitivity mode (applying lower laser energy). The peak colloid concentration was reached after 60 minutes and the concentration of extracted bentonite colloids decreases slowly to background level of GTS groundwater colloids at about 250 minutes. The background levels before the injection and after the completion of bentonite colloid extraction were found to be the same.

Based on the 2-D spatial distribution of breakdown events along the laser beam axis as determined by image-processing of the data obtained by off-line measurements, the average colloid size and concentration were appraised quantitatively. The measurements were performed off-line, partly *in situ* and partly in the laboratory. The results are illustrated in Figure 3.10.

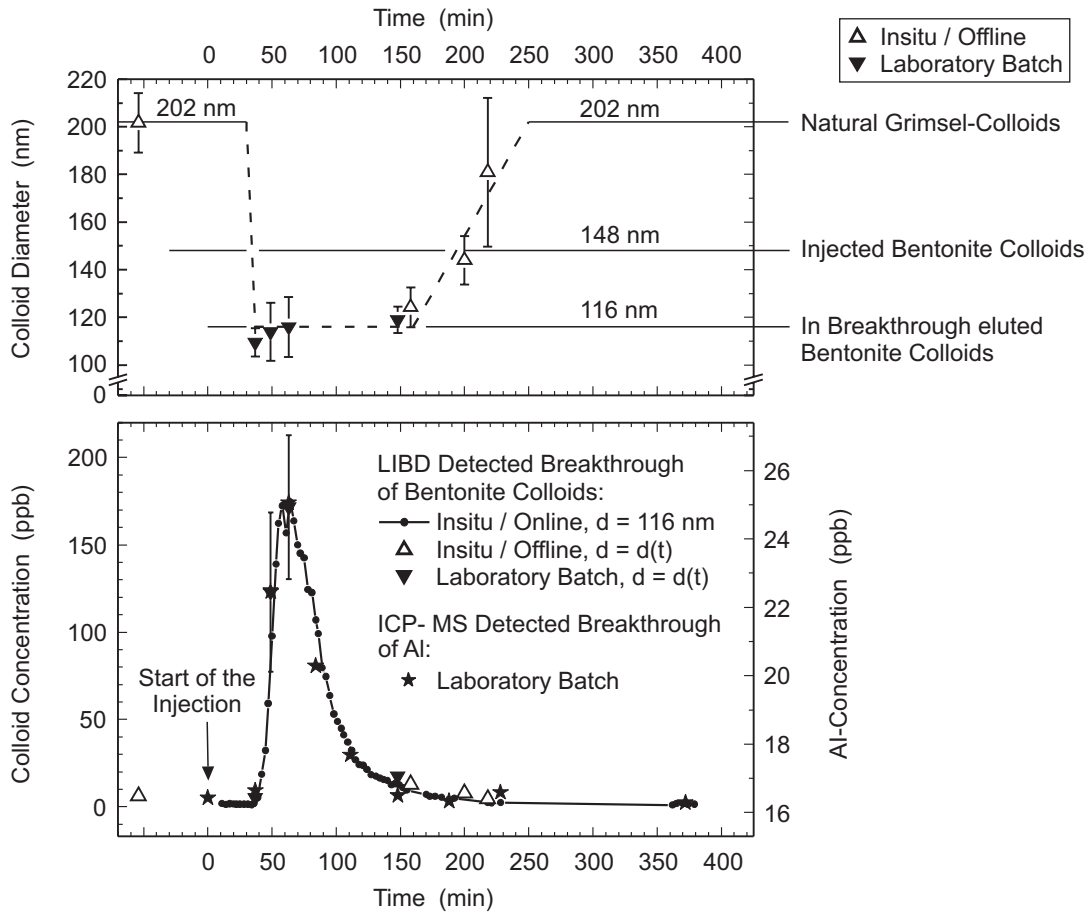

Fig. 3.10: Colloid diameter and concentration in the bentonite colloid migration experiment

The background colloids in the GTS groundwater extracted before the breakthrough of the injected bentonite colloids showed an average size of 202 ± 12 nm (see above). The average size of the extracted bentonite colloids was found to be 116 ± 12 nm, which is lower than the value of the initial colloid dispersion of 148 ± 8 nm. The maximum concentration of the extracted colloids was found to be 175 ± 20 ppb. Increase in the colloid concentration due to changes in the flow rates were eliminated after 1 h of constant flow conditions.

Batch samples collected during the field-experiment were later analysed by ICP-MS for the aluminium content. The breakthrough patterns of the colloid concentration determined by both

LIBD and ICP-MS are in good agreement with each other, as shown in Figure 3.10 (lower part). This indicates that, in the GTS groundwater system, aluminium can be taken as an appropriate indicator for the bentonite colloids.

The recovery of the extracted bentonite colloid fraction relative to the injected mass concentration was evaluated by integrating the breakthrough curve (after subtracting the natural background level of colloids in the GTS groundwater). The recovery, obtained from both LIBD and ICP-MS, is calculated to be identical at 55 ± 5% by mass.

3.3.1.3 Bentonite colloid and uranine breakthrough

The peak maximum of the bentonite colloids arrived after about 60 minutes, slightly earlier than the uranine peak in the preceding injection (run #6) in the same flow field (Figure 3.11). The tailing of the uranine curve is also more pronounced than for the bentonite colloids. This observation can be interpreted as concentration of the colloids in the centre of the flow stream (where higher velocities occur) or, and more likely, to the fact that uranine has access to small pores in both the rock matrix and the fault gouge[11] while the 50 to 400 nm particles of the bentonite colloids have not. This is confirmed by the fact that the uranine curve showed a broader tailing than found for the colloid breakthrough, indicating size or charge exclusion of the colloids leading to considerably less diffusion of bentonite colloids into the pores of the fracture infill and granodiorite matrix.

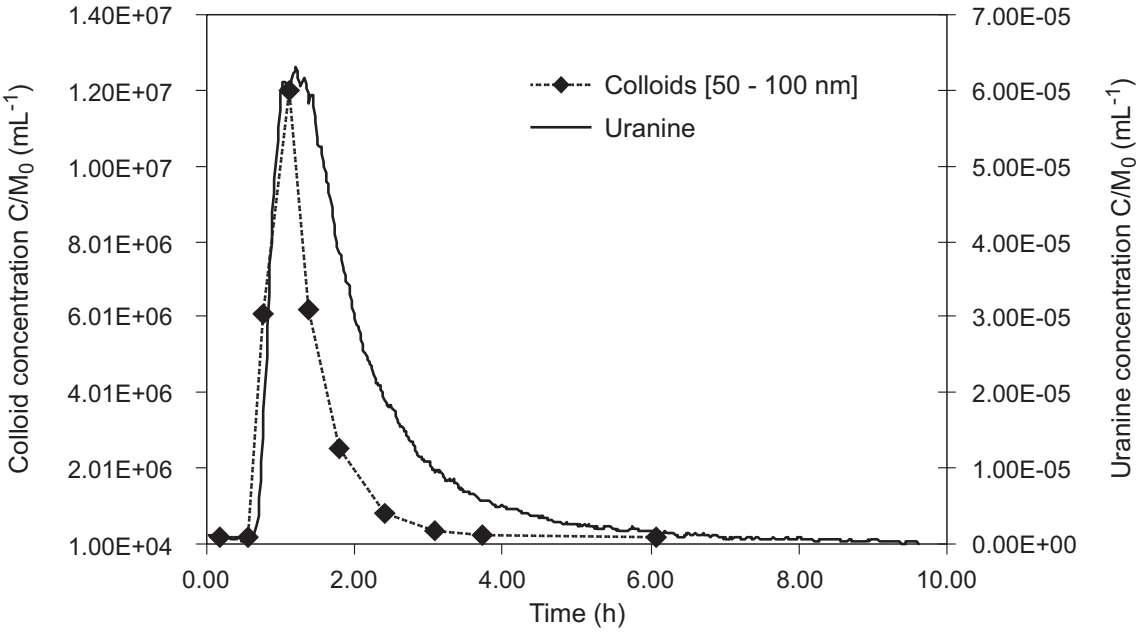

Fig. 3.11: Comparison of colloids and uranine breakthrough curve in dipole 3 (5 m)

3.3.1.4 SPC measurements

The particle size distribution in the GTS groundwater samples and the bentonite colloid solution are given in Figure 3.12. Clearly the colloid concentration background in the MilliQ water is

[11] Smith et al., (2001) noted evidence for uranine retardation in the same shear zone.

well below that in the GTS groundwater (see Figure 3.12, data points for samples taken at 0.18 and 6.08 h after injection) which itself is, for the small sizes, well below that in the samples collected during breakthrough (samples between 0.18 and 6.08 h), which finally is also below that in the starting suspension (bentonite in Figure 3.12). In the breakthrough samples and the starting solution, the majority of the colloid population (normalised by the injection mass, in mL^{-1}) is in the classes 50-100 (79%) and 100-150 (20%). The fraction of colloids is 1% for the class 150-200 nm.

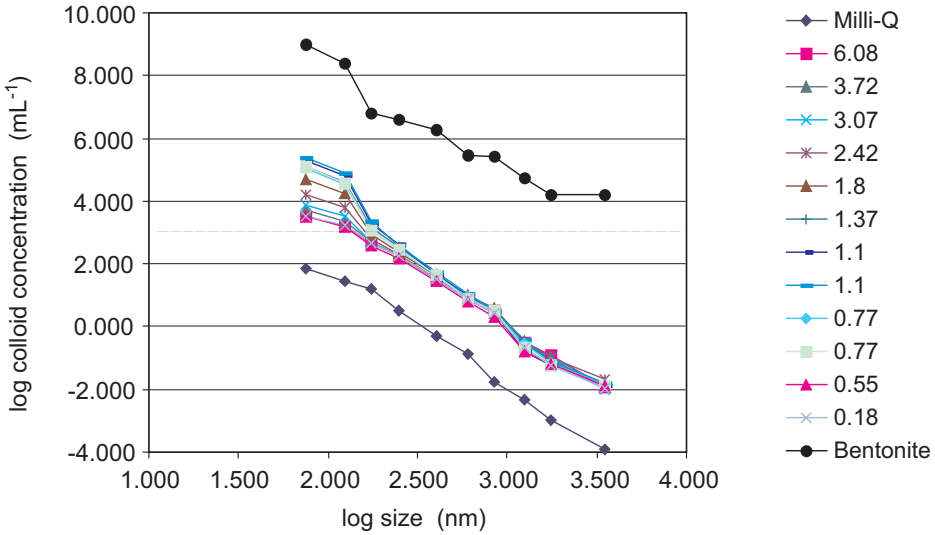

Fig. 3.12: Colloid size distribution in the studied samples [12]

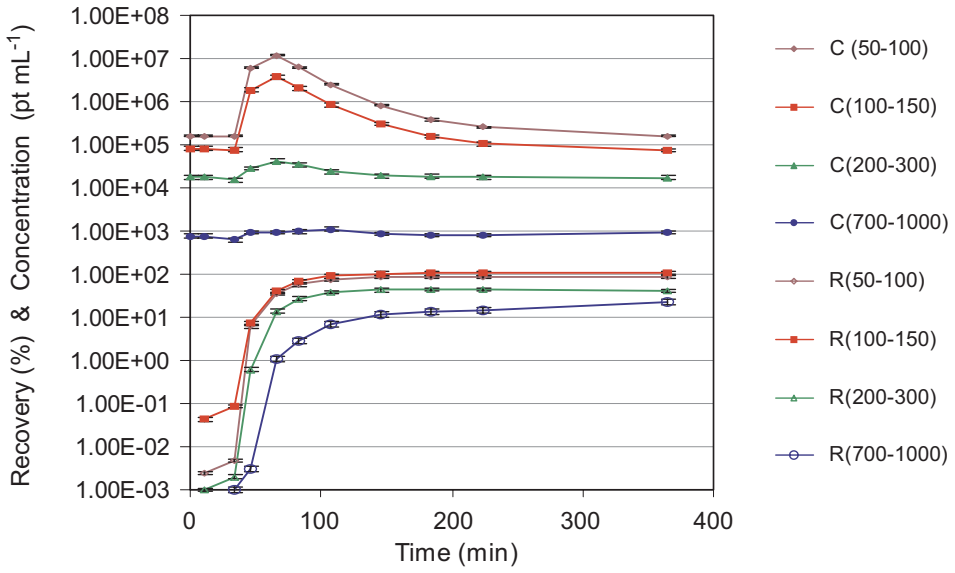

Fig. 3.13: Breakthrough (C) and recovery (R) curves of the bentonite colloids for 50-100, 100-150, 200-300 and 700-1000 nm size classes [13]

[12] Note: the colloid size corresponds to the average size and the normalised concentration is calculated per size class. The slope of the GTS groundwater colloid distribution is around –4, as found earlier during the Grimsel colloid exercise (see Degueldre et al., 1990 for details).

The recovery curve for the bentonite colloids can be determined on a class by class basis. Figure 3.13 shows that, after 6.08 h, the recovery of the colloids for the size class 50-100 nm is 98.3 and that for the 100 – 150 nm class is 108%. For larger size classes, a decrease in recovery to 44% for the 200 – 300 nm colloids and to 22% for the 700 – 1000 nm colloids is observed, giving a preliminary indication for filtration effects in the experimental shear zone.

3.3.2 Homologue migration

Four homologue tracer tests were performed in the experimental shear zone: run #14 in dipole 1 (2.23 m), run #10 in dipole 2 (1.71 m) and run #15 and #7a in dipole 3 (5.25 m), the last in presence of 20 mgL^{-1} bentonite colloids (see above).

The main aim of these homologue injections was to study the migration behaviour of the polyvalent metal ions which are considered as strongly sorbing tracers in the absence of bentonite colloids and to improve the *in situ* methodology for tracer testing with strongly sorbing tracers. The homologue samples collected at the extraction borehole were analysed off-site by ICP-MS.

3.3.2.1 Preparation of homologue tracer cocktails

The homologue tracer cocktails were prepared at FZK using GTS groundwater as solute. The concentration of ^{159}Tb, ^{178}Hf and ^{232}Th in the injection cocktails for run #10, #14 and #15 (see Table 2.3 for details) was kept in the range of the recommended solubilities for the trivalent actinides and of ^{232}Th as given in Duro (2000). For trivalent ^{159}Tb, the final concentration in the cocktail lies a factor of 10 below the solubility limit predicted for ^{243}Am. Small aliquots of acidic stock solutions of the respective elements were spiked to the GTS groundwater, causing no change in the pH of the GTS groundwater. Even though the thermodynamic solubility limits were not exceeded in the final solution, temporary oversaturation leading to colloid formation due to the spiking procedure cannot be excluded. The speciation of the elements under investigation, therefore, is ambiguous.

Recent studies on the solubility of amorphous $Th(OH)_4$ using LIBD reveal the onset of colloid formation even below supposed solubility limits (see Neck et al., 2002). The "true solubility" of, especially, tetravalent ^{178}Hf and actinides in alkaline conditions, *ie* the concentration where these elements exist as mono-nuclear $Me(OH)_4$ species, might clearly be lower than assumed in predictions based on available thermodynamic data[14]. This makes clear that the solution chemistry of the actinides in the near neutral pH range might be widely dominated by colloidal species. Due to the presence of natural colloids in GTS groundwater, the sorption of ^{159}Tb, ^{232}Th and ^{178}Hf on these colloids also cannot be excluded. Ultracentrifugation of the injection cocktail for run #15 suggests a considerable fraction of the tracer elements to be indeed colloid-borne.

In run #7a, the homologue elements were oversaturated, according to the thermodynamic solubility data reported in Duro (2000) which assumes the absence of colloids. However, the addition of 20 mgL^{-1} of bentonite colloids appears to prevent the formation of precipitates or the formation of oxide/hydroxide colloids as ultracentrifugation indicated that all of the homologue elements were associated with the bentonite colloids.

---

13 The error on the concentration is around 4% for the 50-100 nm size range but increases to 15% for larger colloids and particles, the precision for recovery is 8% and 25% respectively.

14 This is something which has been observed many times over the last 15 years in thermodynamic database testing in natural analogue studies (see, for example,Alexander et al., 1992, Linklater et al., 1996, and Miller et al., 2000)

3.3.2.2 Homologue tracer test in dipole 1

The experimental data for the three homologues reveal breakthrough behaviour close to that of uranine (see Figure 3.14). The tailing in the homologue and uranine curves show almost identical shapes. The peak time of the homologue curve was slightly earlier compared to that of uranine. This behaviour was also observed in the bentonite colloid experiment #6a even if in run #14 the homologues were injected without adding bentonite colloids and the concentration was below the calculated solubility values at the given pH of the solution (see discussion above). However, the broader tailing for uranine compared to that of the bentonite colloids observed in run #6a was not observed in run #14, which might be a result of a decreased size of the colloids produced by the homologues.

Based on mass balance calculations, the recovery for ^{232}Th was 45 %, for ^{178}Hf 39% and for ^{159}Tb 32 %. The PEEK injection tubing was treated with nitric acid and the sorbed ^{232}Th, ^{178}Hf and ^{159}Tb was analysed: 64 ng ^{232}Th, 6 ng ^{178}Hf and 29 ng ^{159}Tb were found in the acid, corresponding to 27 % of the injected ^{159}Tb, 3 % of the ^{178}Hf and 16 % of the ^{232}Th, giving total recoveries of 44 % of the ^{159}Tb, 40.2 % of the ^{178}Hf and 61 % of the ^{232}Th.

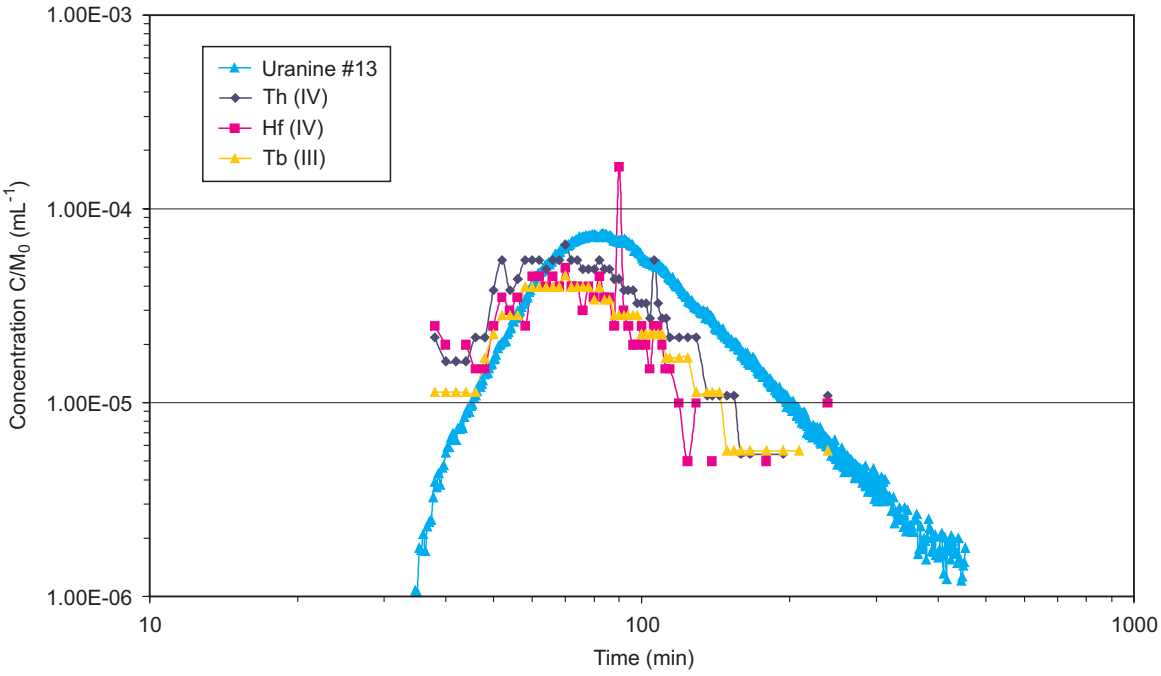

Fig. 3.14: Tracer breakthrough curves of homologues (run #14) and uranine (run #13) in dipole 1

The faster transport compared to uranine was previously observed in the colloid test #6a in dipole 3 where it was assumed that colloids would travel in the centre of the flow stream and colloid diffusion into the surrounding pores is hindered due to size effects but not for the uranine and therefore uranine would be slightly retarded. This is supported by the markedly longer tail of the uranine breakthrough curve. However, even if the homologues were injected without adding bentonite colloids it must be assumed that homogeneous or heterogeneous homologue colloids could have formed in the vial, or later within the dipole flow field, so accentuating the difference in the homologue and uranine breakthrough curves. The formation of heterogeneous homologue colloids can not be ruled out, even if the background concentration

of natural colloids in GTS groundwater is quite low (see Degueldre et al., 1990 and natural colloid background studies in this report). On the other hand, even though the homologues were added below their calculated thermodynamic solubility limit, it is also possible that they formed homogeneous oxyhydroxide colloids under "real" conditions. Whether homogeneous colloids or heterogeneous colloids were formed can not be determined.

3.3.2.3 Homologue tracer test in dipole 2

Preceding tracer testing with uranine revealed that dipole 2 appears to have a very direct connection between the inlet and the outlet borehole, resulting in very short shear zone residence times of conservative tracer of the order of 10 to 15 minutes. It was therefore decided to inject the three sorbing homologues without bentonite colloids into this dipole in order to find out if sugnificant retardation of the metal ions can be observed during the relatively short residence time within this dipole. 73.6 mL of a solution consisting of 4.0E-09 mol^{L-1} ^{232}Th, 5.0E-09 $molL^{-1}$ ^{178}Hf and 6.9E-09 $molL^{-1}$ ^{159}Tb in GTS groundwater were injected. As can be seen in Figure 3.15, a major fraction of the tracer elements was recovered with no retardation. The previously observed faster breakthrough of the bentonite colloids in dipole 3 or of the homologues in dipole 1 compared to uranine was not observed in this dipole. The recovery of the tetravalent elements ^{232}Th and ^{178}Hf was around 70 % and that of trivalant ^{159}Tb was 27 %.

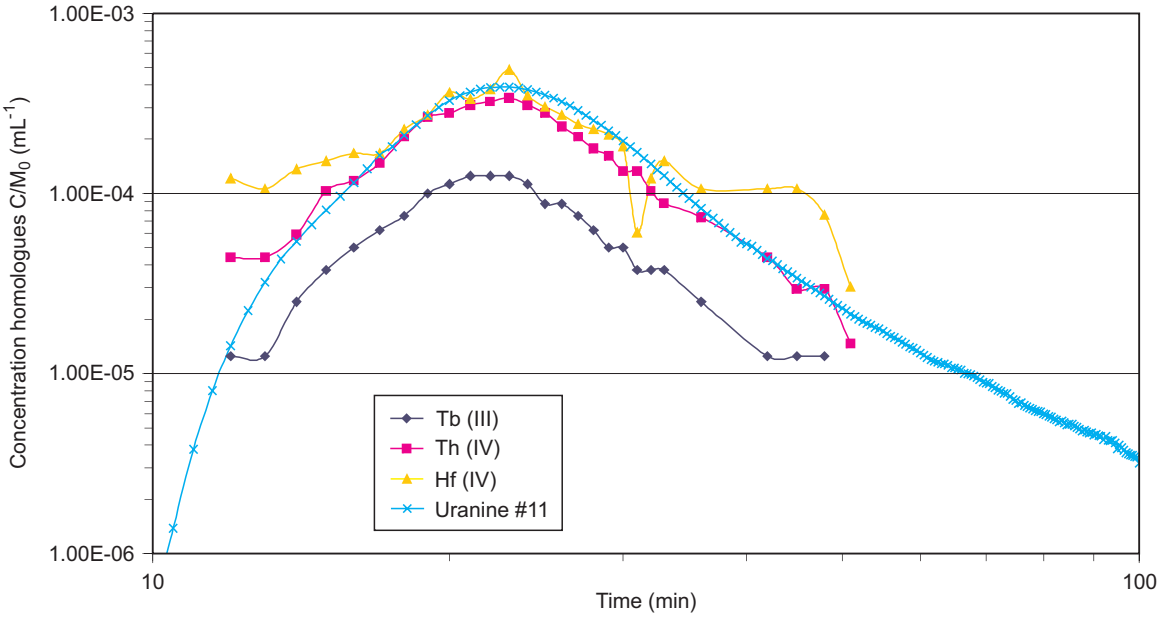

Fig. 3.15: Tracer breakthrough curves of homologues and uranine (run #11) in dipole 2

The high recoveries of the sorbing tetravalent metals (70% for tetravalent homologues and 27% for ^{159}Tb) might again imply the occurrence of colloid-mediated migration, even though no bentonite colloids have been added. Another explanation for the observed behaviour could be sorption kinetics which hinders the retardation of the metals within the experimental time scale of this second dipole (about 22 minutes peak time). The reason for the discrepancy between ^{159}Tb and the tetravalent homologues is not yet clear. Different kinetic properties of sorption on fracture filling material and/or different reversibility of sorption on colloids and/or fracture filling material might influence the recovery. There are, however, hints that the ^{159}Tb and ^{232}Th undergo considerable interaction with the surface of the PEEK capillary (see findings in run

#14, where about 27% of the injected ^{159}Tb and 16 % of ^{232}Th were found sorbed on the PEEK tubing) and therefore ^{159}Tb and ^{232}Th recovery data have to be treated carefully and should not be over-interpreted.

3.3.2.4 Homologue tracer tests in dipole 3

The experimental data reveal that the homologue breakthrough behaviour is comparable to that of uranine (Figure 3.16), even if the homologues arrived slightly earlier than the uranine. Compared to the results obtained for uranine, a clearly reduced recovery for ^{178}Hf, ^{232}Th and ^{159}Tb is observed at 26%, 29% and 23% respectively. Under the simple assumption that sorption to the PEEK line was the same as for run #14 in dipole 1, this would mean that 32% of the ^{159}Tb, 27% of the ^{178}Hf and 34% of the ^{232}Th that reached the fracture passed through without any retardation.

^{178}Hf and ^{232}Th peak concentration was about 3 times higher in the experiment with bentonite colloids compared to the run without added colloids. ^{159}Tb showed almost the same breakthrough behaviour in the presence and absence of colloids (see run #7a).

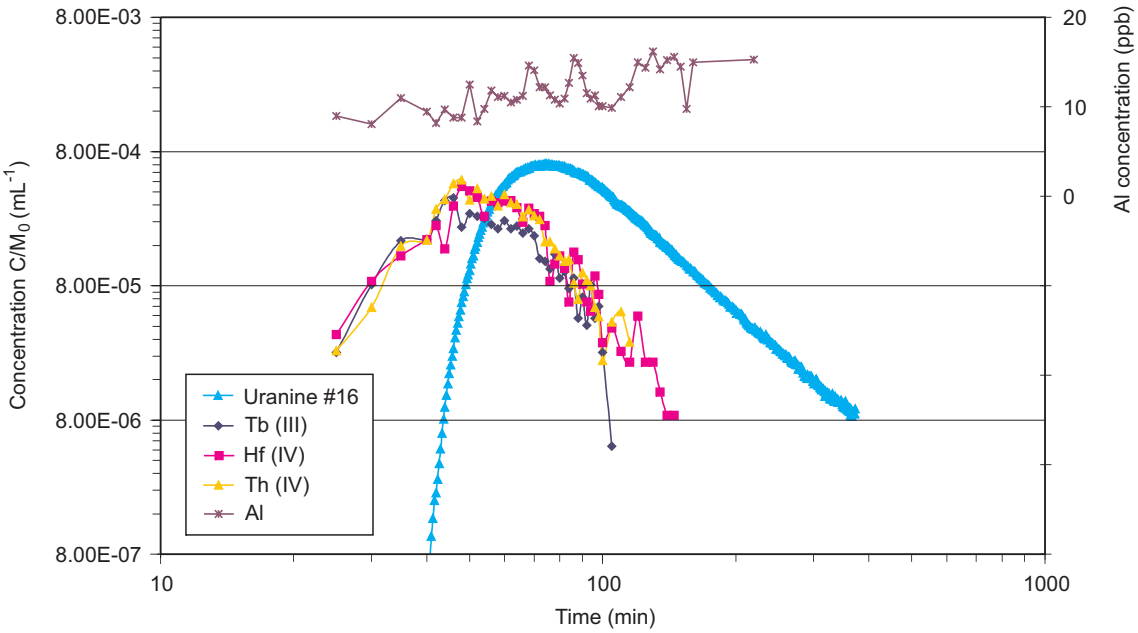

Fig. 3.16: Tracer breakthrough curves of homologues (run #15) and uranine (run #16) in dipole 3 including aluminium concentration in the GTS groundwater

The colloid suspension for run #7a was prepared in the same manner as run #6a, but spiked with ^{178}Hf, ^{232}Th and ^{159}Tb to a final concentration of 30 ppb for each element. For spiking, a solution containing 1000 µg mL^{-1} of each element in 1 M HNO_3 was diluted with distilled water 50 fold to pH 1.7 for using as a stock solution. To 200 mL of the GTS groundwater containing 20 ppm bentonite colloids, 300 µL of the stock solution was added on shaking, thus resulting in the final molar concentration of 1.3E-07 molL^{-1} for ^{232}Th, 1.7E-07 molL^{-1} for ^{178}Hf and 1.9E-07 molL^{-1} for ^{159}Tb. Addition of the tracer solution caused no change to the GTS groundwater pH (within 0.2 units). According to the calculated thermodynamic solubility of each tracer element, the final concentrations of these elements are, in the absence of colloids, in a state of over saturation at the given pH. This procedure was selected as all tracer elements were expected to be sorbed

quantitatively onto bentonite colloids after spiking and as an increased element concentrations in the tracer solution facilitates the element analysis. The disadvantage was that the chemical states of the sorbed homologues were not known (colloidal or ionic form). The injected volume of traced colloidal dispersion is 82.5 mL.

Colloid analysis was conducted on-line by LIBD with some samples checked off-line. Samples were transported to the laboratory for trace element and aluminium analysis by ICP-MS after acidifying with HNO_3. As shown in Figure 3.17, each of the breakthrough curves for aluminium, ^{232}Th, ^{178}Hf and ^{159}Tb determined by ICP-MS are in good agreement with one another and also in good accordance with the bentonite colloid breakthrough determined by LIBD. The results indicate that the homologue migration in the presence of colloids under the present experimental conditions is facilitated by bentonite colloids acting as a carrier.

The calculated colloid recovery was 56 ± 6 %, which corresponds to the value of run #6a. The evaluation of the colloid recovery by measuring the aluminium concentration is hampered by relatively large scatter in the data and lies in a range of 37 to 47 %. Recoveries for both tetravalent elements, ^{232}Th and ^{178}Hf, were 78 ± 8 %, which is significantly higher than the recovery of the bentonite colloids. The recovery for ^{159}Tb was considerably lower at 33 ± 3 %. There is, up to now, no explanation for this behaviour of ^{159}Tb.

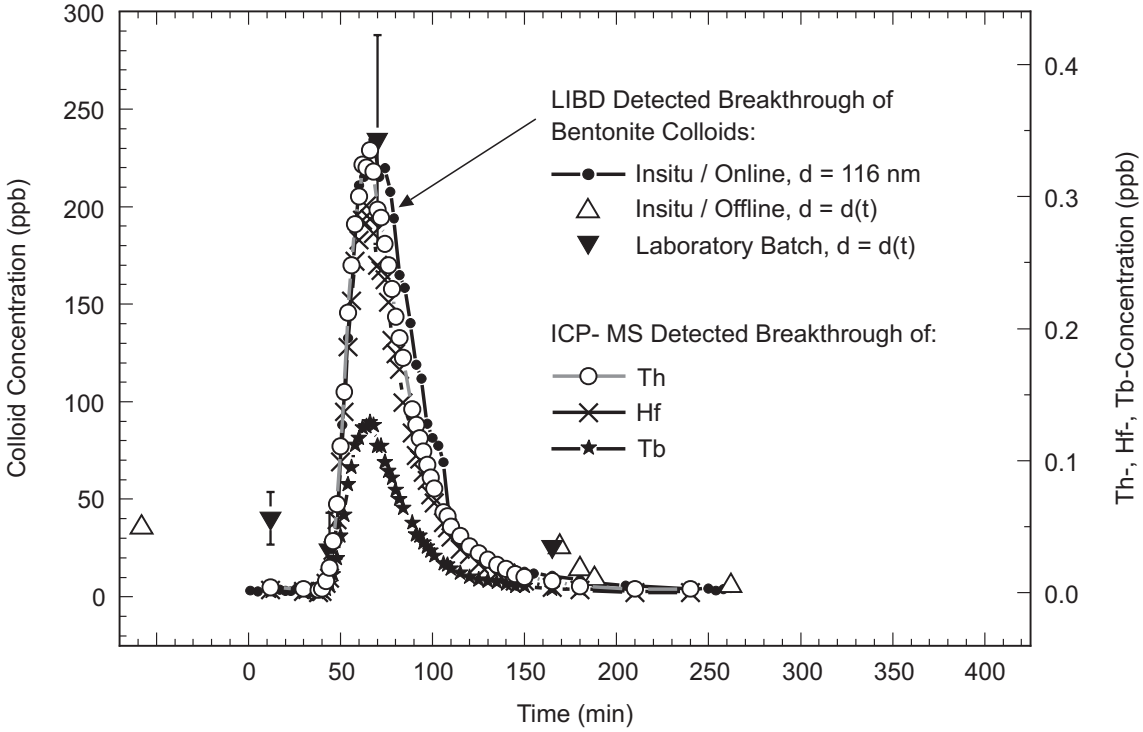

Fig. 3.17: Bentonite colloid and homologue breakthrough curves in run #7 (dipole 3)

Homologue tracer recovery in dipole 3 in the presence of bentonite colloids was found to be greater in the case of the tetravalent homologues (78 % compared with ^{178}Hf 27 % and ^{232}Th 34 % without bentonite colloids). The colloid recovery was almost the same as for the colloid injection #6a, where no homologues were added, but it was smaller than for the tetravalent homologues. This discrepancy can be explained by the fact that the metal ion loading onto colloids depends on their surface area. As shown in this experiment, bentonite colloids

underwent a change in their average size towards smaller diameters (from 148 ± 8 nm in the initial colloid dispersion to 116 ± 12 nm in the breakthrough) and hence a larger surface area results for the same mass concentration. In order to corroborate this assumption, the total "recovered colloid surface" was compared with the total surface of the injected particles. Assuming a spherical geometry of the injected colloids (148 nm) and a total mass of 1.65 mg, their total surface is 2.5E-08 cm^2. For the extracted bentonite colloid fraction (56 ± 6%) with an average colloid size of 116 nm, the total surface is calculated to be 1.8E-08 cm^2, which corresponds to a recovered surface area of ~ 72%. This value is very close to the recovery of ^{232}Th and ^{178}Hf, which may thus explain the discrepancy between the mass fraction recovery obtained for colloids and the concentration fraction recovered for ^{232}Th and ^{178}Hf. Again, trivalent ^{159}Tb did not behave like the other two homologues and showed a recovery of only 33% in the presence of bentonite colloids. One possible explanation for this behaviour might be that ^{159}Tb ions have a reduced sorption affinity on bentonite colloids compared to the tetravalent metal ions. For this reason, the ^{159}Tb ions sorbed onto colloids may be dissociated in the course of migration and sorbed on the rock matrix surface as well as on the surface of experimental equipment. For the moment, this may explain the low recovery obtained for this metal ion, but this has to be checked in the laboratory.

3.3.3 ^{82}Br and ^{85}Sr migration

^{82}Br and ^{85}Sr were injected into dipole 1 together with uranine. The injection of the two active tracers was intended to:

- test the experimental setup, including the HPGe detectors, pumps and the radioprotection measures for the final *in situ* tracer experiments,
- compare the breakthrough curves of uranine and ^{82}Br (both conservative tracers) in order to replace the uranine with ^{82}Br in the actinide injections if possible (uranine molecules could possibly interact with the actinides in the final tracer cocktail) and
- investigate the migration behaviour of the moderately sorbing ^{85}Sr in dipole 1 in order to compare this result with results from the MI experiment where the same tracer was injected into a 1.7 m dipole in the same shear zone (see Frick et al., 1992 and Smith et al., 2001, for details).

Figure 3.18 shows the almost identical peak arrival time for uranine and ^{82}Br, with a slightly earlier arrival of the uranine. The tailing of both tracers is identical. In agreement with the previous observations of Frick et al., (1992) and Smith et al., (2001), ^{82}Br can therefore be used as a substitute for uranine in the main injections. Also in agreement with previous experimental work at the site, ^{85}Sr shows some degree of retardation with lower peak height and later peak arrival time compared to uranine and ^{82}Br in dipole 1. The experimental setup, the on-line measurements of the γ-emitting radionuclides as well as the radioprotection measures worked faultlessly and could therefore be applied in the final tracer tests.

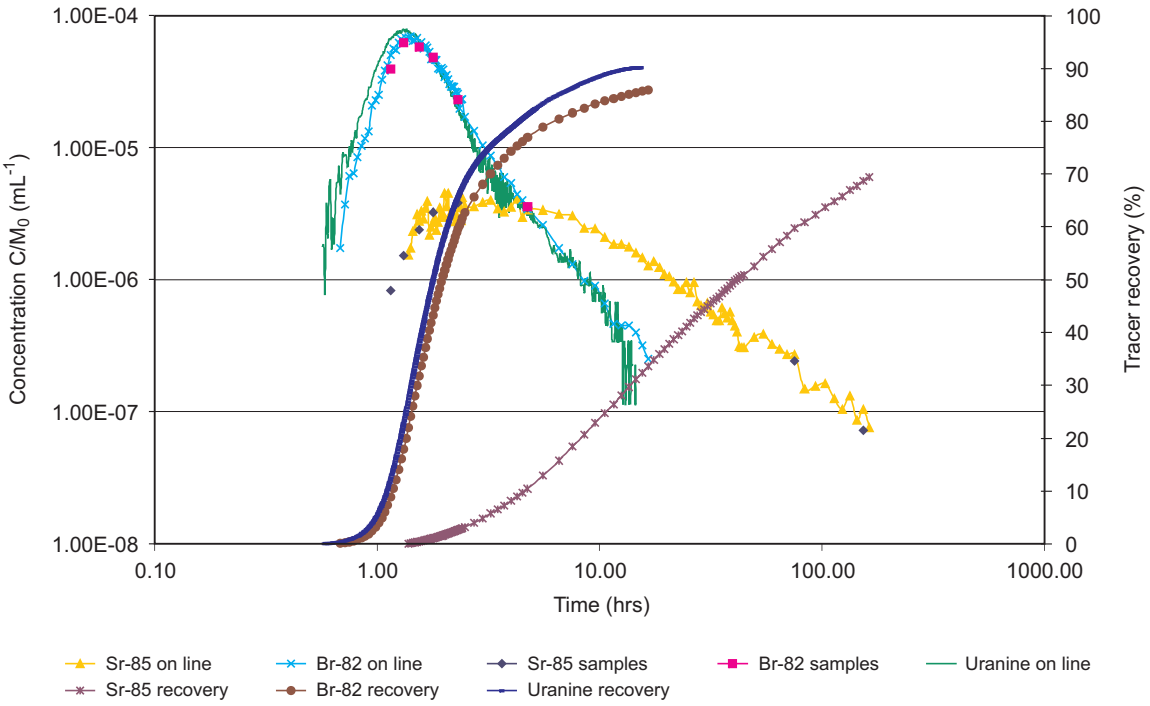

Fig. 3.18: Tracer breakthrough curves and recovery of uranine, ^{82}Br and ^{85}Sr

3.3.4 Summary of preparatory tracer tests

3.3.4.1 Colloid testing

The results of the preparatory tracer tests confirmed that the experimental shear zone is suitable for migration tests with bentonite colloids as well as with conservative and reactive tracers. The colloid dispersion which was produced by washing FEBEX bentonite with GTS groundwater remained stable for several weeks in the laboratory. The on-site LIBD measurements proved to be a very powerful tool for simultaneously monitoring colloid breakthrough in the GTS groundwater and subsequent size analysis of the GTS groundwater colloids. The breakthrough curves of the colloids which were derived from the LIBD measurements were independently confirmed with ICP-MS aluminium concentration data in the samples (in terms of recovery and shape/position of the breakthrough curve). The combination of on-line data with analysis of backup samples revealed the possibility of cross checking the field measurements (*eg* determination of aluminium content for the evaluation of the colloid content in the GTS groundwater or determining the average size or the size class distribution by off-site analysis with LIBD and SPC methods).

The natural colloid background in the GTS groundwater of the experimental shear zone was around 5 ppb. Perturbations in the flow field conditions due to manipulating the experimental setup revealed a measurable increase in the background colloid concentration for about one hour before the original background values were re-attained. The average size of natural GTS groundwater colloids was found to be about 200 nm. This relatively large colloid size infers that the forced hydrodynamic flow of GTS groundwater in the fracture zone due to the dipole flow field might have induced enough mechanical stress on the fracture filling material to generate colloids of larger sizes by erosion. Furthermore, homologues showed an apparent higher mass recovery than the simultaneously injected bentonite colloids, a fact which can be explained by

the larger surface area of the smaller bentonite colloids compared to the larger colloids which were filtered out during migration.

The injected bentonite colloid suspension had an average colloid size of 148 nm, as determined by LIBD. The peak solution revealed an average colloid size of about 116 nm. The same observation was made by the SPC measurements which showed a decrease in recovery from 89.3% for the size class 50 – 100 to 22.0% for the size class 700 – 1000 (after 365 min), indicating that the recovery may be biased by filtration processes in the system. Bentonite colloids arrived slightly earlier than did the uranine and the tailing of the colloid breakthrough curve was steeper than the tailing of the uranine curve. This observation can be interpreted as indicating concentration of the colloids in the centre of the flow stream (where higher velocities occur) probably due to charge repulsion effects and to a slight interaction of the uranine with the matrix or with the fault gouge in the experimental shear zone ("matrix" diffusion).

3.3.4.2 Homologue migration

In general, the breakthrough behaviour of actinide homologues in all experiments was similar to that obtained for the conservative tracer uranine although the peak maxima of tracer breakthrough are slightly shifted to earlier arrival times, suggesting either the presence of homologue colloids or some retention of uranine (see comments in Frick et al., 1992 and Smith et al., 2001 on uranine retardation). As noted in Frick et al., (1992), this could be tested against ^{3,4}He breakthrough behaviour.

In the absence of bentonite colloids, a clearly lower recovery is found for the homologues. The different migration behaviour of both the tri- and tetravalent homologues in the experimental shear zone in the absence and presence of bentonite colloids clearly shows the enhancing effect of bentonite colloids on homologue migration. Whether the homologue migration behaviour without added bentonite colloids is mainly determined by sorption kinetic effects or the existence of colloid-borne species has to be further studied. However, ultracentrifugation studies suggest the presence of colloidal ^{232}Th-, ^{178}Hf- and ^{159}Tb-species in the injection cocktail. The mechanism of colloid formation and the nature of these colloids are again unclear. Generation of colloidal hydroxide/oxide phases due to local oversaturation during the spiking procedure or interaction with GTS groundwater colloids both appear possible and it therefore cannot be ruled out that the colloidally mediated transport of the homologues was not, at least in part, in the form of homogenous homologue oxyhydroxide colloids.

However, the studies showed that particular attention needs to be placed on the cocktail preparation and characterisation for any *in situ* tracer tests. Colloid formation during spiking of GTS groundwater with the radionuclides should be prevented as much as possible and the tracer cocktail needs to be analysed with regard to the formation of colloids within the vial before the injection takes place. This effect has never been reported before and needs to be studied in detail in the future – only then can previous radionuclide tracer experiments be placed in proper context.

4 Main tracer tests

H. Geckeis, Th. Fierz, J. Eikenberg, C. Degueldre, W. Hauser, Th. Schaefer, F. Geyer and A. Möri

4.1 Overview of main tracer tests

In total, eight tracer tests were performed between January and March 2002 in dipole 1: runs #31 and #32 containing the actinide cocktails and six supporting uranine-^{131}I tracer injections. The entire test programme was performed within a very tight time schedule of 3 months and laboratory analyses were started immediately after *in situ* injections had been completed (see Table 4.1).

Tab. 4.1: Overview of tracer tests in 2002

Calendar week in 2002	**Tracer run**	**On site activity**	**Off site activity**
W 01 & 02	---	Site preparation, installation of radioprotection measures	Preparation and charact. of tracer cocktail #31
W 03	#28-#30 ^{131}I & uranine	Tracer injection, on-line monitoring of uranine input and tracer breakthrough Sampling for lab. analysis	Preparation of tracer cocktails #28-#30 γ-spectrometry of selected samples
W 04 & 05	#31 ^{243}Am, ^{237}Np, ^{242}Pu, ^{238}Pu, ^{238}U, ^{85}Sr, ^{131}I & ^{232}Th; (no bent. coll.)	Tracer injection On-line monitoring of ^{85}Sr and ^{131}I tracer breakthrough Sampling for lab. analysis	α- and γ-spectrometry, ICP-MS measurements Single particle counting
W 06 & 07	#33 ^{131}I & uranine	Tracer injection On-line monitoring of uranine input and tracer breakthrough Sampling for lab. analysis	Continuation lab. anal. of #31, γ-spectrometry of selected samples, Preparation and character. of tracer cocktail #32
W 08 & 09	#32 ^{241}Am, ^{237}Np, ^{244}Pu, ^{238}Pu, ^{233}U, ^{85}Sr, ^{99}Tc, ^{137}Cs, ^{131}I & ^{232}Th; (incl. bentonite coll.) #34 ^{131}I & uranine	Tracer injection On-line monitoring of ^{85}Sr, ^{137}Cs and ^{131}I tracer breakthrough On line detection of colloid breakthrough (LIBD, PCS) Sampling for lab. analysis	α- and γ-spectrometry, ICP-MS measurements LIBD and PCS evaluations Single particle counting
W 09-13	#35 ^{131}I & uranine	Tracer injection On-line monitoring of uranine input and tracer breakthrough Sampling for lab. analysis	Continuation of lab. analysis of #32 γ-spectrometry of selected samples

4.2 Supporting tracer test with uranine and iodine

Originally it was planned to inject ^{82}Br as a conservative tracer before, during and after the injections of the actinides as it was expected that the large uranine molecules would interact with the actinides. Therefore ^{82}Br was already used during a preparatory tracer test (see section 3.3.3) and it was seen that the tracer behaved like uranine and could serve for on-site detection of the breakthrough of a conservative tracer during the actinide injections. However, as there was no bromine available at PSI during the planned *in situ* test phase (the beam line used for ^{82}Br production was undergoing revision at the time), it was decided to use ^{131}I instead of ^{82}Br. Previous injections in the MI and EP experiments revealed similar breakthrough behaviour for both elements.

The supporting tracer injections during the main test phase were necessary as there was no possibility to measure the input functions during the actinide injections because of the absence of uranine in the main runs[15]. Six runs with the conservative tracers uranine and iodine were performed in order to evaluate the stability of the flow field during the test phase and to verify the reproducibility of the input functions before, between and after the actinide runs. Figure 4.1 shows the pressure reactions in the test and observation boreholes during the tracer testing. Even the MI boreholes at distances of several metres from the test dipole showed an increase in pressure at the times of injection.

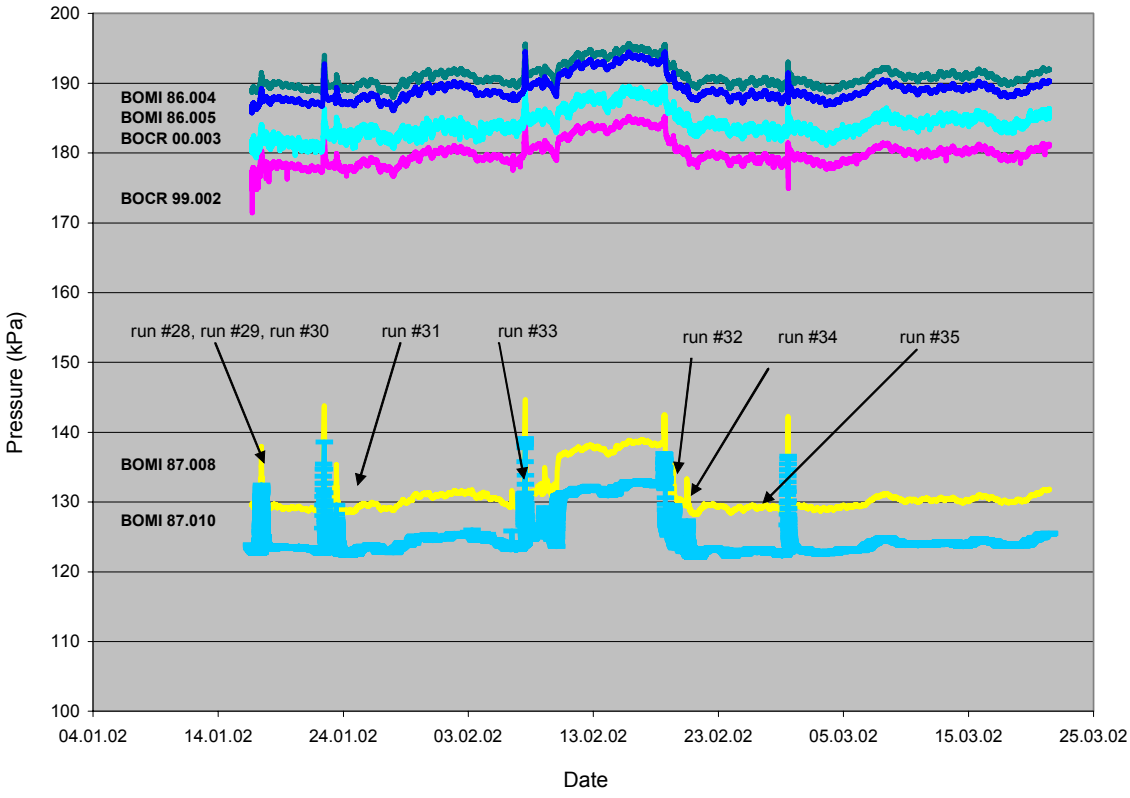

Fig. 4.1: Pressure response (kPa) in observation boreholes during *in situ* experiment

[15] Uranine is the only tracer that could be detected downhole at the input side (see comments above).

4.2.1 Uranine input functions

Figure 4.2 shows five input functions of uranine. The input function of run #30 could not be measured due to a malfunction in the uranine detection device. The input functions of run #28 and #29 (performed before the injection of the actinide tracer cocktails) are in good agreement to each other. Runs #33, #34 and #35 which were performed between and after the actinide tracer injections indicate a slight shift to lower peak concentrations and to a change in the shape of the tail. These deviations are affected by an increase in the uranine concentration in the injection vial by a factor of 10 and by the lower flow rate applied to the injection device (9.5 mL min^{-1} compared to 10 mL min^{-1}). Evaluations of the influence of these small shifts in the uranine input functions to the uranine breakthrough curves, which were investigated within the modelling task of the experiment (see Guimera et al., 2004), revealed no significant influence and can therefore be neglected. Moreover, it can be assumed that the release of the actinides into the injection interval is well represented by the uranine input functions.

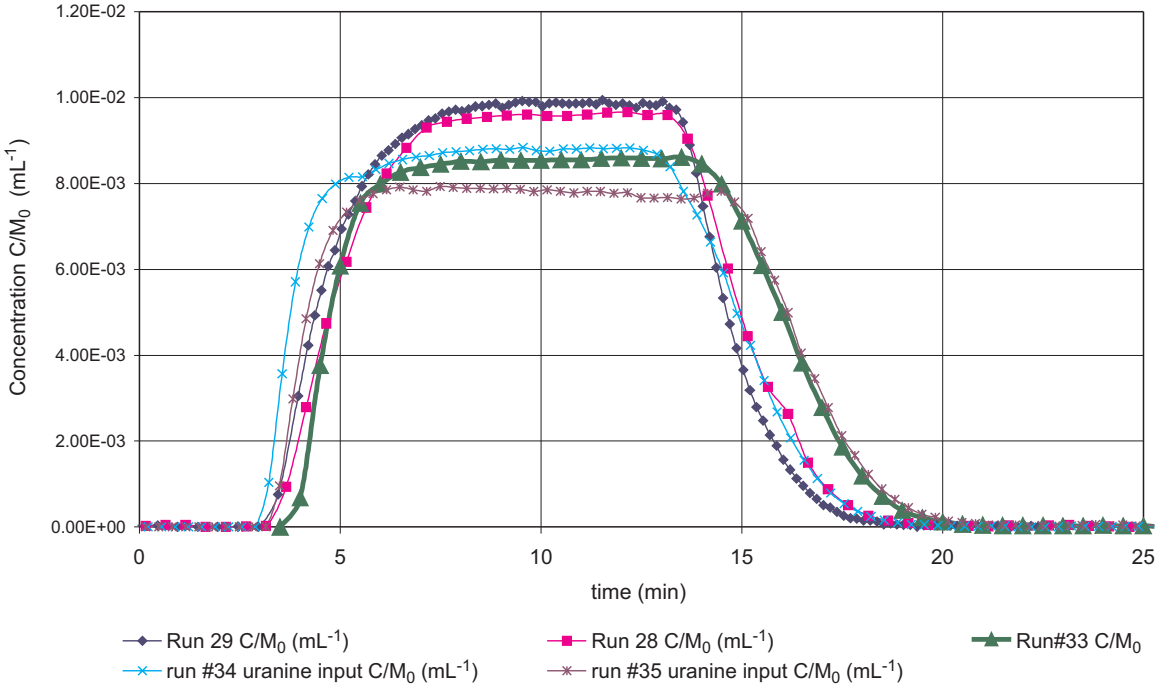

Fig. 4.2: Uranine input function for runs #28, #29, #33, #34 and #35

4.2.2 Uranine breakthrough curves

With increasing duration of the main test phase in 2002, the breakthrough curves of the six tracer tests shifted slightly towards lower peak heights, more pronounced tailing and increasing recovery (see Figures. 4.3 and 4.4). This systematic change may be due to small changes in the geometry of the active flow paths within the flow field which might be related to the duration of testing of more than 2 months. However, it seems to be more probable that the better recovery results from the lower detection limit in runs #33, #34 and #35, as in these runs, 10 times higher uranine concentrations were injected compared to runs #28, #29 and #30. Peak times, residence times and recoveries are summarised in Table 4.2.

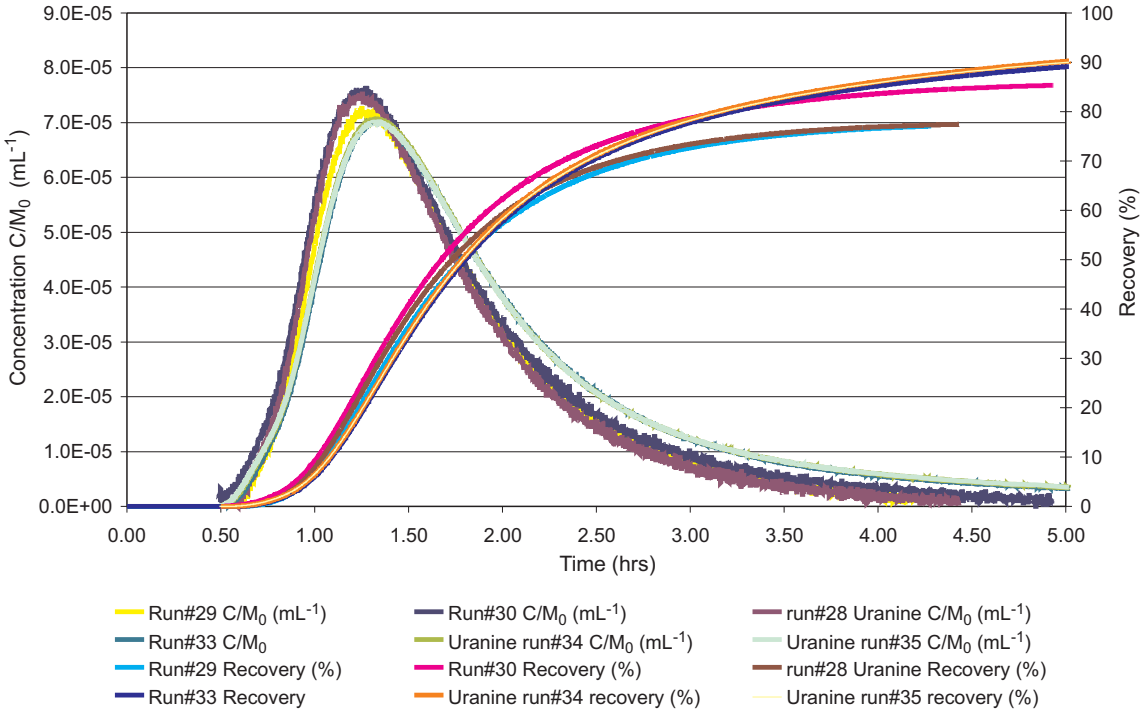

Fig. 4.3: Uranine breakthrough curves, linear scale

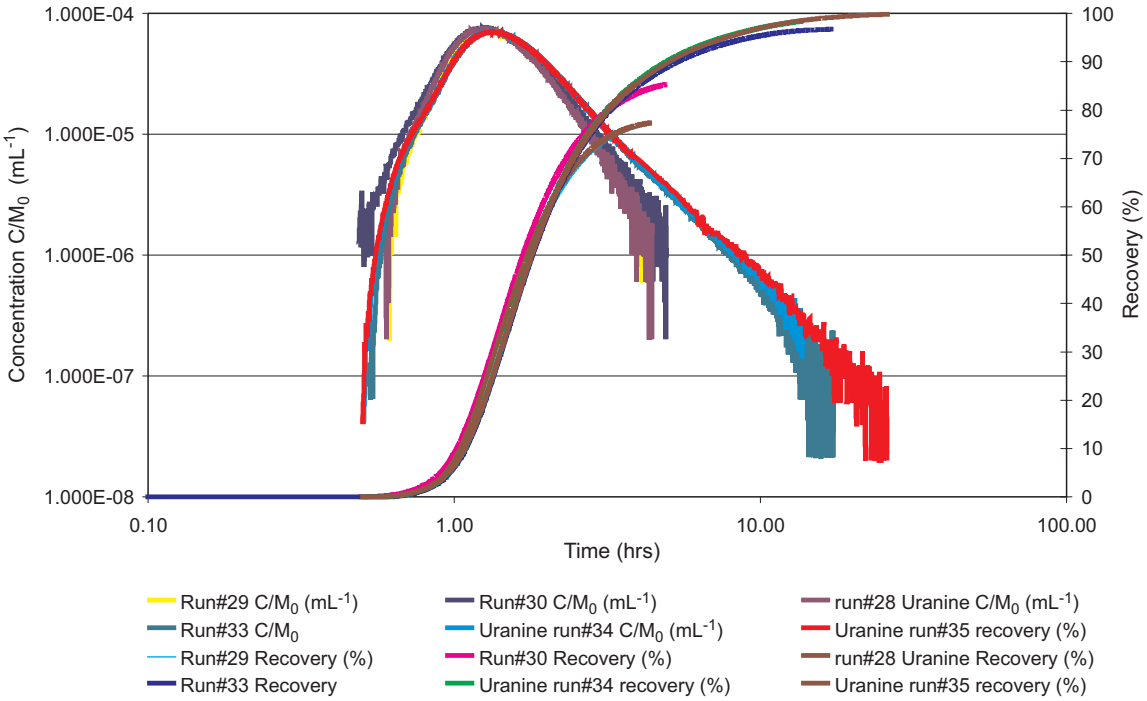

Fig. 4.4: Uranine breakthrough curves, log-log scale

Tab. 4.2: Uranine and Iodine recoveries and the peak times run #28 -#35

Run	Peak time breakthrough uranine [min]	Residence time uranine [min]	Recovery uranine [%]	Peak time breakthrough Iodine [min]	Recovery Iodine [%]
28	75	62	77	85	92
29	75	63	77	78	85
30	76	63	85	86	105
31	No uranine injection			82	102
32	No uranine injection			83	92
33	79	65	97	83	102
34	80	70	98	86	154*
35	80	72	100	80	123*

* see text for explanation of recovery >100 %

4.2.3 Iodine breakthrough curves

^{131}I was injected in combination with uranine and detected on-line with an HPGe detector at the outlet borehole BOMI 87.010. Samples were taken for laboratory analysis of the ^{131}I content in the breakthrough solution at different time steps. Figure 4.5 shows the breakthrough curves and the recoveries of all runs together. It is obvious that the runs differ only in the late part of the tails. Peak time was found to be between 78 and 86 minutes and the recoveries between 85 and 154% (see Table 4.2).

The nonsensical recoveries of more than 100% in some of the tests suggested ^{131}I retardation in the detector so leading to multiple counts of the retarded ^{131}I. It was therefore decided to flush the PEEK lines within the HPGe detector with 2% HNO_3 and up to 5% of the injected conservative ^{131}I was remobilised by the flushing procedure[16].

Figure 4.6 shows a comparison between the uranine and ^{131}I breakthrough curves in run #34. There is a good agreement between both curves from the first arrival to the peak and even after the peak until the ^{131}I builds a more pronounced tail to the end of the breakthrough curve which might be due to the higher matrix diffusion of the ^{131}I ions compared to the larger uranine molecules-or, even more likely, is the consequence of ^{131}I retardation on PEEK tubing surfaces.

[16] As noted above, retardation of radionuclides on the equipment is always a problem. During MI, all metals were coated with PTFE to minimise uptake of strontium, among other tracers and, in EP, much of the PTFE was replaced by nylon and high-density PTFE to minimise uranium, selenium *etc* uptake. Here, in CRR, the use of PEEK has greatly minimised uptake of actinides but, clearly, at a cost to the iodine transport through the equipment (note that there were no problems with bromine). Due to the complex nature of such experiments, it is unlikely that a "magic" material which suits all tracers will be discovered and so comprimises such as the use of PEEK will always need to be accepted.

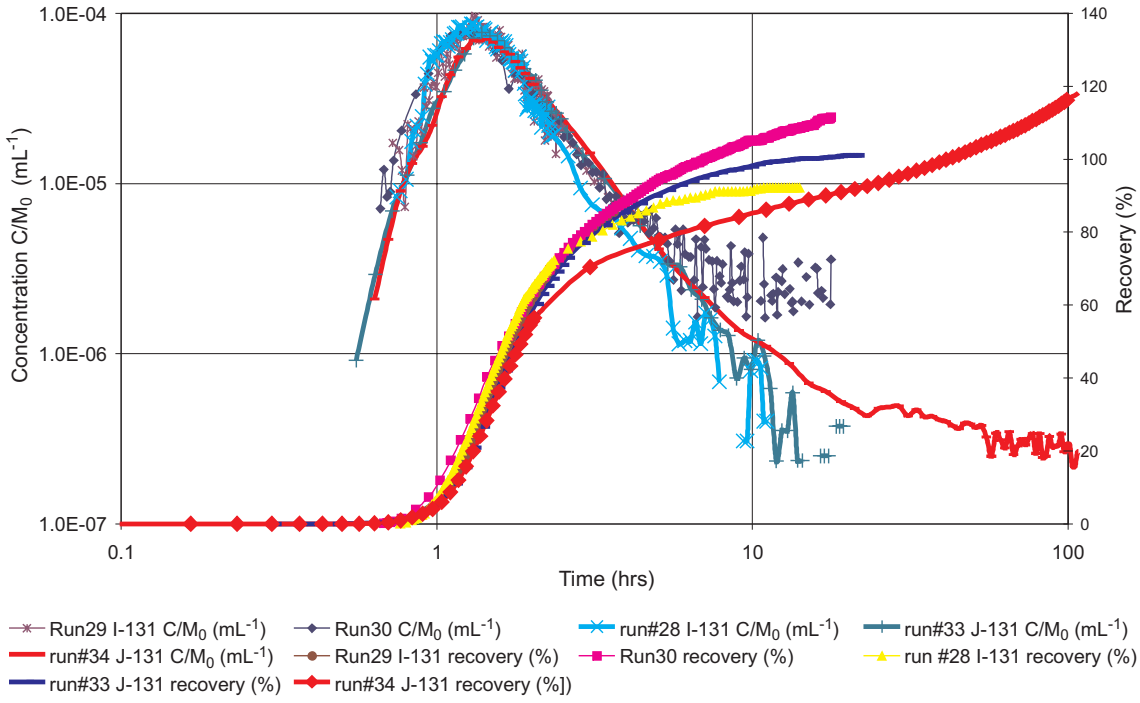

Fig. 4.5: ^{131}I breakthrough curves in log-log scale

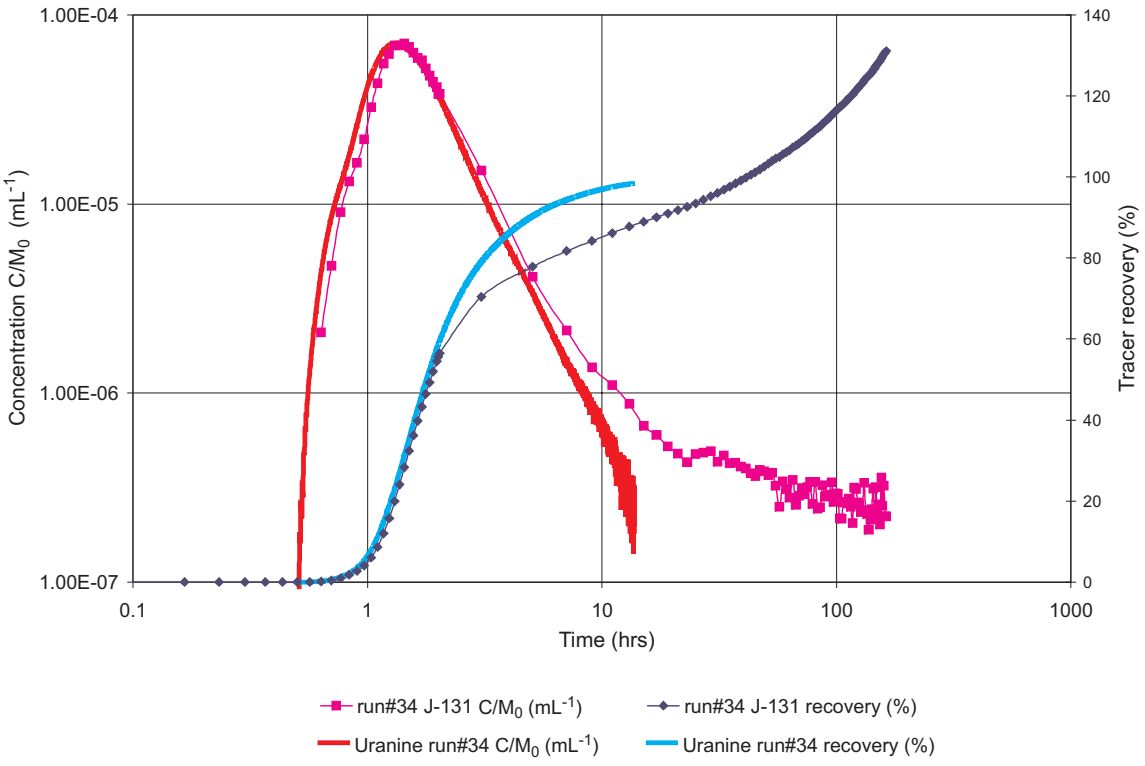

Fig. 4.6: Comparison of uranine and ^{131}I break through curves in log-log scale

4.2.4 Summary of supporting uranine and ^{131}I tracer injections

The slight shift in the recorded uranine input functions was attributed to the increased input concentrations of uranine and to small variations in the injection flow rates. Modelling exercises investigating the sensitivity of the breakthrough curves of uranine on these deviations revealed no relevance, the curves being unaffected by these changes. However, it was observed that, with increasing test duration, the breakthrough curves of the different uranine and ^{131}I injections shifted slightly towards lower peak heights and more pronounced tailing with increasing recoveries. This can be attributed to small changes in the internal build up of the experimental shear zone due to the long test duration of more than two months. However, there is no evidence for a drastic change in either the input functions of the uranine (good reproducibility) or in the breakthrough curves of the uranine and ^{131}I (only minor changes in the flow field due to testing activities). Clogging of the flow paths under the given flow conditions and at the given colloid concentrations or total masses that were injected into this dipole was not observed.

^{131}I showed significant sorption onto the PEEK tubes of the HPGe detector spiral of up to 5%. This was revealed as multiple counting of ^{131}I in the detector and so to calculated recoveries higher than 100%.

4.3 Preparation of actinide tracer cocktails

Handling of the actinide cocktails was carried out under an inert gas atmosphere (Ar with < 1 ppm O_2). Stock solutions of radionuclides were prepared in such a way that only volumes in the range of several µL of the acidified stock were added to the original alkaline GTS groundwater, so ensuring minimal chemical disturbance. 125 mL of each cocktail were prepared in opaque (brown), high density polyethylene (HDPE) bottles. PEEK tubes and valves are connected to the cover of the bottle and allow the direct coupling of the bottle to the *in situ* injection device at the GTS (see above). The bottles were transported to the GTS in a desiccator vessel filled with Ar and the desiccator was opened only immediately before injection to minimise contamination/chemical disturbances. No handling except the connection to the N_2 and the injection lines was necessary.

4.3.1 Preparation and characterisation of injection cocktail run #31

It was a prerequisite of CRR that the injection of the radionuclide tracer cocktail should disturb the *in situ* groundwater/rock conditions to as small a degree as practicably possible. The original pH of the stored GTS groundwater of 9.1[17] dropped to about 3 after the addition on 14.01.2002 of 48 µL of ^{85}Sr stock solution (present as $SrCl_2$ in 0.5 $molL^{-1}$ HCl; specific activity: 3.61E11 Bq g^{-1} $SrCl_2$). To the acidic cocktail, aliquots of the other radionuclide stock solutions were then added (^{232}Th as nitrate; ^{243}Am as nitrate; ^{238}Pu as perchlorate; ^{242}Pu as perchlorate; ^{237}Np as perchlorate). The Pu in the stock solution was reduced electrochemically to the tetravalent state and spectroscopy revealed the presence of < 10% hexavalent Pu. ^{131}I (as NaI) was added on 15.01.2002 and, finally, the pH was re-adjusted to 9.09 by addition of 60 µL 0.1 $molL^{-1}$ NaOH to 200 mL of the cocktail. Note that, due to these pH adjustments, the ionic strength of the solution was increased to 2.9E-03 $molL^{-1}$ (*cf* the original ionic strength of 1.2E-03 $molL^{-1}$; Frick et al., 1992). 125 mL of the cocktail was transferred to the injection bottle. The final radionuclide concentration for run #31 (reference date 22.01.02) is given in Table 4.3.

[17] *cf* normal GGW pH of ~ 9.6; Frick et al., 1992

Tab. 4.3: Final radionuclide concentration (reference date: 22.01.02; 19:00 h) for the injection cocktail for run #31

	Added (nominal) Bq in 125 mL	**Measured** Bq in 125 mL	**Rel. analyt. uncer-tainty (1 σ)** %	**Colloidal fraction** % coll	**Anal. meth.**	**Licensed activity** Bq in 150 mL	**Ordered activity** Bq in 125 mL	**Mass** gL^{-1}	**Concen-tration** $molL^{-1}$
^{131}I	9.33E+04	9.33E+04	1.1	0	γ-spec.	1.00E+05	8.33E+04	1.62E-10	1.24E-12
^{85}Sr	1.19E+05	1.19E+05	4.6	0	γ-spec.	1.50E+05	1.25E+05	1.09E-09	1.28E-11
^{232}Th	1.2E-03	1.32E-03	10	20-30	ICP-MS	1.41E-03	1.18E-03	2.60E-06	1.12E-08
^{238}U	3.8E-01	3.52E-01	10	0-12	ICP-MS	4.50E-01	3.75E-01	2.26E-04	9.50E-07
^{237}Np	7.7E+02	7.28E+02	5	0-10	ICP-MS/ α-spec.	9.26E+02	7.71E+02	2.24E-04	9.44E-07
^{238}Pu	1.2E+03	8.38E+02	2	5-58	α-spec.	1.50E+03	1.25E+03	1.06E-08	4.44E-11
^{242}Pu	4.4E+01	4.38E+01	8	5-58	ICP-MS	5.30E+01	4.41E+01	2.40E-06	9.94E-09
^{243}Am	2.5E+03	1.33E+03	4	6-58	ICP-MS/ α-spec.	3.00E+03	2.50E+03	1.44E-06	5.93E-09

In order to check the fraction of colloidal species present in the cocktail, the cocktail was subjected to ultracentrifugation (90000 rpm for 1 h). For the actinides $^{238/242}Pu$, ^{232}Th and ^{243}Am, the results for the colloidal fraction showed significant scatter (see Table 4.3). The variation in the ultracentrifugation results may be due to the presence of very small colloids that cannot be sedimented under the given conditions or due to the existence of colloids of a very low density (close to that of water), for example gel-like aggregates with a high water content. Even though the results of the ultracentrifugation experiments are ambiguous, it is clear that colloidal $^{238/242}Pu$-, ^{232}Th- and ^{243}Am-species are present.

The concentrations of soluble ^{238}U, ^{237}Np and ^{243}Am remained constant over 50 days within the analytical uncertainty, whereas a slight concentration decrease with time was observed for ^{232}Th and $^{238/242}Pu$ (Figure 4.7). Repeating the analysis after a period of 500 d reveals a dramatic decrease in the colloid-borne actinides ^{243}Am, $^{238/242}Pu$ and ^{232}Th, while ^{238}U and ^{237}Np concentrations remain unchanged. From these data, it is concluded that the colloidal species of tri- and tetravalent actinides are not stable in the GTS groundwater. They either dissolve with time or actinides dissociate from the colloids. Dissolved actinide species, in turn, are scavenged by sorption on the container walls.

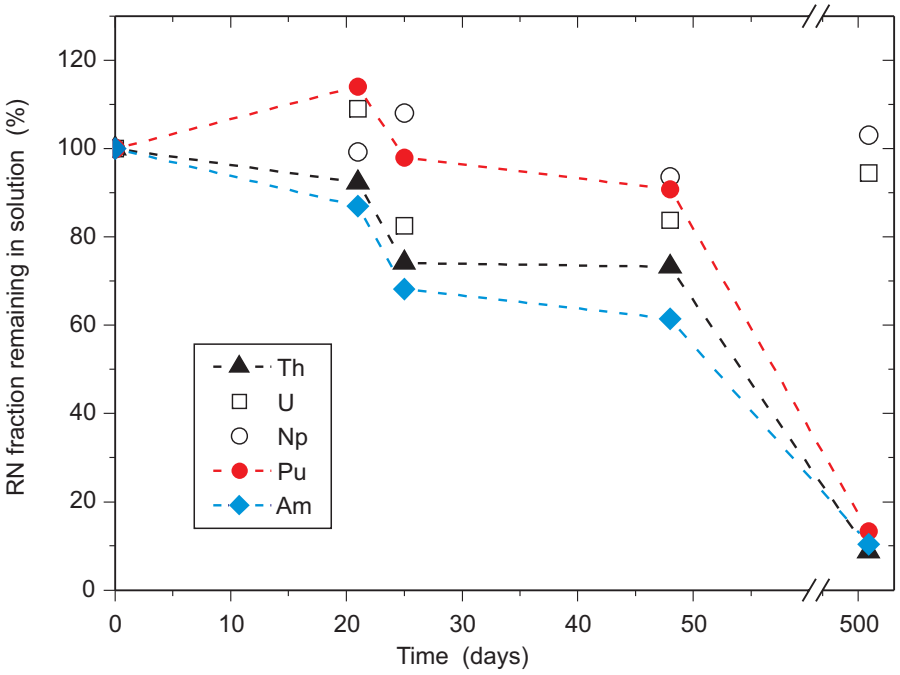

Fig. 4.7: Evolution of the actinide concentration with time in the CRR #31 cocktail

4.3.2 Preparation and characterisation of injection cocktail run #32

The final radionuclide concentration for run #32 at the reference date (18.02.02) is given in Table 4.4. The colloid stock suspension for the *in situ* migration experiment was prepared from a batch of FEBEX Ana Bentonite (grain size < 63 µm) provided by CIEMAT. An initial weight of 0.01 kg was suspended and equilibrated in 1 L GTS groundwater (collected in November 2001) for 7 days under aerobic conditions. Due to storage, the GTS groundwater had an initial specific conductivity of 113 µS cm^{-1} and the pH was at 8.56 (*cf* normal GTS groundwater pH of ~9.6, specific conductivity of 103 ± 5 µS cm^{-1}; Frick et al., 1992). The bentonite colloid suspension was prepared by five consecutive centrifugation steps (4000 rpm for 40 minutes), decantation of the supernatant and re-suspension in GTS groundwater using an ultrasound tip (Bioblock Scientific, Vibracell 75043; 37% amplitude) for 15 seconds. The final suspension (named CRR-TS2) had a pH of 9.21, a specific conductivity of 117 µS cm^{-1} and a gravimetrically determined colloid mass concentration of 540 ± 57 mgL^{-1}. This concentration is comparable to the results of the bentonite quantification using the ICP-AES and ICP-MS measurements of the aluminium concentration using the proposed FEBEX bentonite structural formula

$([Si_{7.66}aluminium_{0.34}][aluminium_{2.68}Fe_{0.34}Mg_{0.91}]X_{0.81}O_{20}(OH)_4)$

given in ENRESA (1998), which gave 484.6 mgL^{-1} and 499.7 mgL^{-1}, respectively. For the run #32 cocktail preparation, the bentonite colloid concentration was adjusted to 20 mgL^{-1} by dilution of an aliquot of the CRR-TS2 stock solution in anaerobic GTS groundwater under an Ar atmosphere.

Spiking of radionuclides into 200 mL of the colloid suspension was made at the 14.02.2002 under an Ar atmosphere. In order to avoid considerable pH shift due to the addition of acidic radionuclide stock solutions, the ^{137}Cs (as chloride), ^{85}Sr and ^{233}U (originally present in 5 $molL^{-1}$ HNO_3) stock solutions were evaporated to near dryness and re-dissolved in 10^{-3} $molL^{-1}$ HCl. 0.5

mL of the ^{99}Tc stock solution (5.6E04 Bq mL^{-1}) was adjusted to 1.5 molL^{-1} HCl and 60 µL of a 20% hydrazine solution was added. The solution was heated to 60°C for 30 min in order to reduce ^{99}Tc(VII) to ^{99}Tc(IV). Aliquots from these solutions were added to the GTS groundwater along with ^{244}Pu (in 0.25 molL^{-1} HCl), ^{232}Th (in 0.01 molL^{-1} HNO_3), ^{238}Pu, ^{237}Np (both as perchlorates), ^{241}Am (in 0.1 molL^{-1} HCl) and ^{131}I (as NaI). The $^{238/244}$Pu stock solution contained $^{238/244}$Pu as $^{238/244}$Pu(IV) and < 10% as $^{238/244}$Pu(VI) as determined spectroscopically. ^{233}U and ^{237}Np were added as their oxidised species ^{237}Np(V) and ^{233}U(VI), respectively. ^{232}Th and ^{241}Am exist in their stable oxidation states IV and III. The final pH was 6.3 and was readjusted by addition of 32 µL of 1 molL^{-1} NaOH to pH = 9.12. 125 mL of this solution were transferred to the injection bottle. The activity concentration for ^{238}Pu was determined indirectly by subtracting the concentration of ^{241}Am analysed by gamma spectrometry from the total activity of ^{241}Am and $^{238/244}$Pu determined by α-spectrometry. The selective extraction of $^{238/244}$Pu from the acidified dispersion failed. Only 20 % of the $^{238/244}$Pu was extracted, possibly due to the interference of bentonite colloids from which the $^{238/244}$Pu could not be desorbed, even after acidification.

Tab. 4.4: Final radionuclide concentration (reference date: 18.02.02; 00:00 h) in the injection cocktail for run #32

	Added (nominal) Bq in 125 mL	**Measured** Bq in 125 mL	**Rel. analyt. uncer-tainty (1 σ)** %	**Colloidal fraction** % coll	**Anal. meth.**	**Licensed activity** Bq in 150 mL	**Ordered activity** Bq in 125 mL	**Mass** gL^{-1}	**Concentration** molL
^{131}I	7.0E+04	6.95E+04	2.9	0	γ-spec.	1.00E+05	8.33E+04	1.21E-10	9.23E-13
^{85}Sr	1.0E+05	1.03E+05	2.5	0	γ-spec.	1.50E+05	1.25E+05	9.41E-10	1.11E-11
^{137}Cs	7.7E+05	7.59E+05	2.3	8	γ-spec.	1.05E+06	8.75E+05	1.90E-06	1.38E-08
^{99}Tc	7.0E+01	8.19E+01	10	12	ICP-MS	9.47E+01	7.89E+01	1.03E-06	1.04E-08
^{232}Th	1.9E-03	1.29E-03	8	94	ICP-MS	1.41E-03	1.18E-03	2.55E-06	1.10E-08
^{233}U	1.0E+04	9.03E+03	8	6	ICP-MS	1.25E+04	1.04E+04	2.02E-04	8.69E-07
^{237}Np	7.7E+02	8.40E+02	8	0-1	ICP-MS	9.26E+02	7.72E+02	2.58E-04	1.09E-06
^{238}Pu	9.0E+02	9.00E+02	10	84	α-/γ-spec.	1.50E+03	1.25E+03	1.14E-08	4.77E-11
^{244}Pu	1.8E-01	1.39E-01	8	84	ICP-MS	2.48E-01	2.07E-01	1.64E-06	6.70E-09
^{241}Am	2.8E+03	2.55E+03	8	99	γ-spec.	3.60E+03	3.00E+03	1.61E-07	6.66E-10

The actinide concentration in this cocktail remained constant (within analytical uncertainty) for up to 500 days after preparation. Ultracentrifugation shows clearly the presence of tri- and tetravalent actinides in the colloidal state, *ie* adsorbed on bentonite colloids. A small fraction of ^{137}Cs also appears to be sorbed on colloids while, for ^{99}Tc, the concentration difference between the ultracentrifuged and the original solution lies within analytical uncertainty. It is consequently unclear whether ^{99}Tc is associated with the colloids or not.

4.3.3 Summary of tracer cocktail composition and preparation

Cocktail characterisation with the LIBD revealed that run #31 also contained a certain amount of radiocolloids in the injection vial. The variations in colloidal fractions between 5 and 58% indicate either the presence of very small colloids or gel-like aggregates of $^{241/244}$Am, $^{238/242/244}$Pu and ^{232}Th. Run #32 showed a considerable fraction of $^{241/244}$Am, $^{238/242/244}$Pu and ^{232}Th (84 – 99%) and a smaller fraction of ^{137}Cs and $^{233/238}$U (8 and 6 % respectively) present as colloids in the injection vial. The mean colloid size of all colloids present (i.e. not only bentonite colloids) in the injection cocktail in the presence of bentonite colloids was determined by the LIBD as 109 nm (cf Fig. 3.10).

The colloidal species of the tri- and tetravalent actinides found in the injection cocktail of run #31 were stable within the experiment time scale but not on a longer time scale of about 500 days. Nevertheless, it was shown that the actinide concentration in cocktail #32 remains constant within the analytical uncertainty for up to 500 days after preparation. Ultracentrifugation shows clearly the presence of tri- and tetravalent actinides in the colloidal state, *ie* adsorbed to bentonite colloids and a small fraction of Cs also appears to be sorbed on colloids.

4.4 Colloid migration

4.4.1 Photon Correlation Spectroscopy (PCS)

On-line measurement of the laser light scattering (LLS) signal intensity of the GTS groundwater showed a variation ranging from 2.0 to 2.7 thousand counts per second (kcps, Figure 4.8) which is below, or close to, the detection limit of the method and corresponds to a colloidal mass concentration of approximately 50-70 ppb. The LLS signal increased to reach a value of 5 kcps at the peak maximum (at 80.5 min) of the run #32 breakthrough curve (Figure 4.8).

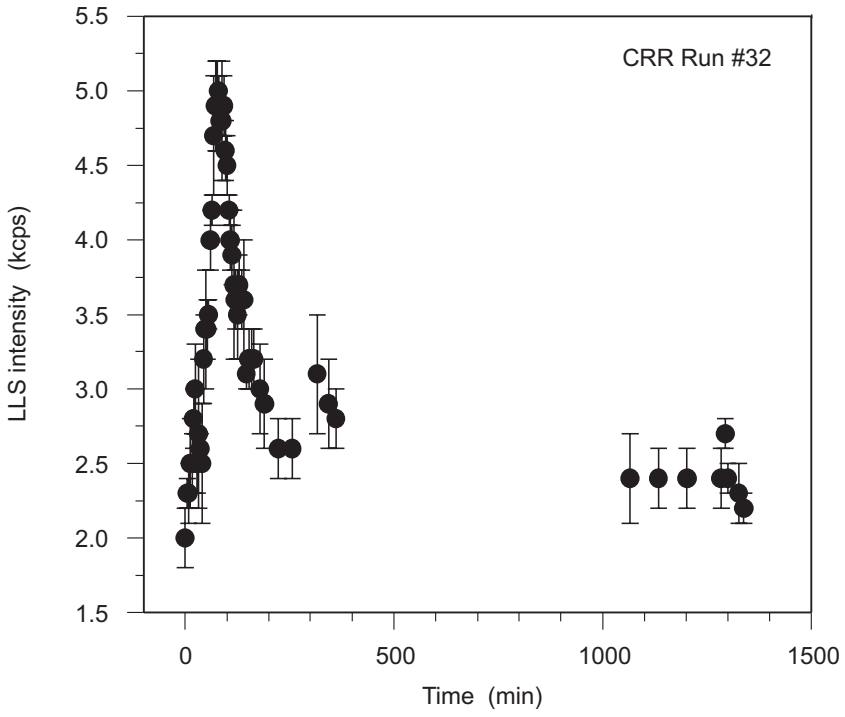

Fig. 4.8: Time-depended variation of the LLS intensity during run #32

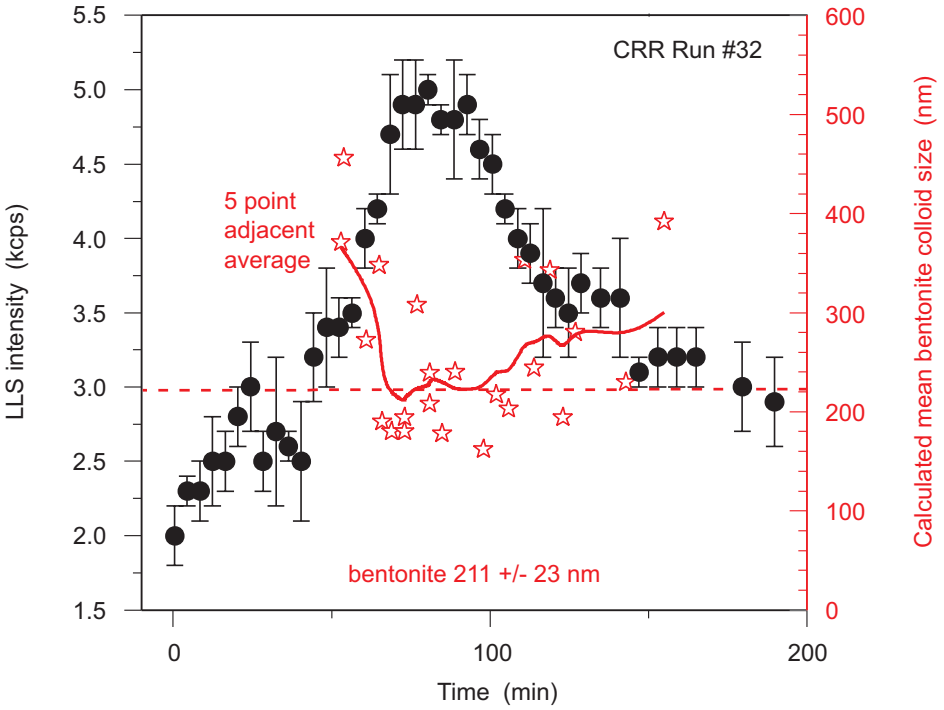

Fig. 4.9: Variation of the PCS calculated mean bentonite colloid size and LLS intensity during run #32 with time after injection start

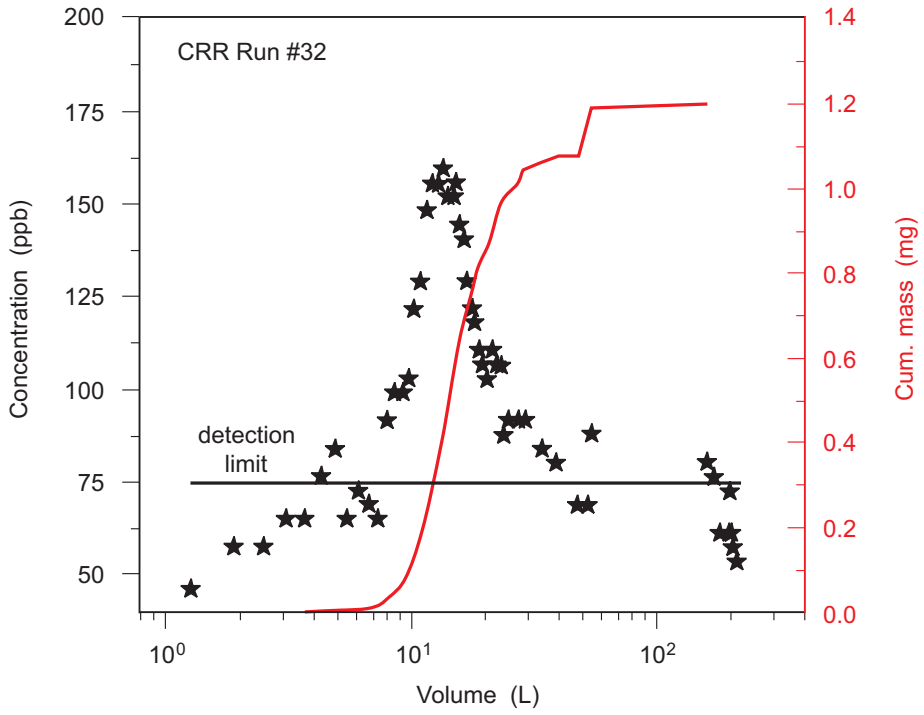

Fig. 4.10: Bentonite colloid concentration variation and recovered cumulative colloid mass

The peak maximum of the breakthrough curve was calculated by fitting the data to a Gaussian distribution and lies at 86 min after injection. Size analyses reveal a mean bentonite colloid diameter of 211 nm in the injection suspension and a very small variation between the different

calculation methods of 23 nm. The background colloid size in the GTS groundwater showed a large degree of scattering around 300 to 500 nm with a high uncertainty documented by the average variation of ± 105 nm.

Although an exact size analysis of the background colloids is difficult, the shape of the measured background auto correlation functions (ACF) provides strong evidence that large colloids are transported under the hydraulic conditions of the *in situ* experiment. The mean colloid size decreases to values around 200 nm during the colloid breakthrough curve. Measured diameters lie in a range from 160 to 260 nm (Figure 4.9). This variation can partly be explained by low scatter light intensities leading to an increase in the measured width of the size distribution but might also be due to the presence of large background colloids. Five point adjacent averaging of the calculated mean colloid size reveals mean diameters of the background colloids comparable with those of the injected colloids. This finding suggests that size exclusion effects in the experimental shear zone should be of minor importance, at least in this size range.

Taking into account the above mentioned negligible size exclusion effect, a colloid recovery of 57 ± 6.5% can be calculated (Figure 4.10) using the calibration curve and a detection limit of 75 ppb. It must be kept in mind, however, that PCS detection tends to overestimate colloids of larger size in those samples which contain colloid population of multimodal or broad size distribution. This is due to the much higher cross section of larger sized colloids for light scattering. It is thus possible that only a part of the larger sized colloids is observed by this technique and smaller colloids are masked out. The uncertainty of the calculated recovery is also attributed to the step in the cumulative mass curve due to the second peak in the breakthrough curve (grey striped pattern in Figure 4.10), which leads to a recovery of > 90% if taken into account in the recovery analysis.

Nevertheless, the PCS measurements demonstrate that a significant amount of bentonite colloids in the ~200 nm size (PCS size) range are mobile under the given conditions of run #32.

4.4.2 Laser-induced breakdown detection (LIBD)

Colloids in the extracted water were detected continuously on-line and occasionally off-line. Figure 4.11 shows the breakthrough of the bentonite colloids displayed by the measured breakdown probability. After cocktail injection, values for the breakdown probability were measured in the range of 8-10% at the high detection sensitivity mode of LIBD (applying the higher laser energy). These signals are attributed to the natural colloid background in the GTS groundwater under the given flow conditions and appear significantly above the value for the ultra-pure water.

Eluting bentonite colloids are first observed 30 min after the injection. Before reaching the breakthrough maximum, the breakdown probability attains saturation. At this stage, the LIBD was switched to a lower detection sensitivity mode (applying the low laser energy). The concentration of the extracted bentonite colloids decreases slowly after the maximum colloid concentration is reached at around 80 min. Between 430 min and 1130 min (dashed line), no data were collected as sampling was interrupted overnight. The colloid background level of the GTS groundwater (~10% breakdown probability) is reached again at about 1300 min.

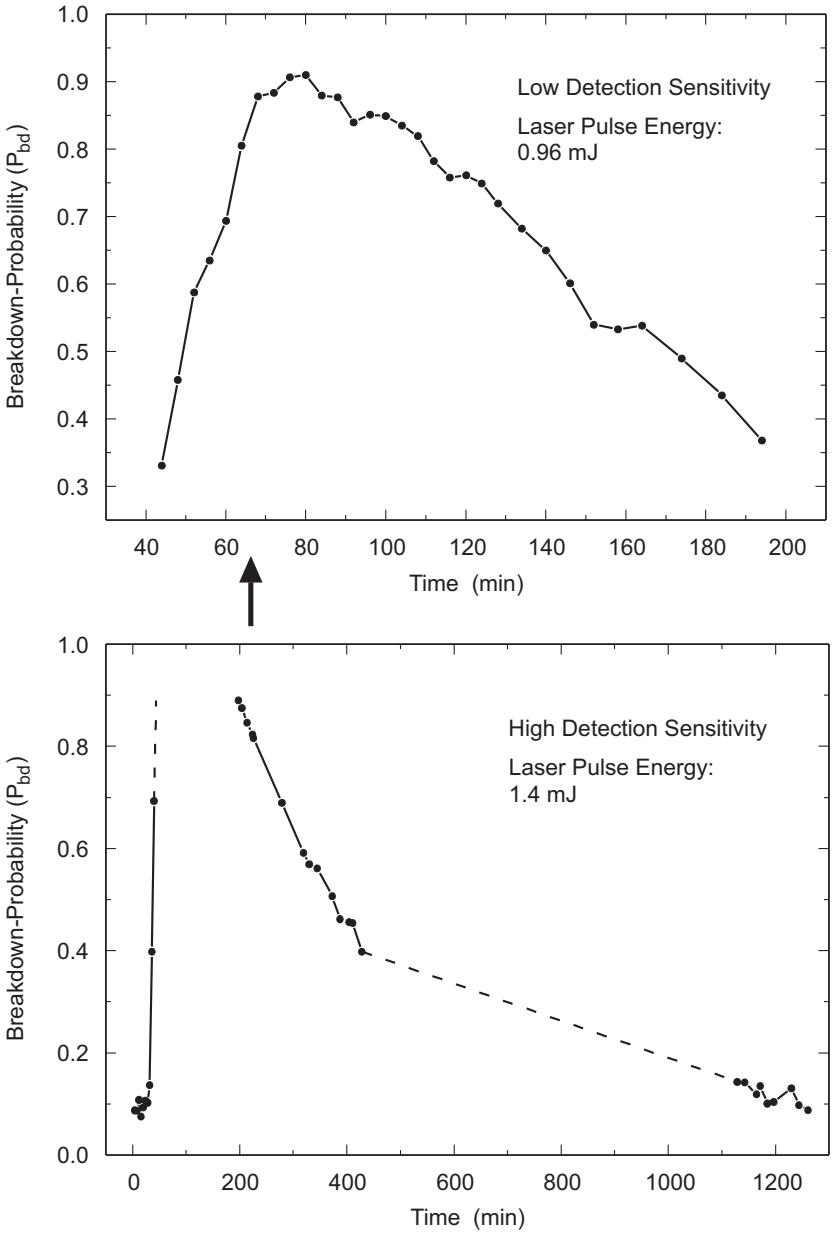

Fig. 4.11: Colloid breakthrough monitored on-line by the breakdown-probability measured by the LIBD

Based on the 2-D spatial distribution of breakdown events along the laser beam axis (as determined by image-processing of the data obtained by off-line measurements), the average colloid size and concentration were appraised quantitatively according to the method described in Hauser et al. (2002). For the calculation of the colloid concentration, a colloid density of ρ_P = 2.7 g cm^{-3} is assumed for the FEBEX bentonite colloids (see ENRESA, 1998, Huertas et al., 2000 and Hauser et al., 2002 for details). Size analyses were performed for a series of collected sample fractions at both the GTS and in the FZK laboratory and the results are illustrated in Figure 4.12. Before the injection started, very large background colloids with a maximum diameter of 480 nm and a maximum concentration of about 22 ppb were detected (note both colloid diameter and concentration decrease with time). This may have been caused by manipulations at the extraction HPLC pump and subsequent washing out of larger colloids from the fracture infill due to flow pulses. From the data given in Figure 4.12, it appears that a steady

state for the colloid background was not attained by the beginning of the injection. At this point, a leak in the sample container was discovered before any cocktail entered the injection line and the leak was sealed and the injection restarted. The slight increase of the colloid diameter from 168 nm to 208 nm after injection might be a consequence of the interrupted injection because such manipulations destabilise the flow rates for a certain time. Immediately before the breakthrough of the injected bentonite colloids, the concentration of the background colloids was about 2-4 ppb with an average size of 208 nm. These values are similar to those observed in the previous experiment (Hauser et al., 2002). The average diameter of the extracted bentonite colloids in the breakthrough was about 100 nm, which is almost identical to the value of the initial colloid dispersion (109 ± 10 nm). Consequently, the breakdown probability was converted to a concentration by a re-calibration of the LIBD with an aliquot of the injected colloids. The maximum concentration of the extracted colloids was then 109 ppb.

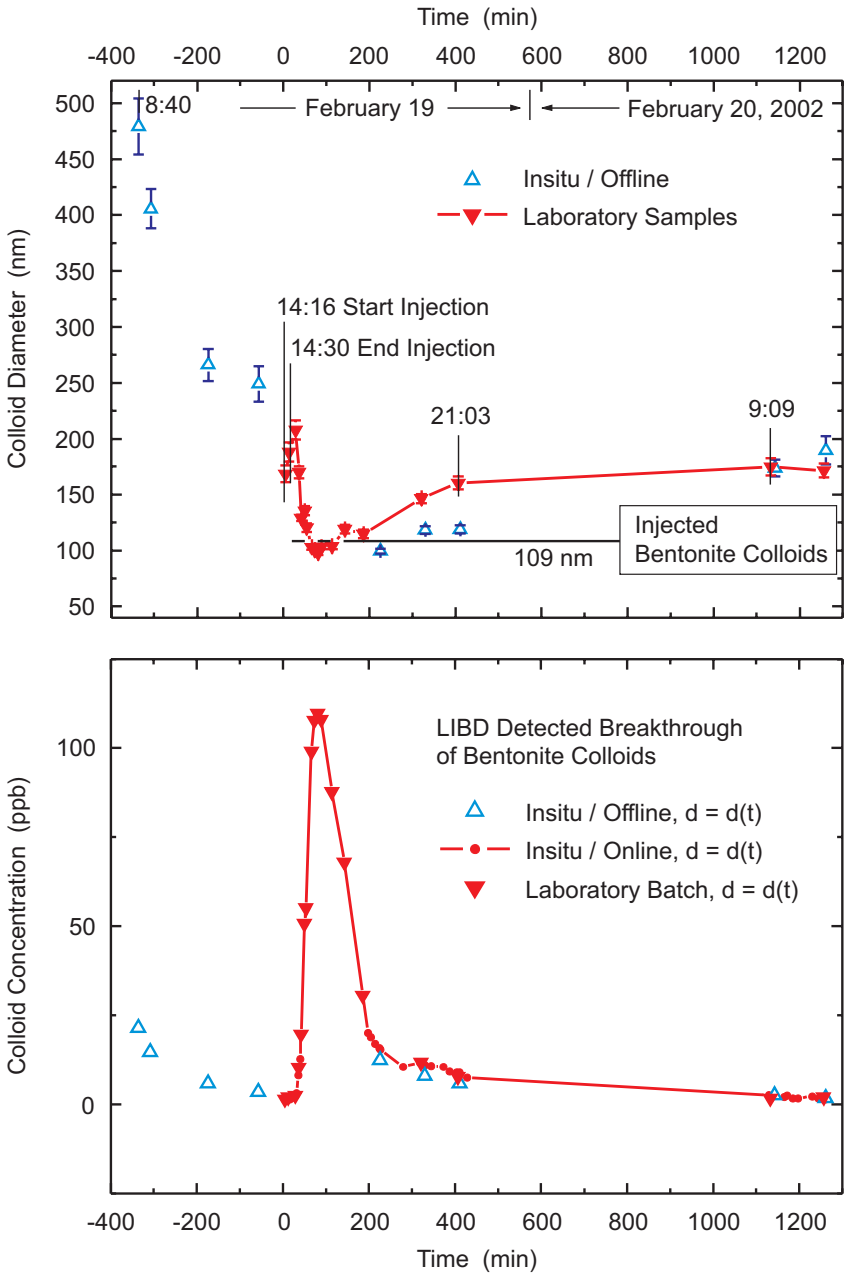

Fig. 4.12: Colloid diameter and concentration in run #32

The extracted bentonite colloid fraction (relative to the injected mass concentration) was evaluated by integrating the breakthrough curve after subtracting the natural background level of colloids in GTS groundwater. The recovery obtained from the LIBD is calculated to be 89-100%, depending on the position of the baseline. The uncertainty results mainly from the selection of the baseline position (determination of effective share of the natural colloid background).

Nevertheless, the mass recovery and the colloid diameters indicate a large fraction of the injected bentonite colloids being moved through the fracture zone. A filtration effect for a fraction of larger sized colloids, as noted in the preparatory experiments (see section 3.3.1 and Hauser et al., 2002) was not observed. This may be due to higher permeability in dipole 1 (compared to dipole 3 in the preparatory experiments) and/or the somewhat smaller average size of the injected colloids (109 nm compared to 149 nm in the previous experiment).

Aluminium concentrations have been determined in the samples taken for off-line LIBD measurements in the INE-laboratory. The result is given in Figure 4.13. The background aluminium concentration is 15 to 16 μgL^{-1} (cf Fig. 3.16), compared with the aluminium concentration in the cocktail of 2.2 ± 0.18 mgL^{-1}. From the molecular formula of the FEBEX bentonite clay, it can be calculated that the aluminium content is 10.9 mass% which would produce a clay colloid concentration in the cocktail of 20.2 ± 1.6 mgL^{-1}, which is in very good agreement with the expected value. A comparison with the concentration of bentonite colloids shows that the peak maxima are in good agreement.

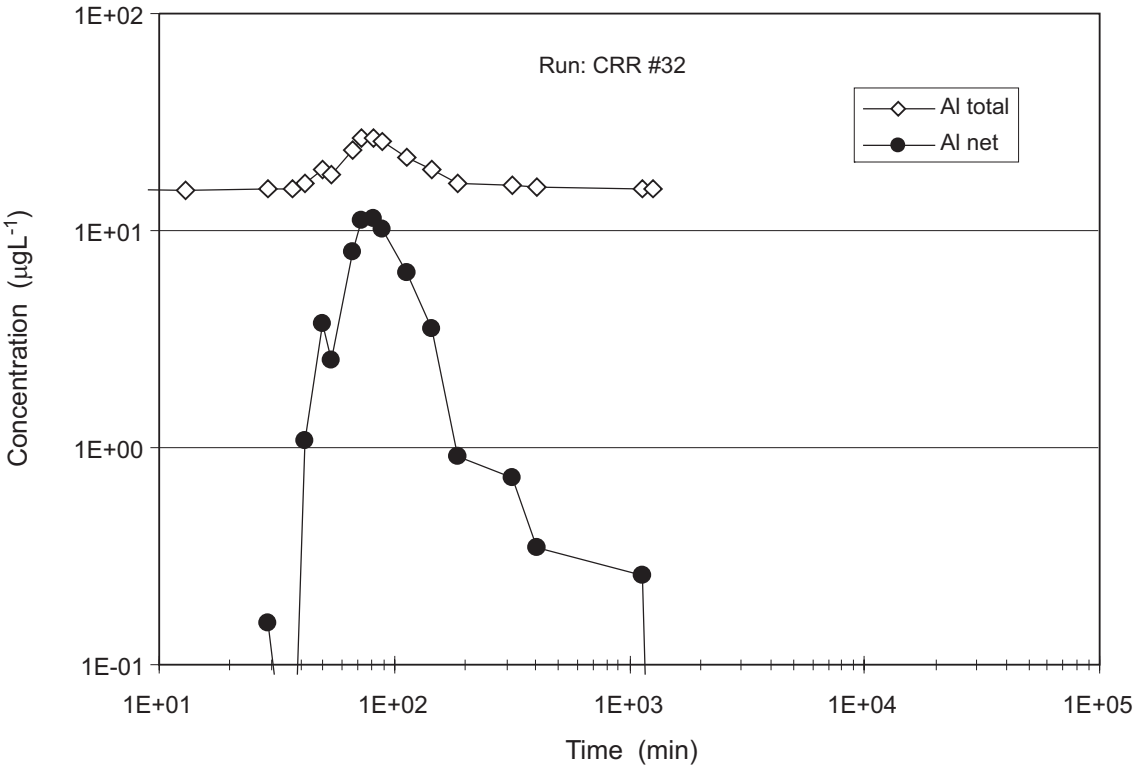

Fig. 4.13: Aluminium breakthrough curve in run #32; aluminium total represents the total aluminium concentration in the samples; aluminium net values are corrected for the natural aluminium-background of the GTS groundwater indicating the aluminium-content of the bentonite colloids

4.4.3 Single particle counting (SPC)

4.4.3.1 Breakthrough curves of colloids in runs #31 and #32

Figure 4.14 shows the colloid concentration for the detected size classes during the breakthrough of the conservative tracer in run #31. The breakthrough curves are compared with the breakthrough curve of the bentonite colloids obtained during run #32 (breakthrough was clearly seen approximately between 30 and 300 minutes after the colloids were injected). In run #31, no colloid breakthrough is observable even for the smallest size class of 50 nm – 100 nm, which is in good agreement with the LIBD analysis made on the injection cocktail in run #31. This means that, if actinide colloids are generated in the tests, they are either smaller than 50 nm or that their concentration is smaller than the natural colloid background in the GTS groundwater. In the actinide cocktail of run #31, the total actinide concentration is 2E-06 M. This could provide an actinide oxyhydroxide colloid concentration of ~ 5E-04 gL^{-1} (based on a molar weight of 250 g mol^{-1}). With an assumed density of 10 g cm^{-3}, the maximum concentration of colloids for 100 nm (corresponding to a colloid volume of 10^{15} cm^3, a single colloid mass of 10^{-14} g per colloid) in the original cocktail would be about 5E+10 L^{-1} or 5E+07 mL^{-1}. During run #31 injection and transport through the experimental dipole, this estimated colloid concentration would be diluted by a factor of about 15, which would reduce the estimated concentration to a maximum of 2E+06 mL^{-1}, which is below the detection limit of the method employed here and which is also below the natural colloid background. In other words, the results of the *in situ* experiment cannot rule out the presence of actinide colloids in the GTS groundwater during run #31.

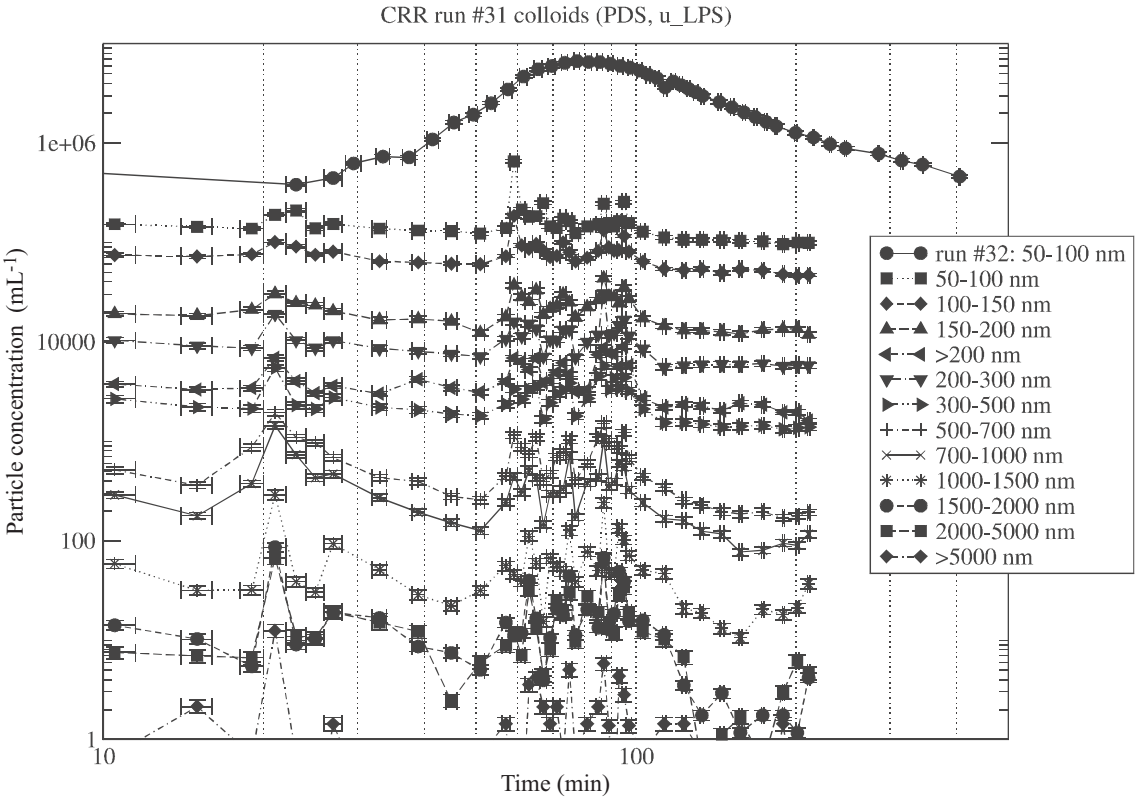

Fig. 4.14: Colloid breakthrough curves for the various size classes in run #31; colloid breakthrough curve for 50-100 nm from run #32 for comparison

For run #32, the time dependent particle and colloid concentration is given for all measured size classes in Figure 4.15. A colloid breakthrough is observable for the size of 50 – 100 nm and a very flat peak is also detectable for colloid sizes of 100 – 150 nm. For the other size classes, the breakthrough of bentonite colloids was not detectable, since the size distribution of the bentonite colloids in the injection cocktail was found to be mostly ranging in the sizes between 50 and 150 nm and since the variation of the natural colloid background is larger than the corresponding peaks of the bentonite colloids. This finding is different to the results of the preliminary experiments with bentonite colloids in dipole 3, where a breakthrough of colloids up to a size of 500–700 nm was observed.

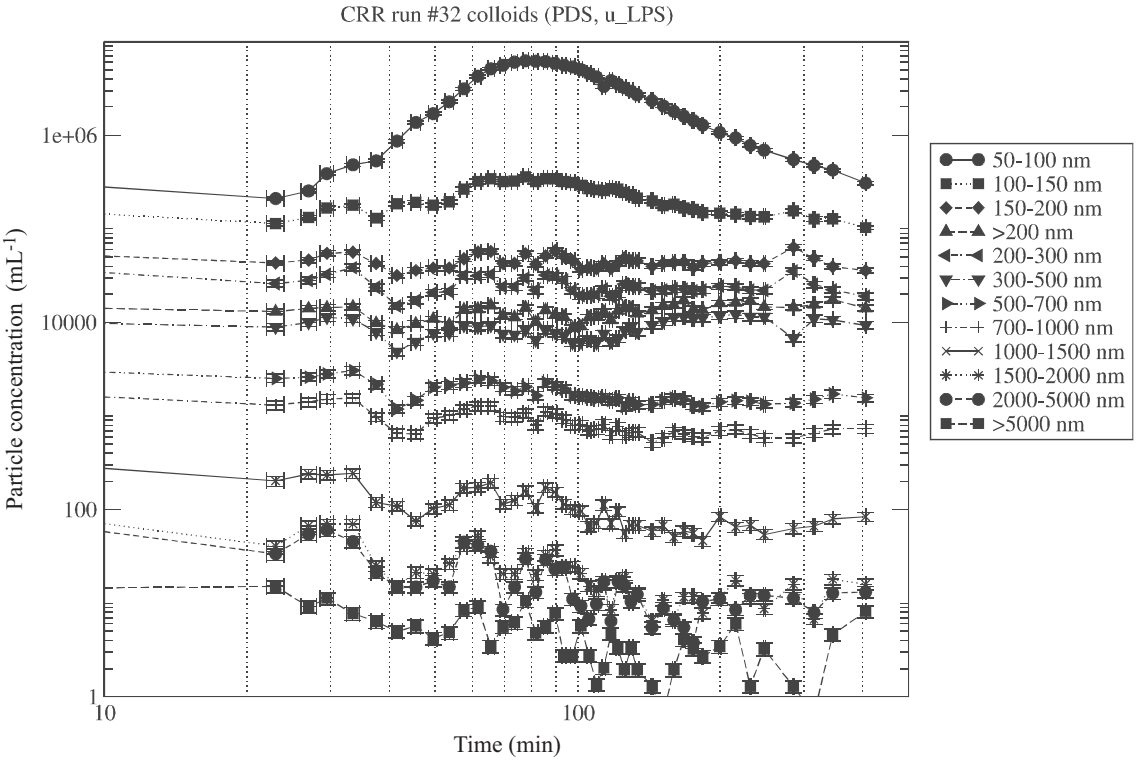

Fig. 4.15: Result of run #32: colloids counted in the various size classes

Figure 4.16 presents the comparison between non-retarded ^{131}I and the 50-100 and 100-150 nm colloid breakthroughs. The background concentration, obtained from sample number 10 from run #32 (compare Table 4.5), was subtracted from the measured colloid breakthrough and the colloid concentration (number of colloids per volume of water) was then normalised by division through the number of colloids in the injection solution for the corresponding size class. Clearly, the colloids arrive slightly before iodine while the tail is also somewhat comparable for ^{131}I and bentonite colloids.

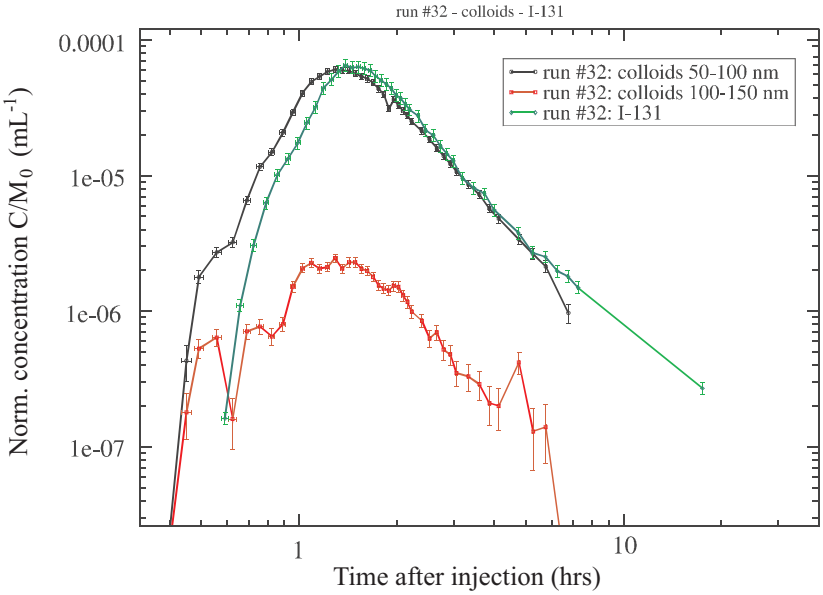

Fig. 4.16: Result of run #32: comparison of the breakthrough of ^{131}I and of colloids for size 50-100 and 100-150 nm

4.4.3.2 Recovery of bentonite particles in run #32

The colloid recovery is calculated independently for every size class $[d_i,d_{i+1}]$. The minimum and maximum particle diameters are represented for each size class by d_i and d_{i+1}, respectively. N_I is defined as the total number of injected colloids for a size class.

$$N_I = \int_{t_0}^{t_1} (q_i \cdot n_I)\, \mathrm{d}t = Q_i \cdot n_I \tag{3}$$

n_I is the number of colloids per volume in the injection solution (mL^{-1}), t is the time (s), q_i the injection flow rate (mL s^{-1}) for a time interval from t_0 to t_1, and Q_i the total injected amount of injection solution (mL). It is assumed that q_i and n_I are constant during injection.

The recovered total number of colloids for a given size class during a given time interval is

$$N_w = \int_{t_0}^{t_1} (q_w \cdot n_w(t))\, \mathrm{d}t \tag{4}$$

q_w is the withdrawal flow rate which is assumed to be constant in time. $n_w(t)$ is the measured number of colloids for this size class for time t and is a superposition of two colloid populations, the natural (background) GTS groundwater colloids and the injected bentonite colloids.

If the total number of natural (background) colloids N_B recovered during a time interval $[a,b]$ is known, it is possible to calculate the recovery R of the injected colloids

$$R = \frac{N_w - N_B}{N_I} \tag{5}$$

If it is assumed that the background colloid concentration is constant over time, N_B can be easily calculated from one measured concentration value n_B

$$N_B = \int_{t_0}^{t_1} (q_w \cdot n_B)\, \mathrm{d}t = (t_1 - t_0) \cdot q_w \cdot n_B \qquad (6)$$

At the beginning of run #32, before bentonite colloids were detected, measurements were taken to obtain the background colloid concentration. From Figure 4.15 it is clear that the first two measurements were not biased by the bentonite colloid breakthrough. Unfortunately these values were increased by a factor of ~5 compared to the values for the background concentration from run #31. The last measurements in run #32 show lower colloid concentrations than at the beginning. This is strong indication that the background concentrations at the beginning of the test were biased by the handling of the test equipment and probably show an overall decrease with test time. The comparison of the total number of recovered colloids with the total number of injected colloids shows that, for the smallest colloid size class, both values are nearly identical. The estimated total number of background colloids (integration along the sampling time) is less than 10% of the total number of injected colloids.

For larger colloid sizes, the total number of recovered colloids was higher than the total number of injected colloids as the total number of background colloids is also higher than the total number of injected colloids. It is therefore very difficult to detect the bentonite colloid breakthrough and it is therefore not possible to estimate accurate recoveries for these size classes.

The time dependent, natural colloid background concentration during the tracer tests was not known but from the colloid background study it is known that, within an hour of the end of an experimental run, the natural colloid concentration returns to the undisturbed background level. Therefore selected values from run #31 and #32 were taken for the calculation of the total number of recovered natural (background) colloids and it was assumed that they are constant during the experiment. The low concentrations from run #31 give a lower limit for the background concentration, whereas the higher values from run #32 give upper limits. The recoveries summarised in Table 4.5 are calculated for various background concentrations in order to take this variation into consideration.

The smallest measured colloids (50-100 nm), show a nearly complete recovery between 90% and 100%. For these recoveries, the maximum uncertainties (average errors) were also calculated. The calculated recovery for bentonite particles sized between 100 nm and 150 nm is somewhere between 15% and 100%. Here the uncertainty associated with the background particle concentration prevents a more accurate calculation. For all other colloid sizes, it is not possible to calculate a recovery because the natural variation of the background colloid concentration is larger than any possible breakthrough peak for the cocktail.

Tab. 4.5: Calculated recoveries and additional parameters needed for the calculation of the recoveries with help of equations 1-4

Size class [nm]	**d_i-d_{i+1}**	**50 - 100**	**Errors for size class: 50-100**	**100 - 150**	**Remarks**
Measured colloid concentration for injection solution [mL^{-1}]	n_I	8.3×10^8	$(+0.6\text{-}0.4) \times 10^8$	3.3×10^7	The errors represent the min. and max. values measured with various dilutions.
Injected number of bentonite colloids	N_I	8.3×10^{10}	$(+0.6\text{-}0.4) \times 10^{10}$	3.3×10^9	100 mL of initial suspension
Measured total number of recovered colloids	N_w	9.5×10^{10}	$(+1.0\text{-}0.9) \times 10^{10}$	1.1×10^{10}	Time interval: 0 – 405.5 min errors: 10% for a single measurement
Background colloid concentration from run #31 (sample 416) [mL^{-1}]	n_B	9.9×10^4	$\pm 1.0 \times 10^4$	4.7×10^4	errors: 10% for a single measurement
Total number of background colloids from run #31 (sample 416)	N_B	6.0×10^9	$\pm 0.6 \times 10^9$	2.9×10^9	Time interval: 0 – 405.5 min extraction flow rate: 150 mL min^{-1}
Recovery	**R**	**1.1**	**±20%**	**2.3**	
Background colloid concentration from run #32 (sample 1) [mL^{-1}]	N_B	3.4×10^5	+0.3-0.3	1.7×10^5	errors: 10% for a single measurement
Total number of background colloids from run #32 (sample 1)	N_B	2.1×10^{10}	$\pm 0.2 \times 10^{10}$	1.0×10^{10}	Time interval: 0 – 405.5 min extraction flow rate: 150 mL min^{-1}
Recovery	**R**	**0.9**	**±20%**	**0.2**	
Background colloid concentration from run #32 (sample 10) [mL^{-1}]	n_B	2.1×10^5	$\pm 0.2 \times 10^5$	1.1×10^5	errors: 10% for a single measurement
Total number of background colloids from run #32 (sample 10)	N_B	1.3×10^{10}	$\pm 0.1 \times 10^{10}$	6.9×10^9	Time interval: 0 – 405.5 min extraction flow rate: 150 mL min^{-1}
Recovery	**R**	**1.0**	**±20%**	**1.1**	

4.4.4 Summary of colloid migration

LIBD (laser induced breakdown detection), PCS (photon correlation spectroscopy) and SPC (single particle counter) analysis were successfully applied on- and off-site in the frame of the CRR project to characterise the colloid population in the outflowing GTS groundwater.

The natural colloid background concentration in the GTS groundwater was found to be around 5 μgL^{-1} (5 ppb). This concentration was determined by LIBD during the preparatory studies and the mean diameter of the background colloids was found to be around 200 nm. In the final tracer tests it was observed that, prior to the tracer injection, the colloid concentration in the GTS groundwater increased up to 22 ppb with maximum colloid sizes of 480 nm due to perturbations of the flow field by various manipulations of the test equipment. Directly before the first arrival

of the colloids in the extraction water, the colloid background values were down to between 2 and 4 ppb for 208 nm colloid size. The peak revealed concentrations of 109 ppb at an average colloid size of 100 nm, which is close to the mean diameter of the injected bentonite colloids of 109 nm.

PCS measurements revealed mean background colloid diameters scattered around 300 to 500 nm and background concentrations of approximately 50 – 70 ppb. This concentration is very close to or even below the detection limit of the method and therefore has to be taken with care. The mean diameter of colloids in the injection cocktail was 211 nm and 200 nm in the peak of the breakthrough curve. Sizes have to be considered as mean intensity weighted sizes, which are known to overestimate mass or number weighted mean sizes in case of colloid dispersions with a broad size distribution.

SPC measurements did not identify a colloid breakthrough in run #31. This implies that if any colloids are involved in this breakthrough they must be smaller than 50 nm (as already suspected by the LIBD measurements of colloids in the injection cocktail) or are too low in concentration (below natural colloid concentration) and therefore could not be recorded. In run#32, on the other hand, a considerable peak was observed for size classes 50 – 100 nm and, to a lower extent, for 100 – 150 nm. Colloids from size classes above 150 nm could not be detected in the colloid breakthrough as expected due to the lower colloid size in the injection cocktail.

Colloid recoveries were determined with all methods. The slightly different colloid recoveries obtained by the different methods are partly due to the analytical uncertainties of the methods (notably, PCS measurements are close to the detection limit of the method and revealed values between 57 and 90%) and partly due to uncertainties given by the difficulty of positioning the baseline. Consideration of the ICP-MS, SPC and LIBD data suggests that > 80% of the colloids passed the fracture without retardation. Filtration was not observed in these tests but occurred in the preparatory tests in dipole 3. It is reasonable to assume that this is due to differences in the flow path geometry in both dipoles or that the resolution of the analytical techniques is below the effect of filtration.

Figure 4.17 combines breakthrough curves of the colloids (determined with LIBD, PCS and SPC), of the aluminium concentration measurements (ICP-MS data) and of the breakthrough of ^{131}I and ^{244}Pu. After the peak maximum of ^{131}I, the curves fit well, even though ^{131}I arrived slightly later than the colloids (all around 80 minutes) as already observed in the preparatory testing. Aluminium again proved to be very useful and mirrored the breakthrough of the colloids perfectly.

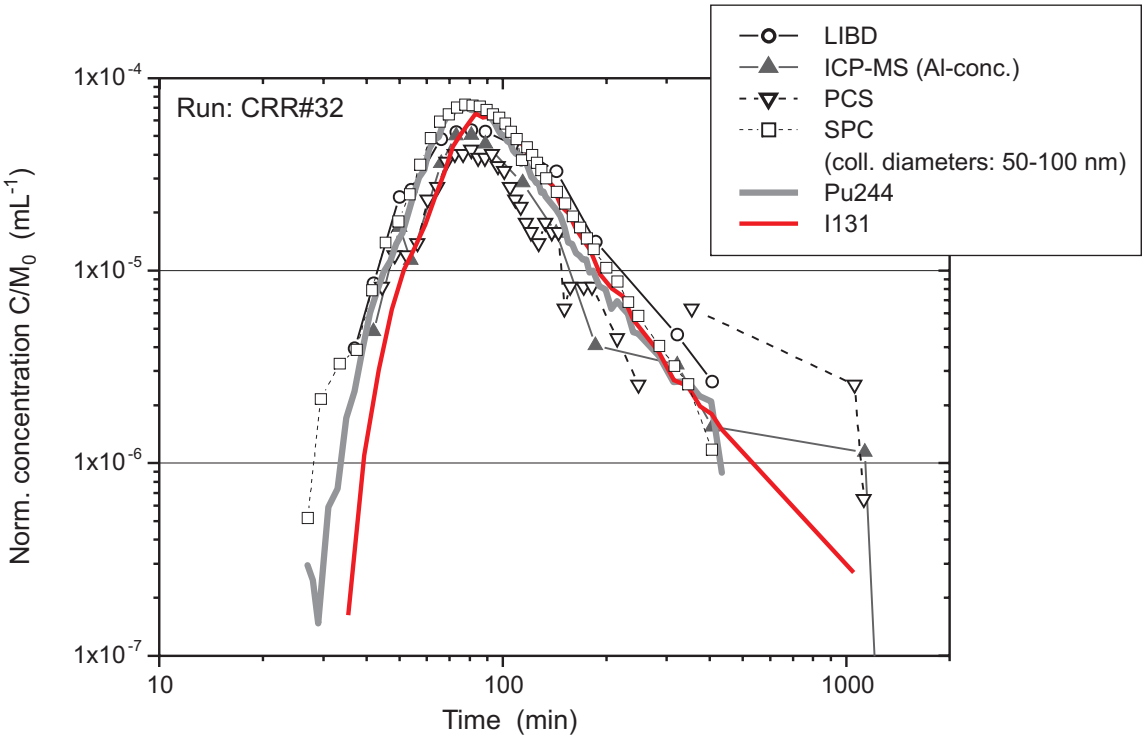

Fig. 4.17: Colloid breakthrough curves detected by LIBD, PCS, SPC and ICP-MS

4.5 Radionuclide migration

The breakthrough solutions in runs #31 and #32 were continuously sampled at the outlet borehole. ^{131}I, ^{85}Sr and ^{137}Cs were analysed using γ–spectrometry. ^{131}I could be detected on-line with the HPGe detector, so providing real-time information on the behaviour of ^{131}I in the experimental shear zone. The equipment was not sensitive enough, however, to detect the low ^{85}Sr and ^{137}Cs breakthrough concentrations. Off-site α–spectrometry analyses were carried out only on the nuclide pairs $^{237}Np/^{233}U$ and $^{241}Am/^{238}Pu$. $^{241/244}Am$, ^{237}Np, $^{233/238}U$ and $^{242/244}Pu$ were analysed also by ICP-MS. ^{99}Tc and ^{232}Th were analysed only by ICP-MS. Peak times and recoveries for the individual elements are summarised in Table 4.6 and discussed in more detail below. The differences in recovery and peak times between the two techniques (ICP-MS vs. α/γ-spectrometry) are almost within the 2-sigma errors of the applied techniques.

Tab. 4.6: Recoveries and the peak times run #31 -#32

Run	Tracer	Peak time **breakthrough** [min]	Recovery [%]	2-sigma errors [±%]	Analysing technique
#31	^{131}I	82	102	10	γ-spec
	^{85}Sr	236	87	10	γ-spec
	^{232}Th	68	n.d.	n.d.	ICP-MS
	^{238}U	78	62	9	ICP-MS
	^{237}Np	84	70	8	ICP-MS
		82	67	10	α-spec
	^{238}Pu	82	33	10	α-spec
	^{242}Pu	68	21	3	ICP-MS
	^{243}Am	68	34	4	ICP-MS
		72	43	10	α-spec
#32	^{131}I	83	92	10	γ-spec
	^{85}Sr	223	88	9	γ-spec
	^{137}Cs	72/10680	70	7	γ-spec
	^{99}Tc	85	n.d.	n.d.	ICP-MS
	^{232}Th	69	63	8	ICP-MS
	^{233}U	87	103	5	ICP-MS
		90	80	9	α-spec*
	^{237}Np	93	82	4	ICP-MS
		90	80	9	α-spec*
	^{238}Pu	84	70	9	α-spec*
	^{244}Pu	73	86	9	ICP-MS
	^{241}Am	71	n.d.	n.d.	ICP-MS
		84	70	9	α-spec*

* Note that U/Np and Am/Pu respectively were analysed in pairs
n.d.: recoveries not determined due to large scatter of analytical data

4.5.1 Radionuclide sorption onto experimental equipment

In order to quantify the sorption of the injected radionuclides on the test equipment, part of the dipole extraction side test setup was rinsed with 2% HNO_3 using a closed loop. Then the HNO_3 rinsing solution was analysed for the used radionuclide tracers (see Table 4.7). Only amounts of tracer activities below 1% of total input activity were found in the samples and sorption of the radionuclides on the test equipment did not bias the experiment to a relevant extent.

Tab. 4.7: Sorption on test equipment runs#31 and #32

Sample No	Flushed equipment components	α- conc. in rinsing solution [Bq/ml]	Percentage of total input activity [%]
Run#31	Total α-concentration		
1 run#31	extraction pumps and electrode flow through cells	0.005	0.13
2 run#31	extraction flow lines and spiral scintillometer	0.017	0.43
Run#32	Am-241 + Pu-238		
1 run#32	extraction pumps and electrode flow through cells	0.0020	0.06
2 run#32	extraction flow lines and spiral around scintillometer	0.014	0.41
4 run#32	dipole injection line	0.011	0.32
Run#32	Np-237 + U-233		
1 run#32	extraction pumps and electrode flow through cells	0.005	0.04
2 run#32	extraction flow lines and spiral around scintillometer	0.002	0.02
4 run#32	dipole injection line	0.007	0.05
Run#32	Sr-85		
1 run#32	extraction pumps and electrode flow through cells	0.0023	0.002
2 run#32	extraction flow lines and spiral around scintillometer	0.0072	0.005
4 run#32	dipole injection line	0.001	0.0007
Run#32	Cs-137		
1 run#32	extraction pumps and electrode flow through cells	0.0015	0.0001
2 run#32	extraction flow lines and spiral around scintillometer	0.0180	0.002
4 run#32	dipole injection line	0.0320	0.003

4.5.2 Mass balance

The detailed balance of radionuclides reported in Van Dorp et al., 2003 is based on the results of the α– and γ-spectrometry and of the ICP-MS analysis (see Table 4.6). The estimate of activity still remaining in the flow field was calculated per radionuclide and kilogram of fault gouge. Further on, these numbers were converted into the number of exemption limits (LE) that this activity represented (decay corrected to 01/01/03 for ^{85}Sr and ^{131}I). The maximum number of LEs remaining in the rock from all CRR injections is estimated to be 5.8 (per kg fault gouge). It should be emphasised that these data are highly pessimistic and represent the uppermost limit of activity remaining in the rock. For comparison, the natural radioactivity in the Grimsel granite gives 33 LE per kg (Möri & Van Dorp 2000). Therefore, the overcoring of the flow field was not recommended from either the radioprotection or from the scientific point of view. However, the activities remaining in the rock will be taken into consideration in the event that the area is to be used for future experiments and the sampling and analysis of the water flowing out of the experimental shear zone will be continued on a regular base (ca. four times per year) for the foreseeable future.

4.5.3 Radionuclide migration without bentonite colloids

The normalized concentrations for ^{237}Np, ^{238}U, ^{243}Am and ^{242}Pu in the breakthrough of run CRR#31 are plotted versus elution time in Figure 4.18.

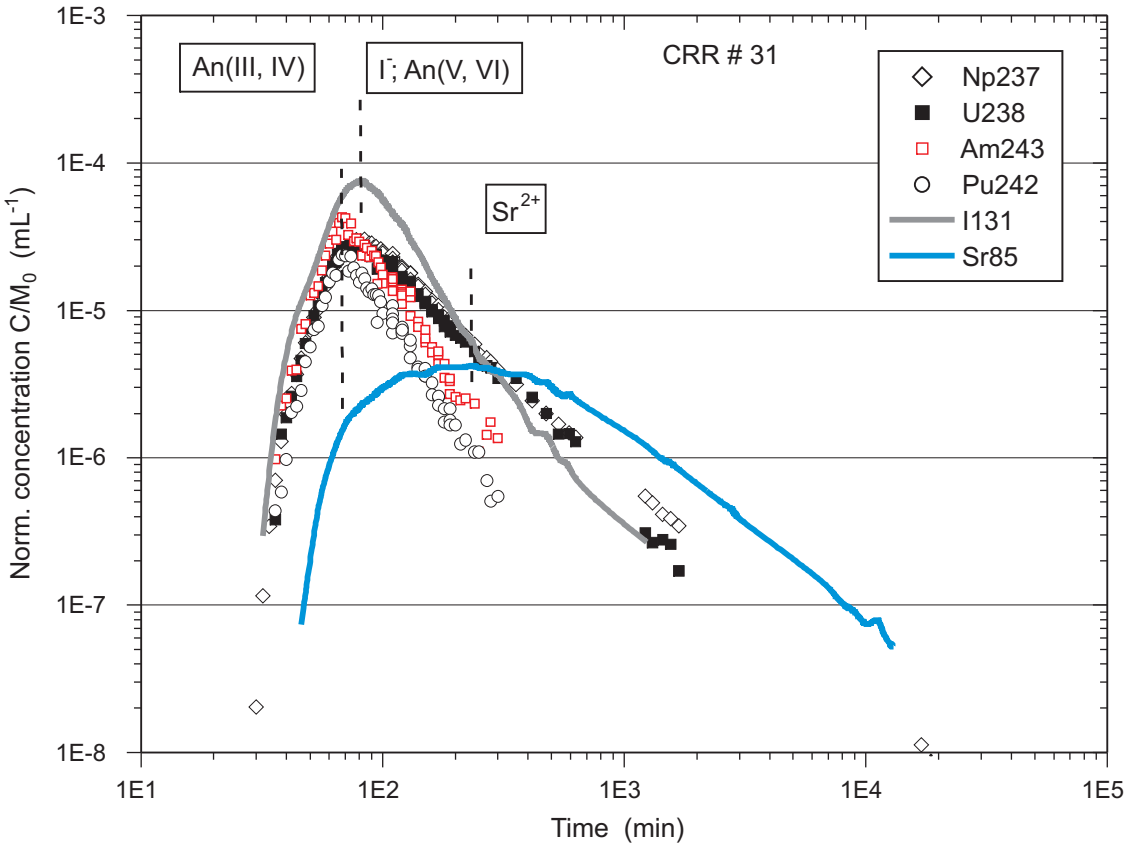

Fig. 4.18: Breakthrough curves determined in run CRR #31 (normalised concentrations); peak maxima for the different breakthrough curves are marked with vertical dashed lines

The breakthrough curves of ^{237}Np and ^{238}U are identical within error as are ^{243}Am and ^{242}Pu, (whereas ^{232}Th, not plotted in Figure 4.18[18], differs to a small degree before and around the maxima) indicating very similar migration behaviour of the oxidised ^{137}Np and ^{238}U and the reduced ^{243}Am and ^{242}Pu species, respectively. The vertical dashed lines in Figure 4.18 mark the peak maxima of the breakthrough curves and show the significant difference between the two element groups. The aluminium-concentration in the effluent remains quite constant during the observed time period within a range of 13 to 16 μgL^{-1}.

4.5.4 Radionuclide migration in presence of bentonite colloids

Results for the radionuclide concentrations in the breakthrough of run CRR #32 as determined by ICP-MS are plotted in Figure 4.19. Data for ^{99}Tc are not included for the same reasons as discussed above for ^{232}Th. There were also problems with the accuracy of the ICP-MS data for

[18] Data for ^{232}Th are quite scattered, lie close to the detection limit of the ICP-MS and are therefore not plotted in the figure. A quantitative determination of the Th-recovery is not possible without considerable error.

^{241}Am, for which the data obtained by α-spectrometry are certainly more reliable. Colloid concentrations were determined by measuring the aluminium concentrations in some of the samples collected during the experiment. Maxima of the breakthrough curves for ^{244}Pu, ^{232}Th and ^{241}Am appear similar to those of run #31 with the maxima occurring about 10 min earlier than those for ^{233}U, ^{237}Np and ^{99}Tc. The colloid breakthrough is indistinguishable from those for ^{244}Pu, ^{232}Th and ^{241}Am. A fraction of ~1% of the ^{137}Cs also shows a colloid-borne breakthrough while the major part appears strongly retarded as expected from the results of the earlier MI experiments. ^{85}Sr also behaves as expected, namely as a weakly sorbing tracer in both runs, irrespective of the absence or presence of bentonite colloids.

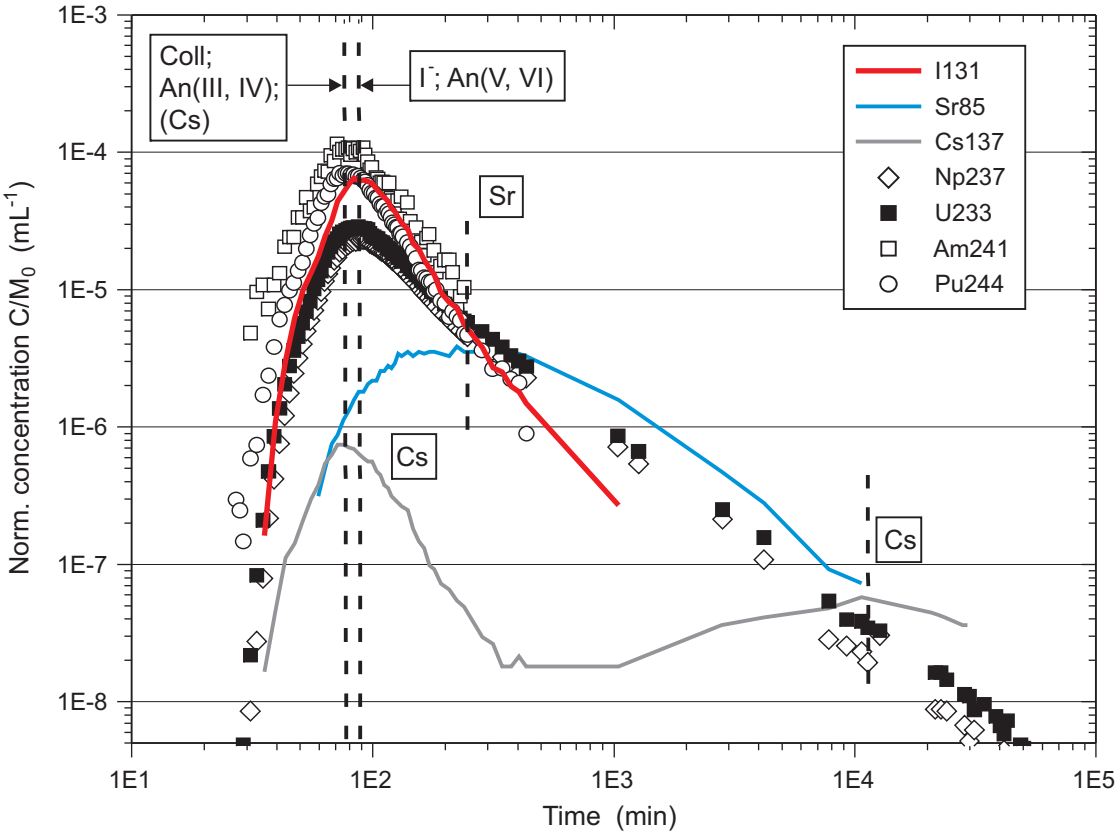

Fig. 4.19: Synopsis of breakthrough curves determined in run #32 (normalised concentrations); peak maxima for the different breakthrough curves are marked with dashed lines

4.5.5 Discussion of the influence of bentonite colloids on radionuclide migration

4.5.5.1 Radionuclide migration without bentonite colloids (run#31)

Breakthrough curves obtained for ^{232}Th, ^{243}Am and $^{238/242}$Pu are significantly different from those found for ^{238}U, ^{237}Np, ^{137}Cs, ^{85}Sr and the non-retarded tracer ^{131}I (see Figure 4.18). The peak maxima for the ^{232}Th, ^{243}Am and $^{238/242}$Pu breakthrough curves appear about 10 min earlier than those found for ^{131}I, ^{237}Np, and ^{238}U. 20 to 30% of the injected ^{243}Am and $^{238/242}$Pu were recovered, which is clearly less than that found for ^{237}Np and ^{238}U (up to 70%), ^{85}Sr (87%) and ^{131}I (100%). The ^{237}Np- and ^{238}U breakthrough curves are characterised by a more pronounced tail than found for ^{131}I, ^{243}Am and $^{238/242}$Pu.

These findings imply colloid-mediated migration of the "reduced" actinides ^{243}Am, $^{238/242}$Pu and ^{232}Th. As has been discussed previously, ultracentrifugation of the injection cocktail, while not providing a precise definition of the colloid content of these elements, does indicate colloidal fractions for these elements of up to 60%. It is therefore possible that the recovered ^{243}Am, $^{238/242}$Pu and ^{232}Th simply represent the colloidal fraction of the injected cocktail while the "dissolved", *ie* mononuclear aquatic species, are retained in the fracture as expected. Whether it is oxyhydroxide colloids (homogeneous radiocolloids) generated by the spiking procedure or existing natural GTS groundwater colloids hosting ^{243}Am, $^{238/242}$Pu and ^{232}Th (heterogeneous radiocolloids) is not yet clear and this would need to be studied further. This could be done in two ways:

- the outflow solution could be analysed for the presence of colloids and, where present, the colloid types could be identified
- additionally, because laboratory tests have shown that the colloidal fraction of the radionuclide cocktail is unstable over longer timescales (tests carried out up to 500 days; see Fig 4.7), a long-term migration experiment could be carried out[19]. This should be able to rule out the affects of the short-term colloids thought to be present in the cocktail.

Solubilities were calculated to lie in a range of 6.0E-08 – 4.7E-09 molL^{-1} for ^{232}Th and 2.0E-09 – 1.0E-10 molL^{-1} for ^{238}Pu (Duro, 2000). However, laboratory tests indicated some uncertainty in these numbers (Missana & Geckeis, 2004) and so it was felt reasonable to increase the injection cocktail concentrations to slightly above these levels as this would aid in the tracer determination in the breakthrough samples. Thus, from the thermodynamic data, the precipitation of colloidal ^{238}Pu species cannot be excluded and may explain the observed presumed colloidal migration behaviour.

Precipitation of pure amorphous solids is not likely for ^{243}Am (concentration in the cocktail: 5.9E-09 molL^{-1} or two orders of magnitude less than the calculated solubility of 1-2E-07 molL^{-1}). Thus, the co-appearance of colloidal ^{243}Am and ^{238}Pu phases cannot be unequivocally explained on the basis of existing thermodynamic data. However, as noted above, the formation of colloids upon spiking the alkaline GTS groundwater with the acidic radionuclide stock solution may also occur due to local oversaturation.

The interaction of dissolved reduced actinide species with existing GTS groundwater colloids could also explain the observed experimental findings. Taking the experimentally obtained K_d-values for the sorption of ^{238}Pu and ^{243}Am on colloids and the background colloid concentration in the GTS groundwater of 5 ppb, it is possible to calculate that a minor fraction of the total actinide species could be colloidally bound, even in the absence of added colloidal matter. It is, however, debatable whether the sorption capacity, *ie* the amount of available surface sites, of these natural colloids is sufficient to bind considerable fractions of ^{243}Am and ^{238}Pu/^{232}Th and this would need to be checked experimentally.

The breakthrough behaviour of ^{238}U and ^{237}Np suggests that a fraction of these elements migrates like a non-retarded tracer (as displayed by the rising part of the breakthrough curve) while another fraction is retarded (as shown by the pronounced tailing of the peak, resembling that of the strontium curve). Colloid mediated transport of these actinide ions can be ruled out as:

1. the ultracentrifugation experiment indicates only small to no significant amounts of colloidal ^{237}Np and ^{238}U species in the injection cocktail (see Table 4.3),

[19] Indeed, just such an experiment (CFM: Colloid Formation and Migration) has begun within GTS Phase VI (see www.grimsel.com for details).

2. the completely identical shape of the ^{237}Np and ^{238}U breakthrough curves in run #31 (without colloids) and run #32 (with colloids) demonstrates the irrelevance of colloids for the speciation of both actinide ions and
3. the maxima in their breakthrough curves are similar to that of the conservative tracer and arrives about 10 min after that of the colloid-borne, reduced actinides.

The kinetic hindrance of ^{238}U and ^{237}Np reduction to the tetravalent state has been shown in previous laboratory experiments where ^{237}Np, ^{238}U and ^{99}Tc have been found to remain stable for a long time in the reducing GTS groundwater (Missana & Geckeis, 2004, Alexander et al., 2003). The significantly different shape of the breakthrough curves for ^{238}U and ^{237}Np as compared to that of the "reduced" actinides ^{243}Am, ^{232}Th and ^{238}Pu, and the almost complete recovery indicates that the oxidation states for these elements remain V and VI, respectively, during the passage through the experimental shear zone (see also the earlier comments about ^{99}Tc).

Rather weak sorption on fracture infill minerals has been observed in laboratory sorption studies for ^{238}U, ($K_d \sim 5$ mL g^{-1} after 1 h) and for ^{237}Np (Missana & Geckeis, 2004). K_d-values for ^{237}Np were < 1 mL g^{-1} at short time scales but increased slightly upon extending the contact time to 24 h (~2 mL g^{-1}). The very limited sorption of these actinide ions may be due to their aquatic speciation. Under given GTS groundwater conditions, ^{238}U probably exists primarily as the anionic carbonato- and hydroxo-complexes $UO_2(CO_3)_3^{4-}$, $UO_2(CO_3)_2^{2-}$, and $UO_2(OH)_3^-$ (Duro, 2000). Formation of anionic carbonato-complexes is known to strongly reduce the interaction of ^{238}U with surfaces (see *eg* Payne et al., 1998). The sorption of ^{237}Np to mineral surfaces is even less pronounced than that of ^{238}U. The weak sorption of the NpO_2^+ ion on fracture infill minerals may be further decreased by the presence of $NpO_2CO_3^-$.

Breakthrough curves for ^{237}Np and ^{238}U therefore indicate the probability that sorption process on fracture surfaces in both runs is kinetically hindered. As has been mentioned before, ^{238}U and ^{237}Np species are dominated by negatively charged complexes. Repulsion from the negative mineral surfaces combined with the delayed exchange of OH^- and CO_3^{2-} ligands on mineral surface sites might be responsible for the retarded sorption reaction.

However, the exact reasons for the observed kinetics remain hitherto unclear. It is very likely that, under slow groundwater flow conditions and at longer residence times in the fracture, both actinide species will be retarded. Moreover, their reduction to lower oxidation states with subsequent strong sorption or precipitation at very long time scales is also within bounds. Further investigations in core experiments will be carried out in the laboratory in order to better understand the kinetics of the ^{238}U and ^{237}Np interaction with fracture surfaces.

Sr and the non-colloid borne Cs fraction injected in run #32 are retarded in a way that is expected from the results of the earlier Migration experiments (Frick et al., 1992, Smith et al., 2001). Under the GTS groundwater conditions, both elements exist almost exclusively as hydrolised cations and thus readily interact with the negatively charged fracture surface sites.

4.5.5.2 Radionuclide migration with bentonite colloids (run#32)

Breakthrough curves for the colloids detected by the different analytical methods and those for $^{238/244}Pu$, ^{241}Am and ^{232}Th are very similar in form and the peak maxima are slightly shifted to earlier elution times relative to that of the conservative tracer (as expected by analogy to earlier colloid in *situ* experiments - see Figure 4.17 for a comparison of ^{244}Pu and colloid breakthrough curves). However, the tails of the curves differ from those in previous experiments with

bentonite colloids in dipole 3 (run #6, #7) insofar that the present experiment is similar to that of the conservative tracer. This finding suggests that the mechanisms responsible for peak broadening and tailing, *ie* diffusive processes or dispersion in the heterogeneous structure of the flow field, are the same for colloids and non-retarded tracers in the fracture zone studied here. Making the reasonable assumption that the geochemical conditions in both flow fields are the same, it is proposed that the flow field used for the earlier colloid migration experiments has a different physical form with regard to the occurrence of channelled structures and the presence of fracture filling material. It is proposed that dipole 1 contains less fine pores (*eg* present in the fracture filling material) which normally allow access of ionic species but exclude colloidal species and dipole 3, on the other hand, could contain more channelled flow paths. This physical difference in the two flow fields could simply be a reflection of the heterogeneity of the experimental shear zone (see also Möri et al., 2004) or it could be due to the extended testing in dipole 3, leading to gradual wash-out of the finer material.

The main difference in the results of the two runs is that the recovery of the "reduced" actinides ^{241}Am, ^{244}Pu and ^{232}Th is increased from about 30% to values >60 to 86%. This is easily explained by the predominantly colloidal state of these metal ions as revealed by the ultra-centrifugation tests in the laboratory. The migration of ^{237}Np and ^{233}U is essentially identical in both runs. For ^{137}Cs, it appears that a minor part is transported by colloids and the major part is retarded as expected. ^{99}Tc migration follows that of ^{131}I, indicating the likelihood of kinetically hindered reduction of TcO_4^- to the tetravalent form of Tc, also in agreement with previous observations for this groundwater system. It thus seems likely that the injected ^{99}Tc was not in the tetravalent state, but either remained heptavalent due to insufficient reduction by hydrazine in the cocktail or has been re-oxidized thereafter. This is also suggested by the ultra-centrifugation experiment, where only a minor part of the technetium was found in the colloidal fraction. A quantitative assessment of the ^{99}Tc behaviour has, however, not been attempted due to the very low concentrations in the cocktail resulting in ^{99}Tc concentrations in the effluent close to the detection limits. Measured data are thus affected by pronounced scattering, demonstrating the analytical uncertainty of these data. According to the results of the ultra-filtration study, ^{85}Sr does not undergo significant interaction with the bentonite colloids, which is reflected by the clearly retarded elution without any visible contribution of colloid-borne transport.

The bentonite colloid influence on the migration of the individual radionuclides is wholly consistent with the results of earlier laboratory experiments. In Table 4.8, the colloid-bound radionuclide concentrations are calculated using the measured K_d-values and compared with the colloid fractions determined by ultrafiltration. There is a reasonable agreement between measured and calculated colloid fractions, with a total concentration of colloid-borne radio-nuclides of < 1.3E-07 molL^{-1}. According to an estimation given in Geckeis et al., (2003a), the capacity of available sorption sites at the colloidal smectite edges corresponds to 2.3E-06 molL^{-1}. As a consequence, less than 6% of the totally available number of surface sites available at the bentonite colloids would appear to be occupied by metal ions.

The colloid concentration obviously does not influence the aquatic speciation of ^{233}U and ^{237}Np considerably, and thus does not affect their migration behaviour in this system. In the case of ^{244}Pu, ^{232}Th and ^{241}Am, however, speciation is dominated by colloids. Significant desorption of these elements from the colloids does not occur during the time of the experiment (nor over the 500 days laboratory observation period) and an almost complete recovery is obtained (as is the case for the colloids). The situation appears to be different for ^{137}Cs. Even though ~ 10% of the ^{137}Cs is colloid-borne in the injection cocktail, only about 1% is eluted from the fracture together with the colloids. This might indicate that a major part of the ^{137}Cs desorbs from the colloids and subsequently is retarded on the fracture surfaces. This behaviour is consistent with

the fact that ^{137}Cs is presumed to partly interact with the permanent charges on the smectite planes in the bentonite by ion exchange, a readily reversible reaction. Nevertheless, kinetic hindrance of desorption of a part of the ^{137}Cs from smectites is also known and explained by the collapse of the interlayer structure capturing the ^{137}Cs and thus preventing a rapid dissociation. The kinetically hindered dissociation of a part of the bentonite colloid-borne ^{137}Cs has indeed been observed in GTS groundwater (Missana et al., 2004).

Tab. 4.8: Calculated and measured colloid-bound radionuclide concentrations (colloid concentration: 20 mgL^{-1}) – see Missana & Geckeis (2004) for details

	^{233}U	**^{237}Np**	**^{244}Pu**	**^{232}Th**	**^{241}Am**	**^{137}Cs**	
K_d ($mL\ g^{-1}$) for sorption on bentonite coll.	8.2 E+02	< 5.0E+03	1.0E+05	2.0E+06	2.0E+06	8.8E+03	
Total radionuclide conc. in cocktail ($molL^{-1}$)	8.7E-07	1.0E-06	6.7E-09	1.0E-08	8.0E-10	1.6E-08	
Calculated colloid bound radionuclide fraction (%)	2	< 9	67	98	98	15	
Measured colloid bound radionuclide fraction (%)	6	<1	84	94	99	8	**Total**
Colloid bound radionuclide conc. ($molL^{-1}$)	1.4E-08 1.6%	< 1E-07 10%	4.5E-09 67%	1.1E-08 110%	6.5E-10 81%	2.1E-09 13%	**1.3E-07**

5 Summary and conclusions

W.R. Alexander, H. Geckeis and A. Möri

The presented *in situ* experiment where, for the first time, actinides and bentonite colloids were injected into a water-conducting feature in a fractured rock, was preceded by an intense preparatory field, laboratory and modelling campaign. Such complex experiments always require compromises in the layout and experimental concept and so an in depth evaluation of the pros and cons of different hydraulic and geochemical boundary conditions were carried out in order to minimise any experimentally induced artefacts on the results. However, an *in situ* experiment can never be entirely free of experimental influences and so some processes which are irrelevant for a repository PA, such as kinetic effects due to the relative short residence time of the tracers in the experimental shear zone, have to be taken into account when interpreting the results.

5.1 Preparatory testing

The careful hydraulic characterisation of the test site required hydro- and tracer testing with conservative tracers. The data were fed into a transmissivity model of the test area and predictions on tracer breakthrough were produced. The optimum compromise site - with a narrow, homogeneous flow field, 100% recovery of a conservative tracer and with long residence times - will always be difficult to find, but the selected 2.23 m long dipole served best for the final *in situ* injection as it showed 100% tracer recovery at residence times of about two hours.

Homologue pre-tests with ^{178}Hf and ^{232}Th for the tetravalent actinides and ^{159}Tb for the trivalent actinides (also in combination with bentonite colloids) proved to be very useful for the prediction of the *in situ* behaviour of the actinides and colloids in the experimental shear zone. Little was known about the *in situ* migration behaviour of bentonite colloids in water conducting features and it was found that a considerable part of the injected colloids travel unretarded through the flow field, increasing also the recovery of the homologues. Travel times of colloids and colloid-bound homologues were found to be even faster than for the conservative uranine as their relatively large size presumably hinders diffusion into the matrix (or in the case of this experiment, the fracture fill material).

The interaction of the strongly sorbing tri- and tetravalent actinides with the equipment was tackled by producing as many as possible of the parts that are in direct contact with the tracers in PEEK. Tracer loss on the equipment was checked by flushing with HNO_3 and this showed that losses were negligible for the given test layout and duration.

5.2 Tracer cocktail

The general tracer cocktail composition reflects the requirements of the various project partners involved in the project. The selected concentrations and activities were influenced by the thermodynamic solubility calculations, by radioprotection limitations and by constraints concerning the detection limits of the available analytical methods. In addition, there was an extended discussion on the oxidation states of the radionuclides in the cocktail, especially for ^{237}Np, which was used in a pentavalent state, and $^{233/238}$U, which was finally used in a hexavalent state. The selection of the actinides in these redox states was the result of laboratory experiments, the kinetics of redox reactions and practicality constraints on the *in situ* use of

these elements. It can be seen that every oxidation state between -I and VII was intendet to be present in the injection cocktail.

The preparation of an injection cocktail which contains tri- and tetravalent actinides proved to be problematic as shown by the presence of a variable colloidal fraction for ^{243}Am, $^{238/242}$Pu and ^{232}Th, even in the absence of bentonite colloids (run#31). Long term investigations of the cocktail (up to 500 days) revealed that the stability of these colloids is temporally limited. The scatter in the measured colloidal data might be attributed to i) colloids with a very low density or ii) gel-like aggregates with high water content. It remains debatable whether these observed colloids are a reflection of the GTS groundwater background colloid levels or whether they are an artefact of the cocktail preparation (*eg* oversaturation during spiking) or both and this needs to be investigated further. The other elements showed no significant colloid formation in the cocktail.

The injection cocktail of run #32 showed high colloid association and long term stability for the tri- and tetravalent actinides with the bentonite colloids in the range of 84 to 99%. For the moment, it is assumed that these radionuclides are all attached to the added bentonite colloids, but this has not been shown experimentally and therefore any interference from the above noted mechanisms cannot be ruled out. The ^{99}Tc in the oxidation state VII appears to have been reduced to tetravalent ^{99}Tc but it remained unclear whether the ^{99}Tc was bound to colloids in the injection cocktail. A small fraction of ^{137}Cs, on the other hand, could be clearly related to colloids. Almost 90% of the $^{238/244}$Pu was found to be in oxidation state IV.

5.3 Tracer migration

In run #31, the tri- and tetravalent actinides ^{243}Am, ^{232}Th and $^{238/242}$Pu displayed different breakthrough behaviour to the other elements (less recovery, less tailing and a peak time which is about 10 min earlier than for ^{238}U and ^{237}Np). This indicates that a fraction of these actinides was transported in a colloidal state. With regard to the colloid content in the injection cocktail, the source of the colloids cannot yet be uniquely defined (homogeneous- or heterogeneous radiocolloids) however, it is clear that these colloids show a considerable instability within a time period of one to two years and they either dissolve or release actinide ions. ^{238}U and ^{237}Np both remained in the oxidised state during the experiment and colloid-mediated transport of these elements can probably be ruled out. This is also the case for ^{85}Sr, which behaved as in previous migration experiments, both in this particular experimental shear zone and elsewhere.

Run #32, on the other hand, indicated an increase in the fraction of the colloid- mediated migration of ^{241}Am, $^{238/244}$Pu and ^{232}Th (significant increase in the tracer recovery). The shape of the breakthrough curves did not change significantly as the peak in the first experiment was also affected by a colloidal fraction. The colloid mediated transport was confirmed by ultracentrifugation of the breakthrough solutions and by the comparison of the breakthrough of the bentonite colloids with those of the actinides. Significant desorption of tri- and tetravalent actinides from the bentonite colloids within the experimental time frame were not observed. ^{237}Np and ^{233}U showed no difference in their breakthrough behaviour in comparison to run #31. About 1% of the ^{137}Cs was colloidally transported which implies that 90% of the initially colloid bound ^{137}Cs in the injection cocktail (10% ^{137}Cs in the injection cocktail was in colloidal form) desorbed. ^{99}Tc behaved like the conservative tracer ^{131}I, even if it was intended to inject ^{99}Tc in its reduced form as ^{99}Tc(IV) where it would be assumed to be associated with colloids under *in situ* conditions. The conservative behaviour indicated that this reduction did not take place in the time frame of the *in situ* experiment. ^{85}Sr showed no significant interaction with the bentonite colloids.

5.4 Colloid migration

The four different colloid detection techniques (LIBD, ICP-MS, PCS and SPC) which were applied in this study produced internally consistent colloid breakthrough data. Uncertainties in the background determination are responsible for a certain scatter in the results, but recovery of about 90% of the injected colloids seems likely. In contrast to earlier *in situ* experiments with bentonite colloids, size fractionation due to filtering was not observed in the final injection, but this effect could be below the detection limit of the applied technique.

The study indicated a considerable influence of the internal structure of the flow field on the migration behaviour of the colloids. Importantly, these (presumably small-scale) differences in the flow paths do not necessarily show up in the measured transmissivities. Indeed, the experiment where the transmissivity field distribution indicated a transmissivity boundary within the test dipole produced less filtration of colloids than in the dipole where no transmissivity boundary could be discerned, suggesting that field transmissivity data, even when measured on small-scale flow paths such as here, are poor indicators of potential *in situ* colloid filtration. This has obvious implications for repository site characterisation programmes and needs further investigation: should the interpretation and design of the tests be improved and/or other tests be employed? Could further improvements be made in the interpretation of conservative tracer data to elucidate the likely degree of *in situ* colloid filtration?

5.5 Recommendations

The *in situ* data produced in CRR must be viewed in context and not be taken over into repository PAs without very careful analysis of their relevance. In particular,

- the formation of actinide colloids *in situ* has been little studied and additional work is required to fully ascertain the mechanisms involved. Until it can be clearly shown that this is not simply an experimental artefact, these data should be treated as provisional.
- while field transmissivity data may be used for the overall understanding of a repository site hydrogeology, the clear dichotomy between the colloid filtration data and the transmissivity data indicate that care must be taken when applying such data to predict small-scale physical processes.
- the kinetic effects previously observed in radionuclide tracer tests and observed once more here are of little relevance to a repository other than to indicate the limitations of short-term experiments when trying to assess repository timescale relevant processes and mechanisms

Finally, it must be mentioned, that a long-term *in situ* experiment will be carried out within Phase VI of the Grimsel Research Programme in the CFM (Colloid Formation and Migration) project. This experiment aims to improve on the spatial and temporal limitations of CRR and to add knew knowledge on speciation, kinetics and desorption processes of actinides in presence of colloids, not only with the *in situ* experiment but also with an associated laboratory and modelling programme.

6 Acknowledgements

The CRR project involved many people from a wide range of organisations and we would like to extend our thanks to all of them. In particular, thanks go to Tiziana Missana (Ciemat), Max Rüthi (PSI) and Lukas Inderbitzin (GI) for their support during the *in situ* experiment, to Andreas Laube (PSI) for analytical support and Wolfgang Hauser (FZK) and his LIBD team. Special thanks also to the staff of the GTS for their support and to Johannes Vigfusson (HSK) for his careful examination of the project radioprotection activities. Finally we would like to thank to the funding organisations, namely ANDRA (F), ENRESA (E), FZK-INE (D), JNC (J), Nagra (CH) and the USDoE/Sandia (USA), who made this project possible.

7 References

ADAMS, J. & E. WYSS, (1994): Hydraulic Packer Testing in the Wellenberg Boreholes SB1 and SB2 - Methods and Field Results. - Nagra Technical Report, NTB 93-38, February 1994.

AGARWAL, R. G. (1980): A New Method to Account for Producing Time Effects When Drawdown Type Curves Are Used to Analyze Pressure Buildup and Other Test Data. - Soc. Petrol Eng., SPE Paper 9289, presented at SPE-AIME Meeting, Dallas, Texas, September 21-24.

ALEXANDER, W.R. (ed.) (1991): Redox state of the Grimsel Test Site (GTS) radionuclide Migration Experiment groundwater/rock system. Unpublished Nagra Internal Report, Nagra, Wettingen, Switzerland

ALEXANDER, W.R., FRIEG, B., K. OTA, & K. BOSSART, (1996) The RRP Project: Investigating Radionuclide Retardation in the Host Rock. Nagra Bulletin No.27 (June, 1996), pp43-55.

ALEXANDER, W.R., R. DAYAL, , K. EAGLESON, J. EIKENBERG, E. HAMILTON, C.M. LINKLATER, , I.G. MCKINLEY & C.J. TWEED, (1992): A natural analogue of high pH pore waters from the Maqarin area of northern Jordan II: results of predictive geochemical calculations. J. Geochem. Explor. 46, ppl33-146.

ALEXANDER, W.R., K. OTA, & B. FRIEG, (eds.) (2003): The Nagra-JNC *in situ* study of safety relevant radionuclide retardation in fractured crystalline rock II: the RRP project methodology development, field and laboratory tests. Nagra Technical Report NTB 00-06, Nagra, Wettingen, Switzerland.

ALEXANDER, W.R., A. MOERI, & P.A. SMITH, (2004): The CRR final project report series: IV – project overview and synthesis of results. Nagra Technical Report NTB 03-04, Nagra, Wettingen, Switzerland (in prep).

BAEYENS, B., A. MAES & A. CREMERS (1985). *In situ* Physico-chemical Characterization of Boom Clay; Rad. Waste Manag. Nucl. Fuel Cycle; 6, 391.

BOSSART, P. & M. MAZUREK, (1991): Grimsel Test Site: Structural geology and water flow-paths in the migration shear zone. Nagra Technical Report 91-12, Nagra, Wettingen, Switzerland.

BOURDET, D., J. A. AYOUB, & Y. M. PIRARD, (1989): Use of Pressure Derivative in Well-Test Interpretation. - SPE Formation Evaluation, Vol. 4, pp. 293-302.

BROOKHAVEN INSTRUMENTS CORPORATION (1990): Brookhaven Instruments Corporation's Data Analysis Software (BI-ISDA), version 8.0; Brookhaven Instruments Corporation (www.bic.com): Holtsville, New York.

CHAPMAN, N.A., I.G. MCKINLEY, M.E. SHEA & J.A.T. SMELLIE (1993). Poços de Caldas: nature`s experiment. Nagra Bulletin 1/1993, Nagra, Wettingen, Switzerland.

COOPER, H. H. & C. E. JACOB, (1946): A generalized graphical method for evaluating formation constants and summarizing well-field history. – Trans. Amer. Geophys. Union, Vol. 27, No. IV, pp 526-532.

DEGUELDRE, C., H.R. PFEIFFER, , W.R. ALEXANDER, , B. WERNLI, & R. BRUETSCH, (1996). Colloid properties in granitic groundwater systems. I Sampling and characterisation. Appl. Geochem., 11, 677-695.

DEGUELDRE, C., G. LONGWORTH, V. MOULIN, & P. VILKS, (1990): Grimsel colloid exercise: An international intercomparison exercise on the sampling and characterisation of groundwater colloids. Nagra Technical Report NTB 90-01, Nagra, Wettingen, Switzerland.

DIERCKX, A., M. PUT, P. DE CANNIÈRE, L. WANG, N. MAES, M. AERTSENS, A. MAES, J. VANCCLUYSEN, W. VERDICKT, R. GIELEN, M. CHRISTIAENS, P. WARWICK, A. HALL & J. VAN DER LEE (2000). Transport of Radionuclides due to Complexation with Organic Matter in Clay Formations - TRANCOM-Clay. EUR19135EN, Final Report Nuclear Science and Technology, European Commission, Brussels, Belgium.

DURO, L. (ed.) (2000): Prediction of the solubility and speciation of radionuclides in Febex and Grimsel waters. Appendix A in MISSANA, T. and H. GECKEIS, (eds), (2004): The CRR final project report series: II - results of the supporting laboratory programme. Nagra Technical Report NTB 03-02 (in press).

ENRESA (1998): FEBEX Bentonite: Origin, Properties, and Fabrication of Blocks, ENRESA, Publication Technica Num. 05/98, ENRESA, Madrid, Spain.

FIERZ, TH., H. GECKEIS, , R. GÖTZ, F.W. GEYER, & A. MÖRI (ed.) (2001): GTS V/CRR: Tracer tests #1 - #16 (September 1999 – January 2001). Unpublished Nagra Internal Report. Nagra, Wettingen, Switzerland.

FISCH, H.R. (2002): Task 5a: Hydraulic testing in the boreholes BOCR 99.002 and BOCR 00.003. Unpublished Nagra Internal Report, Nagra, Wettingen, Switzerland.

FRICK, U., W.R. ALEXANDER, , B. BAEYENS, , P. BOSSART, , M.H. BRADBURY, CH. BÜHLER, , J. EIKENBERG, Th. FIERZ, W. HEER, , E. HOEHN, I.G.McKINLEY, & P.A. SMITH, (1992): The radionuclide migration experiment-overview of investigations 1985-1990. Nagra Technical Report Series NTB 91-04, Nagra, Wettingen.

GARDINER, M. P., P. GRINDROD & V. MOULIN (2001). The Role of Colloids in the Transport of Radionuclides from a Radioactive Waste Repository: Implicationon Safety Assessment. Final Project Report EUR 19781, European Commission, Brussela, Belgium.

GECKEIS, H., W. HAUSER, F.W. GEYER, , R. GÖTZ, , TH. SCHÄFER, , TH. FIERZ, , W.R. ALEXANDER, & A. MÖRI, (ed.) (2003a): GTS V/CRR: Preparatory tracer tests with bentonite colloids, homologues, Br-82 and Sr-85. Unpublished Nagra Internal Report. Nagra, Wettingen, Switzerland .

GECKEIS, H., F.W. GEYER, W. HAUSER, C.M. MARQUARDT, TH. SCHÄFER, J. EIKENBERG, TH. FIERZ, , A. MÖRI, (ed.) (2003b): GTS V/CRR: Tracer tests #28 - #35 (January – March 2002); raw data report. Unpublished Nagra Internal Report, Nagra, Wettingen, Switzerland.

GUIMERA, J., G. KOSAKOWSKI, K. IIJIMA, A. PUDEWILLS, & P. SMITH, (2004): The CRR final project report series: 3 - results of the supporting modelling programme. Nagra Technical Report NTB 03-03. Nagra, Wettingen, Switzerland (in press).

HAUSER, W., H. GECKEIS, J.I. KIM, , & Th. FIERZ, (2002): A mobile Laser-Induced Breakdown Detection System and its application for the *in situ*-monitoring of colloid migration, Colloids Surf. A, 203, 37-45.

HAUSER, W., H. GECKEIS, R. GÖTZ, F.-W. GEYER, L.INDERBITZIN, Th. FIERZ, & A MÖRI, (2003): GTS Phase V: CRR Experiment Laser-Induced Breakdown Detection of Natural Colloid Background at the Grimsel Test Site. Unpublished Nagra Internal Report, Nagra, Wettingen, Switzerland.

HSK (1998) Unpublished internal note. HSK, Villigen, Switzerland

HUERTAS, F., J.L. FUENTES-CANTILLANA, P. JULLIEN, F. RIVAS, J. LINARES, P. FARIÑA, M. GHOREYCHI, N. JOCKWER, W. KICKMAIER, M.A. MARTINEZ, J. SAMPER, E. ALONSO, F.J. ELORZA, (2000): "Full scale engineered barriers experiment for a deep geological repository for high-level radioactive waste in crystalline host rock (FEBEX Project)" Contract No. FI4W-CT95-0006 E.C. Final report EUR 19147, CEC, Brussels, Belgium.

JAMES, S.C. & C.V. CHRYSIKOPOULOS, (1999). Transport of polydisperse colloid suspensions in a single fracture. Wat. Resour. Res., 35, 707-718.

KRUSEMAN, G.P. & N.A. DE RIDDER, (1991): Analysis and Evaluation of Pumping Test Data. 2nd Rev. Edition. ILRI Publication 47. International Institute for Land Reclamation and Improvement, Wageningen.

LINKLATER, C.M., Y. ALBINSSON, W.R. ALEXANDER, I .CASAS, I.G. MCKINLEY, & P. SELLIN, (1996): A natural analogue of high pH cement pore waters from the Maqarin area of northern Jordan: comparison of predicted and observed trace element chemistry of uranium and selenium. J.Contam. Hydrol. 21, pp 59-69.

MAZUREK, M., W.R. ALEXANDER, & P.M. MEIER, (2001) Geological and hydrogeological characterisation of the Migration shear zone. Ch 4 in SMITH, P.A., ALEXANDER, W.R., W. HEER, P.M. MEIER, B. BAEYENS, M.H. BRADBURY, M. MAZUREK, & I.G. MCKINLEY, (2001): The Nagra-JNC *in situ* study of safety relevant radionuclide retardation in fractured crystalline rock I: The radionuclide migration experiment – overview of investigations 1990-1996. Nagra Technical Report NTB 00-09, Nagra, Wettingen, Switzerland.

MEDINA, A., G. GALARZA, & J. CARRERA, 1996. Transin-II. Fortran code for solving the coupled flow and transport inverse problem in saturated conditions. In El Berrocal Project. Topical Report, 4(16), ENRESA, Madrid, Spain.

MEIER, P.M. 1999. Estimation of representative groundwater flow and solute transport parameters in heterogeneous formations. Ph.D. dissertation, School of Civil Engineering, Polytechnical University of Catalonia, Barcelona, Spain.

MEIER, P.M. (2001) Characterisation of heterogeneity in the MI experimental shear zone using hydrogeological test data. Appendix 1 in SMITH, P.A., W.R. ALEXANDER, W. HEER, P.M. MEIER, B. BAEYENS, M.H. BRADBURY, M. MAZUREK, & I.G. MCKINLEY, (2001): The Nagra-JNC *in situ* study of safety relevant radionuclide retardation in fractured crystalline rock I: The radionuclide migration experiment – overview of investigations 1990-1996. Nagra Technical Report NTB 00-09, Nagra, Wettingen, Switzerland.

MILLER, W.M., W.R. ALEXANDER, , N.A. CHAPMAN, , I.G. MCKINLEY, & J.A.T. SMELLIE, (2000): Geological disposal of radioactive wastes and natural analogues. Waste management series, vol. 2, Pergamon, Amsterdam, The Netherlands.

MISSANA, T., & H. GECKEIS, (eds) (2004): The CRR final project report series: II - results of the supporting laboratory programme. Nagra Technical Report NTB 03-02 (in press).

MÖRI, A., & F. VAN DORP (2000): Grimsel Test Site, Radionuclide Retardation Project: Excavation Project (EP): Mass balance of radionuclides injected into the MI experimental granitic shear zone in the GTS: Degree of radionuclide recovery and radiological aspects. Unpublished Nagra Internal Report, Nagra, Wettingen, Switzerland

MÖRI, A. & M. ADLER; (2001): GTS, Excavation project (EP): The Nagra-JNC *in situ* study of safety relevant radionuclide retardation in fractured crystalline rock: Structural description and conceptual model of flow paths and radionuclide retardation sites. Unpublished Nagra Internal Report, Nagra, Wettingen, Switzerland.

MÖRI, A., B. FRIEG, K. OTA, & W.R. ALEXANDER, (eds.) (2004): The Nagra-JNC *in situ* study of safety relevant radionuclide retardation in fractured crystalline rock III: the RRP project final report. Nagra Technical Report NTB 00-07 (in prep), Nagra, Wettingen, Switzerland.

NAGRA (2002). Project Opalinus Clay: FEP management for safety assessment. Nagra Technical Report Series NTB 02-23, Nagra, Wettingen, Switzerland.

NEALL, F.B. & P.A. SMITH, (eds.) (2004) H12: examination of safety assessment aims, procedures and results from a wider perspective. JNC Technical report, JNC TY1400 2004-001, JNC, Tokai, Japan.

NECK V., R. MÜLLER, M. BOUBY, M.ALTMAIER, J. ROTHE, M.A. DENECKE, & J.I. KIM, (2002): Solubility of amorphous Th(IV) hydroxide – application of LIBD to determine the solubility product and EXAFS for aqueous speciation. Radiochim Acta. 90, 485-494.

PAYNE, T.E., G.R. LUMPKIN, & T.D. WAITE, (1998): Uranium(VI) Adsorption on Model Minerals-Controlling Factors and Surface Complexation Modelling, in Jenne, E.A. (ed.), Adsorption of Metals by Geomedia, Academic Press, San Diego, USA, p. 75-97.

SABET, M.A. (1991): Well Test Analysis. Contributions in Petroleum Geology and Engineering. Volume 8. Gulf Publishing Company, Houston, USA

SMITH, P.A., W.R. ALEXANDER, W. HEER, P.M. MEIER, B. BAEYENS, M.H. BRADBURY, M. MAZUREK, & I.G. MCKINLEY, (2001): The Nagra-JNC *in situ* study of safety relevant radionuclide retardation in fractured crystalline rock I: The radionuclide migration experiment – overview of investigations 1990-1996. Nagra Technical Report NTB 00-09, Nagra, Wettingen, Switzerland.

VAN DORP, F., C. BIGGIN, A.& MOERI, (2003): GTS Phase V - CRR tracer injections 2002: Final radiation protection report. Unpublished Nagra Internal Report, Nagra, Wettingen, Switzerland